THESIS FOR THE DEGREE OF LICENTIATE OF ENGINEERING

On wind turbine main shaft bearing currents

JIAN ZHAO

CHALMERS

Department of Electricl Engineering
CHALMERS UNIVERSITY OF TECHNOLOGY
SE-412 96 Göteborg, Sweden
Telefon +46 (0)31-772 1000

On Wind Turbine Main Shaft Bearing Currents

JIAN ZHAO

Licentiate Thesis at Chalmers University of Technology

Department of Electrical Power Engineer
Chalmers University of Technology
SE-412 96 Gothenburg
Sweden
Telephone + 46 (0)31-772 1000

Chalmers Digitaltryck
Gothenburg, Sweden 2023

Abstract

This study explores the main shaft bearing currents in wind turbines, examining currents both internally generated from the electrical system and externally induced. The research investigates their origins and transmission paths, starting with an overview of general bearing current phenomena, drawing insights from electrical and mechanical system studies. A downscale laboratory wind turbine, abstracted from various wind turbine subsystems, is developed, and employed.

Potential current sources are explored through both laboratory setups and real wind turbine tests, discussing transmission paths, and coupling mechanisms in simplified configurations. Laboratory experiments with the downsized wind turbine validate proposed paths, emphasizing the existence of two common mode voltage sources in modern turbines. The common mode voltage effect exhibits a periodic current pattern, with its frequency determined by converter and grid frequencies. Additionally, the study reveals Electrostatic Discharge via turbine rotor blades as another major source of main shaft bearing current. The often-unnoticed rotor blades' electrostatic discharge effect is further examined in a laboratory experiment. Placing a downsized wind turbine in an artificial environment filled with free charges, attached to the wind blades via airflow, reveals that the electrostatic discharge effect generates currents as high as hundreds of amperes in a brief instance on the main shaft, posing a considerable risk to bearing lifespan.

To protect the bearing from harmful currents, the study suggests primary strategies involving the elimination of the current sources and alteration of the current paths. The common mode voltage driven pattern bearing current can be reduced by utilizing the common mode voltage filter. Regarding the electrostatic discharge-driven bearing current, better maintaining of the main shaft ground brush is imperative to minimize the current passing through the bearing.

Index Terms: bearing current, common mode voltage, electrostatic effect, power electronics, wind power generation.

Acknowledgment

I would like to thank my supervisor Professor Ola Carlson who gave me great support for my research and great patience during our discussion. I would also like to thank my co-supervisor Xiangdong Xu. His knowledge and experience in understanding the bearing current and the lab test gave me great help in the theory study and lab test. Special thanks to Professor Yujing Liu, for his expertise and insights that greatly assisted the research.

This study was carried out in the scope of the research project “Detecting and eliminating bearing currents for longer lifespan 320 of main shaft bearings” funded by the Swedish Energy Agency (Project ID: 2017-008071/44949-1). This project is launched together with SKF, Rabbalshede Kraft, Göteborg Energi AB, ABB AB, and Skellefteå Kraft. Here I sincerely acknowledge their support.

Acronyms

AC:	Alternative Current
CRB:	Cylindrical Roller Bearing
CMV:	Common Mode Voltage
DC:	Direct Current
DTRB:	Double row Tapered Roller Bearing
EDM:	Electrical Discharge Machining
ESD:	Electrostatic Discharge
FSWT:	Fixed Speed Wind Turbine
PWM:	Pulse Width Modulation
SRB:	Spherical Roller Bearing
TRB:	Tapered Roller Bearing
VSWT:	Variable Speed Wind Turbine

Contents

Chapter 1. Introduction

1.1 Background

Bearings, integral components facilitating the linkage between rotating components and immobile structures, play a pivotal role across diverse facets of daily existence, particularly within industrial settings. In recent decades, propelled by the burgeoning growth of the wind power sector in response to the rising electricity demands of modern society, there has been a notable surge in the utilization of larger and an increasing number of bearings within the wind power industry.

Nevertheless, the operational life of bearings often faces a multitude of challenges, including issues related to proper fitting, adequate lubrication, installation accuracy, material defects, and more. These issues, as illustrated in Figure 1.1, have historically comprised the predominant sources of bearing failures[1, 2]. Solutions to these mechanical and maintenance-related problems have been developed and implemented over many decades.

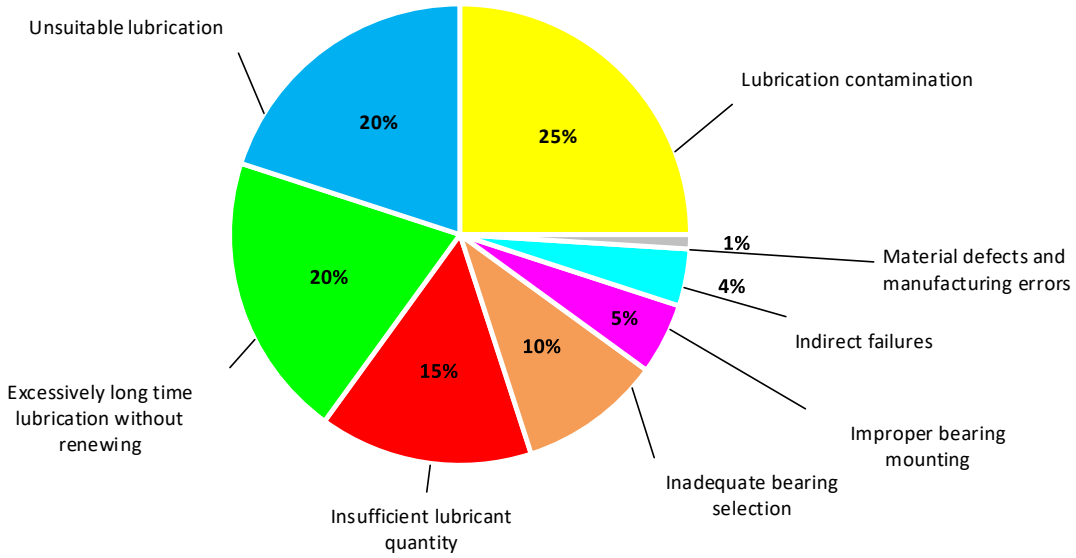

Figure 1.1: Common bearing failure causes in %.

Apart from these traditional failure modes, the emergence of bearing current-induced failure has become a matter of significant concern, especially in the context of wind turbines' main shaft bearings, with the widespread adoption of power electronic solutions[3]. Power electronic converters, renowned for their adaptability and enhanced efficiency, are increasingly integrated into various drive systems, including those within wind turbines. This surge in utilization has brought forth a risk of bearing failures, specifically in the main shaft bearings of wind turbines.

The distinct characteristic of bearing current-induced failure is a long-term process of electrical erosion that often hidden from the early detection by system operators. This phenomenon is particularly common in the context of wind turbines, where the main shaft bearings are subjected to unique environmental and operational stresses.

Notably, in wind turbines, bearing current erosion may not immediately result in bearing breakdown; however, it profoundly influences the bearing's operational condition. Over time, it may trigger subsequent failure patterns, compounding the overall maintenance challenges associated with wind turbine systems. Consequently, while bearing current-induced failure may not always be the most critical issue, it poses challenges within the wind industry and has become a crucial point of research. The specific dynamics of bearing current and its potential sources in wind turbine main shaft bearings will be explored in detail in the subsequent sections of this thesis.

1.2 Bearing current phenomenon

The bearing current phenomenon is a critical concern within the realm of mechanical systems and electrical engineering. It occurs when accumulated electrical charge is dissipated to the ground via the bearing, leading to the formation of pits or fluting on the contact surfaces between the bearing's inner and outer races and rolling elements. From a circuit perspective, this phenomenon manifests as a current flowing through the bearing during the dissipation process.

1.2.1 How bearing current occurs

The fundamental structure of a typical rolling bearing is illustrated in Figure 1.2, consisting of key components such as an inner ring, an outer ring, rollers, a roller cage, and a lubrication medium (oil or grease) that fills the spaces between the races and rollers.

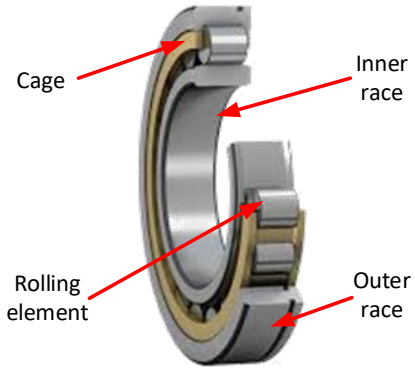

Figure 1.2: Basic structure of a typical roller bearing.

In most cases, the inner race is mechanically connected to a rotating shaft, serving as the driving source or primary action component within a system. Commonly, in various driving systems, there exists a phenomenon known as common mode voltage that sneaks onto the shaft. In specific systems, such as those with belt-driven shafts, charge accumulates on the shaft due to friction. Consequently, a voltage potential is established on both the shaft and the inner race. Conversely, the outer race is typically installed within a bearing housing that is electrically grounded.

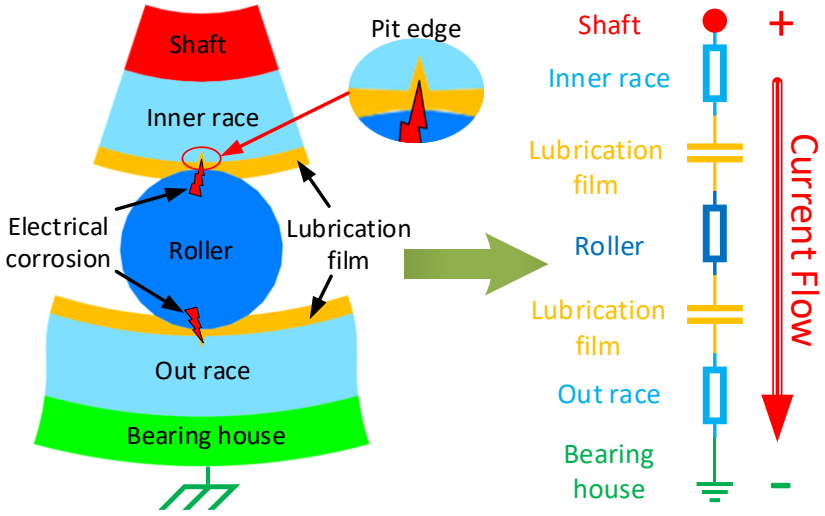

Figure 1.3: Illustration of a typical current path in bearing and its circuit model.

As a result, a voltage potential difference arises between the inner and outer races. While the rollers and the cage exhibit electrically conductive, the lubrication oil or grease tends to act as an electrical insulator. This configuration results in the application of the voltage

potential on the lubrication film, as depicted in the left-hand side of Figure 1.3. As shown in the circuit model presented in Figure 1.3, when the potential differences changes as an alternating current (AC) voltage with a relatively low amplitude, it oscillates through the bearing. However, if the voltage is a direct current (DC) or a high-amplitude AC and exceeds the film's threshold value, electrical discharge occurs. This ionizes the film, allowing current to flow through the bearing, leading to the creation of pits on the bearing races, as demonstrated in the zoomed-in section of Figure 1.3.

1.2.2 Bearing current damage on bearing

In accordance with ISO 15243 [4], the damage resulting from current-induced effects on bearings is termed "electrical erosion." Typical manifestations of this damage include craters (as depicted in Figure 1.4a) and fluting (as illustrated in Figure 1.4b) on the bearing's surfaces.

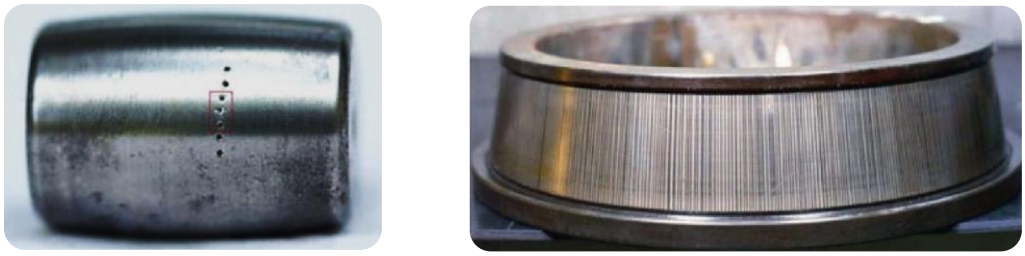

(a) Craters on bearing roller (b) Fluting on bearing raceway

Figure 1.4: Typical bearing failure caused by bearing currents.

A technical report by SKF outlines the process of crater and fluting formation, as illustrated in Figure 1.5*[5]*. This process is characterized by:

a) When discharge occurs on the film, a relatively small current flows through the contact surface, despite its high instantaneous current density (measured in A/mm2).
b) The high current density in the contact area results in rapid and intense heat dissipation over a small surface area within nanoseconds. This leads to the heating, melting, and welding together of the contact surfaces, akin to arc welding.
c) During the welding process, the contact area undergoes tempering, reshaping, or melting in a brief period, with the melted material subsequently solidifying and leading to surface damage.
d) As the rollers continue to rotate, the excess material on the rolling elements wears away [5].

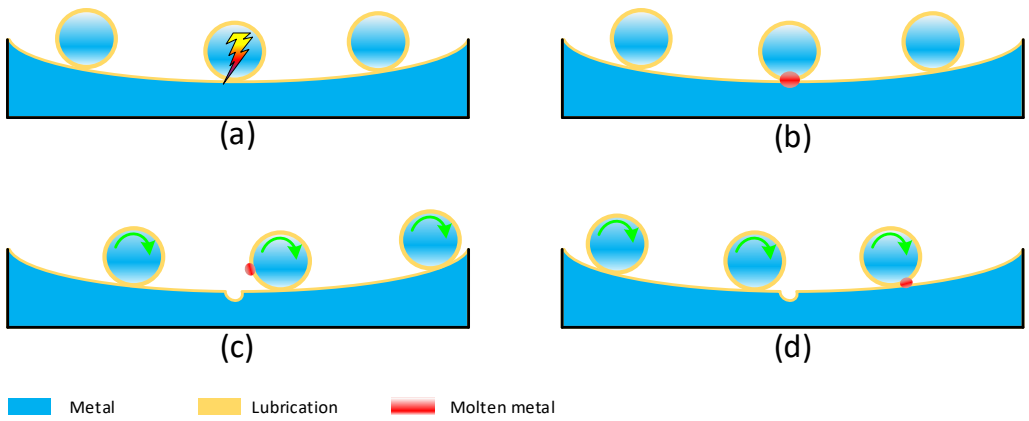

Figure 1.5: Process of electrical erosion on bearing race.

Consequently, these crater formations on the raceway or rollers also contribute to increased surface roughness. This heightened roughness results in an uneven electrical field distribution across the lubrication film, making it more susceptible to breakdown. Over time, these craters may evolve into fluting patterns, exacerbating bearing failure. Additionally, the electrical breakdown of the film causes a reduction in the lubricating properties of the grease, further triggering mechanical wear within the bearing. This vicious cycle accelerates the overall wear and deterioration of the bearing.

1.2.3 Grade of bearing current damage

As discussed in section 1.2.2, bearing current represents a potential threat to the integrity of bearings, ultimately leading to the formation of craters and fluting on the bearing race and, ultimately, bearing failure. In practice, the degradation of bearings is a gradual process, offering ample opportunities for early detection and intervention. Therefore, it is of paramount importance to categorize the level of bearing damage, enabling timely preventive measures to safeguard the bearing from current-induced damage.

To assess the extent of damage inflicted by bearing current, an exhaustive series of tests were conducted by H. Tischmacher within Siemens AG's Large Drives team [6]. These tests involved subjecting bearings to current for approximately 50,000 hours across various machines. The classification of bearing damage levels is predicated on the observation of damage to the rollers, raceways, and alterations in the lubricating grease's properties. The resulting damage has been categorized into five distinct grades [6].

- **Grade 0:** Termed the "gray race," this stage represents the early manifestation of bearing current damage. In Grade 0, the bearing race exhibits a grayish surface, a result of the rollers traversing minor craters on the race.

- **Grade 1:** Referred to as the "frosting race," this stage presents an optical impression characterized by a sequence of numerous minor melting craters traversed by the rollers. At this point, microscopic observations reveal the onset of the fluting effect.
- **Grades 2 to 4:** As the bearing current erosion intensifies, the fluting patterns become increasingly pronounced, and the discoloration of the lubricating grease becomes more evident.
- **Grade 5:** This grade signifies the typical state of bearing wear-out, marked by raceway fatigue failure and corrugation of the bearing balls.

1.3 Bearing current in electrical machine

Bearing current phenomena have been a subject of exploration and analysis for several decades, initially surfacing in grid power-fed motors. However, with the evolution of power electronics, particularly the prevalence of inverter-fed motor systems, the bearing lifespan has witnessed a sharp decline. This shift has also brought forth distinct bearing current patterns unique to inverter-driven systems.

1.3.1 Grid power-fed Circulating bearing currents

In a conventional drive system, the motor is powered by grid electricity, resulting in a pure sinusoidal current waveform. Under such conditions, a current circulates within the motor and flows over the bearing, giving rise to what is commonly referred to as "classical" bearing current [7, 8]. Extensive research has elucidated the mechanism and circulating path of classical bearing current.

The classical bearing current circulating path, depicted in Figure 1.6, emerges due to inherent asymmetries within the motor's construction. Mechanical imbalances within the system lead to the generation of parasitic asymmetric flux linkages when the winding is subjected to symmetric grid current. This flux linkage loop, encompassing the "stator housing - drive-end bearing - motor shaft - non-drive-end bearing," induces a voltage on the shaft and, subsequently, a circulating current, predominantly within the bearing. Notably, as machine size increases, the parasitic flux linkage and induced voltage also experience a corresponding augmentation. Owing to the grid's sinusoidal nature, the frequency of classical circulating current aligns with the grid frequency (50Hz/60Hz).

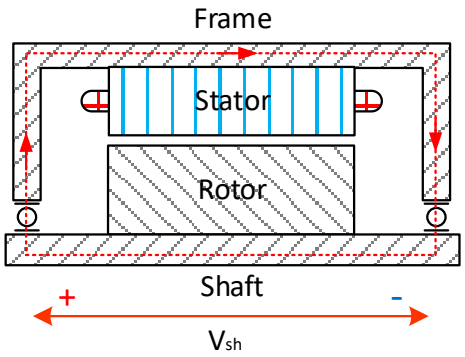

Figure 1.6: Classical electrical machine bearing current circulating path.

1.3.2 Inverter-fed bearing currents

In inverter-fed systems, pulse width modulation (PWM) technology is employed to control the output voltage frequency, resulting in an output waveform comprising pulse signals whose frequency is contingent on the switching frequency. While the fundamental component remains sinusoidal, a multitude of harmonics corresponding to the switching frequency are superimposed onto the output voltage. The fundamental frequency of the converter typically spans from several Hz to several hundred Hz, with switching frequencies ranging from several kHz to, with advancements in wide-bandgap power electronics, several hundred kHz.

Due to dead band effects within each bridge, the instantaneous value of the 3-phase total output voltage is no longer zero. Consequently, a common-mode voltage (CMV) materializes and is applied to the motor winding. Coupled with the rapid switching operations, the CMV is characterized by a high-frequency nature. Within the motor, the instantaneous CMV current circulates, seeking a path to ground, unveiling novel mechanisms for harmful bearing current in motor systems. These harmful bearing current mechanisms are outlined in Table 1.1[2].

Table 1.1 Classification of bearing current under inverter-fed drive system.

a) Electric discharge machining bearing currents	b) High frequency circulating bearing current	c) Rotor to ground currents

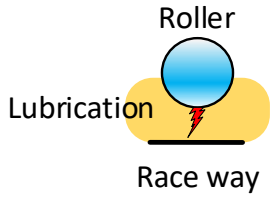	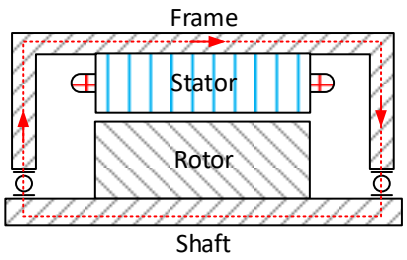	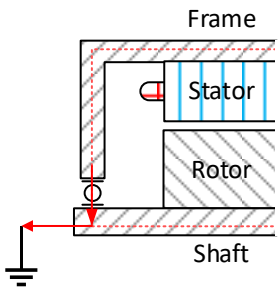
Medium/high rotor speed	Big machine size at low speed	Independent of machine size

a) **Electrical Discharge Machining (EDM) Bearing Currents:** As illustrated in Figure 1.3, the bearing race, bearing roller, and bearing lubrication can be conceptually represented as a capacitor. Under the influence of a low AC voltage, a bearing current flows. However, if this voltage is sufficiently high to generate an intense electric field within the lubrication film, surpassing the discharge threshold, a short-lived arc occurs. This event leads to an immediate discharge of the charged film, resulting in a current spike known as EDM bearing current. This type of current is particularly detrimental, especially in rotor-fed AC machines.

b) **High-Frequency Circulating Bearing Currents:** A circulating current (i_{CM}) is driven in this "loop" through the two non-insulated bearings by the high-frequency (HF) shaft voltage induced in the stator iron, end shields, rotor shaft, and iron due to the stator winding's common-mode current. This "circulating" bearing current is directly proportional to i_{CM} and is dependent on motor geometry. It appears with opposite signs in both bearings and manifests as a pulsed current with a switching frequency due to metallic contact within the bearings.

c) **Rotor-to-Ground Currents:** In scenarios involving a grounded rotor, a portion of the common-mode current flows as a "rotor-to-ground" bearing current, traversing the stator, bearings, rotor, and finally grounding. This current pattern is similar to circulating bearing current but is influenced by the common-mode impedances of the entire drive system, with a proportionality factor to i_{CM} of less than 1.

1.4 Wind turbine main shaft bearing current

1.4.1 Bearings in wind turbine

In a wind turbine, bearings play an indispensable role in the transmission system. These wind turbines encompass various types of bearings to fulfil their operational requirements. Figure 1.7 provides an illustrative depiction of the typical wind turbine nacelle structure.

This structural configuration incorporates main shaft support bearings, gearbox bearings, induction generators, and the yaw drive system, all ensconced within the nacelle. In this operational paradigm, the kinetic energy harnessed from the wind propels the rotation of the blades and hub. Subsequently, this energy is transmitted through the main shaft and gearbox, driving the generator to produce electricity. It is evident that the primary bearings, including the main shaft bearing, gearbox bearing, generator bearing, yaw bearing, and pitch bearing, are integral components of the wind energy generation system [9]. Notably, the main shaft bearing stands out as the costliest and most challenging to maintain among these bearings.

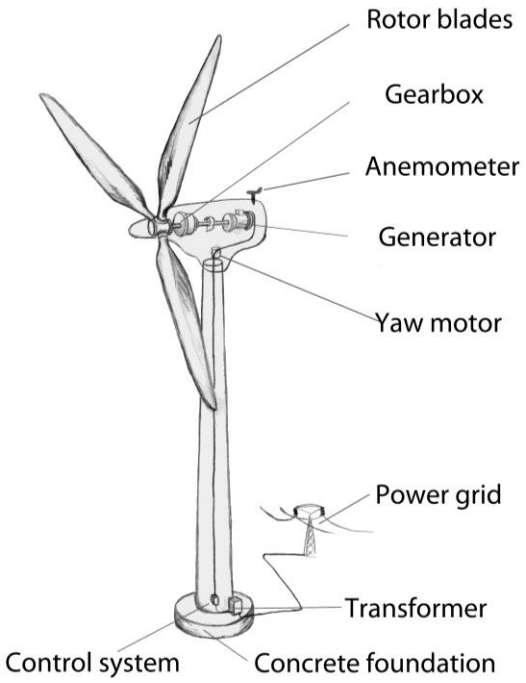

Figure 1.7: Typical wind turbine structure. [10]

As the demand for energy has surged over the years, the wind power sector, characterized by its cleanliness and renewability, has witnessed continuous development. Wind turbines, both onshore and offshore, have been deployed at an escalating pace. The capacity of individual turbines has continually increased, heralding the future direction of wind energy expansion. Achieving higher capacities necessitates a larger sweep area, resulting in taller turbines with larger main shaft bearings. The correlation between wind turbine capacity and main shaft bearing size is graphically illustrated in Figure 1.8.

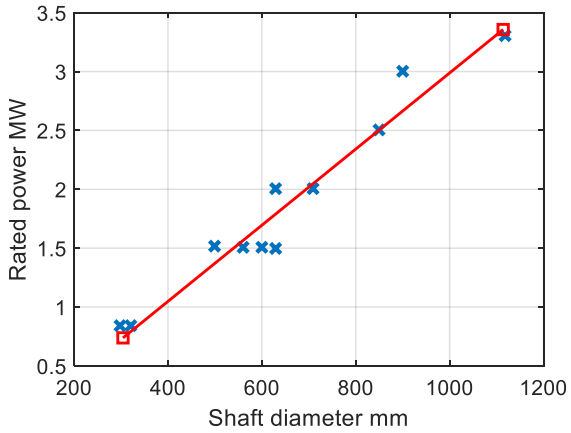

Figure 1.8 Relation between wind turbine capacity and bearing size.

1.4.2 Main shaft bearing breakdown issues

While various bearings are utilized within wind turbine systems, the main shaft bearing, tasked with supporting the rotor's weight and withstanding wind-induced thrust forces, assumes paramount importance. The trend toward larger turbine sizes has correspondingly increased the size and cost of main shaft bearings. This reality has led to elevated maintenance and replacement expenses for these crucial components. According to data from Wind Power Engineering, the replacement of a main shaft bearing can impose costs of up to $450,000, significantly impacting the financial performance of turbine operators[11, 12].

The reliability of the main shaft bearing is a critical determinant of wind turbine reliability and availability. Recent data indicates that over the past two decades, main shaft bearing failures have accounted for up to 30% of total downtime [13]. Furthermore, industry experts have reached a consensus, acknowledging that main shaft bearings have become the second most significant reliability challenge, just behind gearboxes [14].

1.4.3 Main shaft bearing electrical breakdown in the field test and lab test

The factors contributing to main shaft bearing breakdown align with the general bearing failure issues discussed in Section 1.1. Predominantly, mechanical, and maintenance-related issues encompass most failure patterns. However, bearing current, often overlooked, has a substantial impact on main shaft bearing failure.

In a recent study conducted by Chalmers's research group in collaboration with SKF, an exceptionally high current was detected in a main shaft bearing[15]. Figure 1.9 illustrates the fundamental structure of the transmission system and the positioning of current sensors. The tested wind turbine, a direct-drive model equipped with a full-size converter, utilized

several Rogowski coils to facilitate current flow through the bearing. Due to the inaccessibility of the bearing house ground point, direct measurement of the bearing current was unfeasible. Instead, the bearing current was calculated by subtracting the readings from Rogowski coil A and Rogowski coil B, positioned on opposite sides of the main shaft bearing.

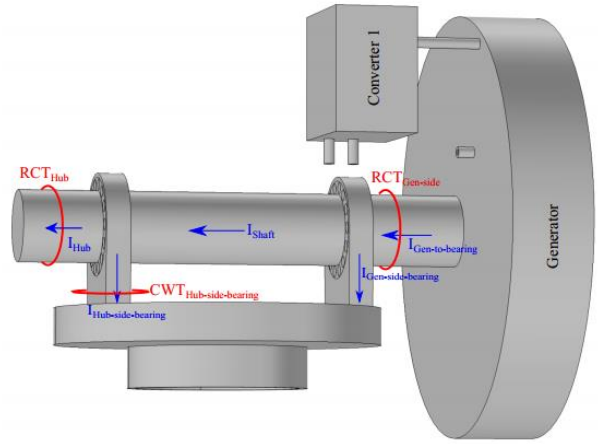

Figure 1.9: The structure of the tested wind turbine.

During the wind turbine's operation at normal power generation mode, the bearing current was continuously monitored using a Pico scope. Figure 1.10 presents the results of the test, where the bearing current is derived from the subtraction of different Rogowski coils. It is evident from the test results that the bearing current exhibits an alternating current (AC) signal, with amplitudes reaching up to 80A. Technical constraints prompted the dismantling of the wind turbine after several years of operation.

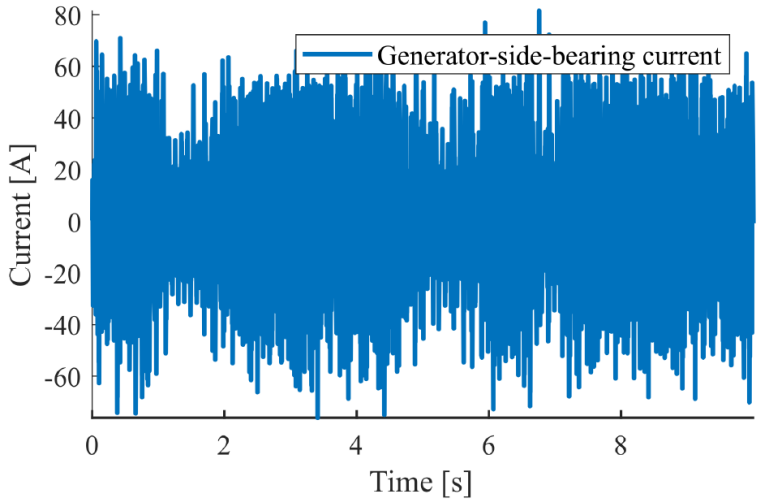

Figure 1.10: Main shaft bearing current in direct drive wind turbine.

To investigate deeper into the impact of current on the main shaft bearing, a series of laboratory tests were conducted within SKF's bearing lab. During these tests, the bearing operated at typical wind turbine speed ranges, with an axial thrust force, simulating wind turbine operation conditions. An alternating current of 2A was supplied through the bearing. After 8 hours of operation, the bearing was disassembled to assess the condition of the raceway and the grease. Figure 1.11 provides an insight of the disassembled components, revealing clear frosting phenomena and the incipient stages of fluting on both the raceway and the rollers.

Figure 1.11: Wind turbine main shaft bearing lab test in SKF.

1.5 Objectives and research questions

Based on the field test results and laboratory experiments, the influence of electrical current on the wind turbine's main shaft bearing has been revealed. Nevertheless, the exploration of this phenomenon within the realm of wind turbine main shaft bearings has remained surprisingly limited. Diverging from conventional bearing currents found within electrical machines, the origins of these currents within wind turbine main shaft bearings have hitherto eluded comprehensive understanding. Furthermore, given the intricacies of the operational environment, the electrical breakdown patterns associated with main shaft bearing currents distinctly deviate from those encountered in traditional bearing current scenarios.

In response to this research gap concerning wind turbine main shaft bearing currents, this study is dedicated to unravelling the complexities associated with these current sources. The main research questions guiding this investigation are articulated as follows:

- Uncover the diverse sources responsible for generating main shaft bearing currents.
- Discover and explain the manifold sources of bearing currents, along with their pathways to grounding.
- Propose viable solutions for mitigating the effects of various bearing currents.

1.6 Structure of the thesis

The thesis unfolds through a structured framework comprising the following chapters.

Chapter 1: This chapter provides an introductory context, elucidating the research background and status of wind turbine main shaft bearing currents. It outlines the research questions and delineates the scope of this thesis.

Chapter 2: Within this chapter, we delve into the structural aspects of wind turbines and enumerate potential factors contributing to main shaft bearing currents. Theoretical analyses are conducted to explore all conceivable causes and possible transmission paths.

Chapter 3: This chapter introduces a laboratory-scaled wind turbine setup and discusses its various subsystems. It also encompasses diverse conditions under which different bearing current mechanisms are tested.

Chapter 4: Primarily, this chapter scrutinizes the impact of Common Mode Voltage (CMV) on the main shaft bearing. Both simulation and laboratory tests are employed to verify the underlying theoretical grounds.

Chapter 5: Chapter 5 shifts the focus to the Electrostatic Discharge (ESD) effect on the main shaft bearing. It encompasses both analytical investigations and practical experiments aimed at validating the observed phenomena.

Chapter 6: In the final chapter, we draw together the threads of the thesis, summarizing key findings and insights. Additionally, we chart a course for future research directions in the field.

1.7 Publication list

J. Zhao, X. Xu and O. Carlson, "Common mode voltage impact on wind turbine main shaft bearing," 2021 23rd European Conference on Power Electronics and Applications (EPE'21 ECCE Europe), Ghent, Belgium, 2021, pp. P.1-P.7, doi: 10.23919/EPE21ECCEEurope50061.2021.9570495.

C. Tang, **J. Zhao** and T. Thiringer, "Circulating Currents and Losses Analysis of an MMC with Using SVM-based Common Mode Voltage Reduction Strategy for a Wind Turbine Application," 2022 IEEE Energy Conversion Congress and Exposition (ECCE), Detroit, MI, USA, 2022, pp. 1-7, doi: 10.1109/ECCE50734.2022.9947709.

J. Zhao, X. Xu, and O. Carlson, "Electrostatic discharge impacts on the main shaft bearings of wind turbines," Wind Energ. Sci. Discuss., vol. 2023, pp. 1-19, 2023, doi: 10.5194/wes-2023-46.

Publication during Phd. But not in this study topic

Q. Xun, Y. Liu, **J. Zhao** and E. A. Grunditz, "Modelling and Simulation of Fuel Cell/ Supercapacitor Passive Hybrid Vehicle System," *2019 IEEE Energy Conversion Congress and Exposition (ECCE)*, Baltimore, MD, USA, 2019, pp. 2690-2696, doi: 10.1109/ECCE.2019.8913170.

Q. Xun, Y. Liu, X. Huang, E. A. Grunditz, **J. Zhao** and N. Zhao, "Drive Cycle Energy Efficiency of Fuel Cell/Supercapacitor Passive Hybrid Vehicle System," in IEEE Transactions on Industry Applications, vol. 57, no. 1, pp. 894-903, Jan.-Feb. 2021, doi: 10.1109/TIA.2020.3035551.

1.8 Contributions

In this study, different wind turbine configurations for bearing current study are proposed. Based on these configurations, the wind turbine main shaft bearing current source are analyzed. The CMV and the ESD effect is confirmed to be the main source of the bearing current. In this study, the sources and the current path are discussed, the main contributions are

a) Proposed the wind turbine configuration for main shaft bearing current study
b) Identity the source of wind turbine main shaft bearing current
c) Analyzed bearing current paths and verify them by lab test and real wind turbine test
d) Highlight the ESD effect's contribution on bearing current which is not noticed in previous study.

Chapter 2. Wind turbine structure for bearing current study

2.1 Main shaft bearing in different types of wind turbines

The main shaft bearing serves as a key component in wind turbines, providing support to the rotor while withstanding the combined forces of radial rotation and axial wind thrust. The operational context of the main shaft bearing, however, exhibits substantial variations across different types of wind turbines. Before delving into an examination of the main shaft bearing's operational conditions, it is imperative to comprehend the classification of wind turbine drivetrains.

2.2 Wind turbine drivetrain classification

Wind turbines can be categorized based on the direction of turbine rotation, resulting in two primary classifications: horizontal axial wind turbines and vertical axial wind turbines. Through operational experience, it has become evident that horizontal axis wind turbines exhibit superior performance in open environments and are notably well-suited for commercial wind farms.

Fixed-speed wind turbines (FSWTs) and variable-speed wind turbines (VSWTs) are the two main categories of horizontal axial wind turbines. While VSWTs possess the ability to adjust their rotational speeds to optimize power output and the generator torque under varying wind conditions, FSWTs maintain a constant rotational speed. Different from FSWTs, which are directly connected to the grid, VSWTs feed power to the grid via an additional power converter.

The classification of wind turbines extends to drivetrain topology, as defined by IEC 61400-27-1, which delineates four primary types[16, 17]. Types 1 and 2 correspond to FSWTs, which require no power converter for grid connection. Conversely, Types 3 and 4 represent VSWTs, necessitating partial or full power converters to feed energy into the grid. Figure 2.1 illustrates their classification map.

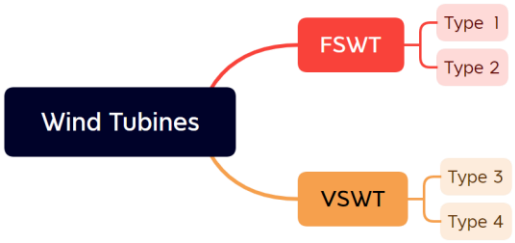

Figure 2.1: Classification of wind turbines according to IEC 61400-27-1.

Type 1: Features direct grid connection with an asynchronous generator, typically employing a fixed-resistance squirrel-cage rotor.

Type 2: Resembles Type 1 but incorporates a variable rotor resistance for output power adjustment.

Type 3: Adopts a double-fed induction generator, with the stator connected directly to the grid and the rotor side linked through a partial-scale converter to regulate power output.

Type 4: Employs a synchronous generator, connecting the wind turbine to the grid via a full power converter. In this configuration, the gearbox is dispensable within the transmission drivetrain.

The classification of wind turbines, as defined, primarily facilitates the development of power generation models. A closer examination of the drivetrain reveals that Types 1, 2, and 3 employ gearbox-driven rotors, while Type 4 can accommodate either gearbox or direct rotor drive. Simplified from a rotor drivetrain perspective, the classification thus dichotomizes wind turbines into geared and gearless categories, as shown in Figure 2.2.

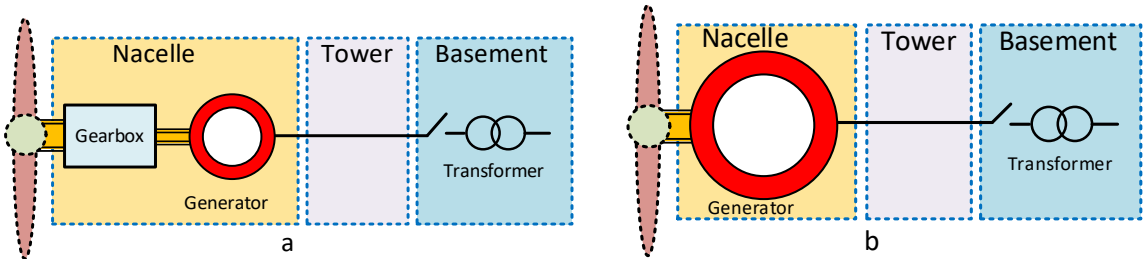

Figure 2.2: Illustration of geared and gearless wind turbine drivetrains.

2.3 Main shaft suspension arrangement in horizontal wind turbine

The rotor suspension system within a wind turbine plays a critical role in supporting the drivetrain's rotor and bearing the radial and axial forces generated by the rotor's operation. These suspension systems rely on a combination of bearings to secure the rotor and withstand these forces. Different types of wind turbines employ distinct suspension

arrangements. In this section, we explore various suspension systems, each tailored to specific wind turbine configurations.

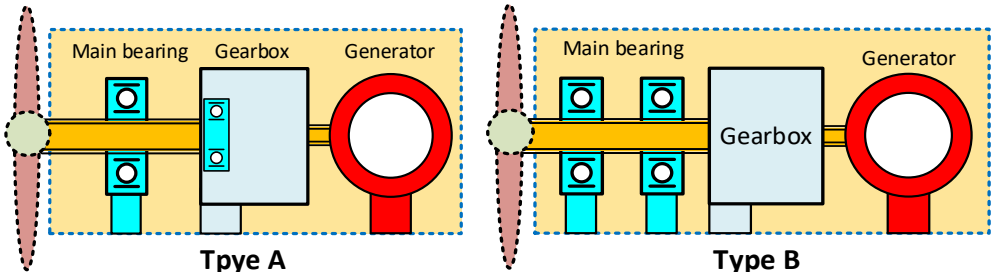

Figure 2.3: Geared drivetrain wind turbine suspension system.

Type A & B: The geared wind turbine suspension system is depicted in Figure 2.3. Type A, the most prevalent configuration, utilizes two bearings in tandem to suspend the rotor system. A spherical roller bearing (SRB) serves as the primary bearing, while a cylindrical roller bearing (CRB) within the gearbox provides additional support. The CRB, however, exclusively handles radial forces, leaving the axial forces to be managed only by the main bearing.

Type B, designed for larger wind turbines with higher loads (>2MW), incorporates two main bearings on the main shaft to handle both axial and radial forces. The bearing on the blade side predominantly manages axial forces, with double row tapered roller bearings (DTRB) or SRBs commonly chosen as the primary bearing.

Type C: In the context of gearless wind turbines, the configuration is simplified by eliminating the gearbox and enlarging the generator to accommodate the torque from the rotor. The generator and main bearings are separate components housed in the nacelle. Figure 2.4 illustrates the suspension system of separate bearings in gearless wind turbines.

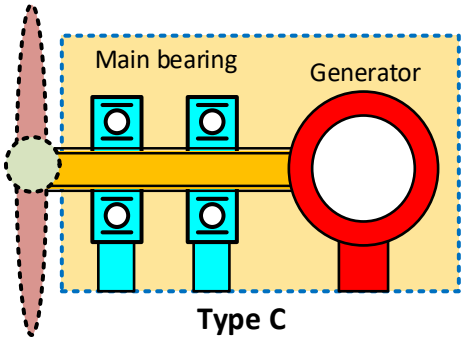

Figure 2.4: Gearless drivetrain wind turbine separate bearing suspension system.

Types D, E & F: As power capacity increases, the nacelle space becomes limited, prompting a more compact structure for gearless wind turbines. The optimal solution involves integrating the generator's rotor with the wind turbine's rotor, forming a unified main rotor. This integration takes two forms: inner rotor and out-rotor wind turbines.

Inner Rotor Configuration (Types D & E): In this design, the generator's rotor is situated inside the generator's stator, with the hub and blades co-mounted with the generator's rotor, as depicted in Figure 2.5. The airgap between the stator and rotor transforms mechanical energy into electrical energy via electromagnetic fields. The generator's stator, mounted with the nacelle frame, generates electrical power, which is conveyed to the converter through a power cable. The main bearing, situated within the rotor, is mounted with the inner race on the stationary generator component and the outer ring on the rotor's inner surface. Gearless wind turbines, like their geared counterparts, can be classified into single-bearing (Type D) and double-bearing (Type E) suspension systems.

Out-Rotor Configuration (Types F & G): In contrast to the inner rotor configuration, the generator's rotor is placed outside the stator and is integrated with the hub and blades. Figure 2.6 illustrates the detailed configurations. Both the stator and main bearings are situated within the rotor in this design. The main bearing's mounting connection is akin to that of the inner rotor. As power capacity increases, out-rotor gearless wind turbines adopt either single-bearing (Type F) or double-bearing (Type G) suspensions.

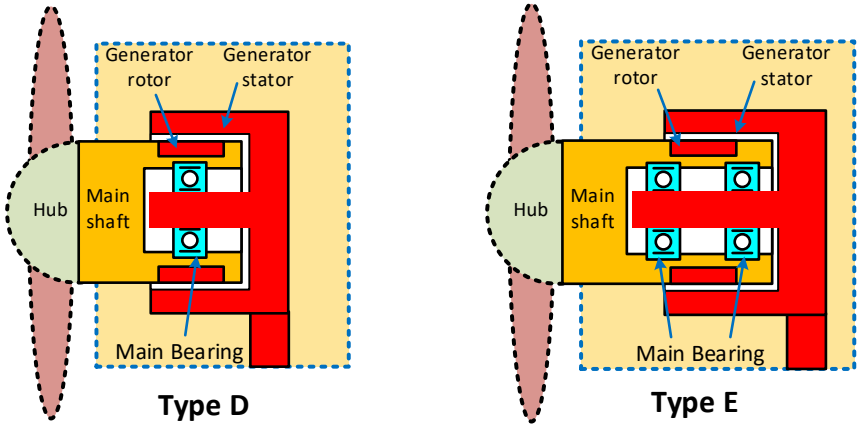

Figure 2.5: Inner rotor gearless drivetrain wind turbine suspension system.

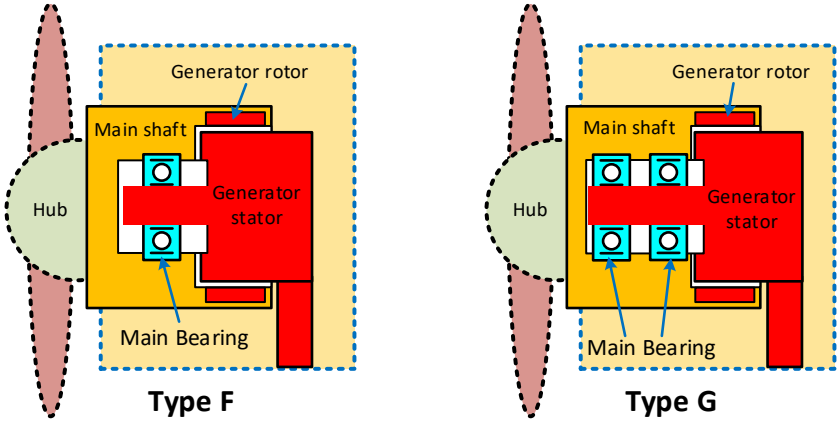

Figure 2.6: Out rotor gearless drivetrain wind turbine suspension system.

2.4 Wind turbine main shaft bearings

The main bearing constitutes the cornerstone of the wind turbine suspension system, providing vital support for the rotating shafts within the transmission system. While the purpose of supporting these rotating shafts remains consistent, the combinations of bearings employed may vary slightly across different drivetrain systems. Table 2.1 provides a summary of potential bearing combinations within various wind drivetrain types[9, 12].

Table 2.1 Suspension bearings in different types of wind turbine.

Suspension type	Blade side bearing	Generator side bearing
Type A	SRB	CRB
Type B/C	SRB/TRB/DTRB	SRB/TRB/CRB
Type D/F	TRB/DTRB	CRB
Type E/G	TRB/DTRB	TRB/CRB

The table outlines different types of bearings utilized in wind turbine main bearings. Notably, all listed wind turbine main bearings are roller bearings, diverging from the prevalent use of deep groove ball bearings in electrical machine applications. Common main bearings encompass Spherical Roller Bearings (SRB), Tapered Roller Bearings (TRB), and Cylindrical Roller Bearings (CRB). The structural configurations of these roller bearings as employed in wind turbines are depicted in Figure 2.7.

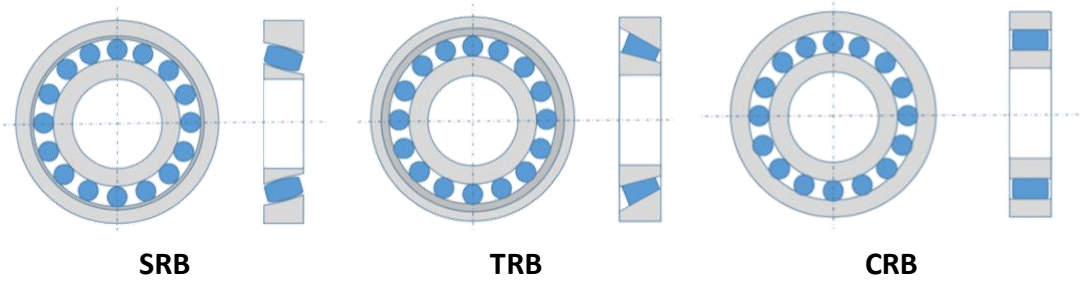

Figure 2.7: Different types of wind turbine main shaft bearings.

Spherical Roller Bearing (SRB): SRBs feature a spherical outer raceway, with rollers precisely designed to follow both the inner and outer raceways. Operating on the principle of self-alignment, SRBs employ spherical rollers (rather than ball rollers) to accommodate larger loads. They excel at withstanding substantial radial loads and light axial forces.

Tapered Roller Bearing (TRB): TRBs comprise conical rollers situated between tapered raceways within the inner and outer rings. The contact angle inherent in TRBs enables them to endure significant radial and axial forces. An imbalanced force due to differing contact angles at the inner and outer raceways causes the roller to engage with its guide flange. The bearing's contact angle, in relation to radial loading, determines the capacity to withstand axial loads. TRBs are frequently configured in double-row setups (DTRB) to enhance radial load-bearing capabilities.

Cylindrical Roller Bearing (CRB): CRBs feature cylindrical rollers and provide optimal distribution of stress elements upon impact. In comparison to SRBs and TRBs, CRBs operate with reduced friction and possess a greater capacity for radial loads. However, they are not suited to withstand axial loads unless a thrust flange is integrated into the bearing housing to tolerate minor axial loads.

Diverging from ball bearings, all components within wind turbine main shaft bearings consist of rollers. The interface between the rollers and the raceway constitutes a line contact zone, significantly larger in area than the point contact spot typical of ball bearings. From an electrical analysis perspective, the capacitance between races and rollers is larger than that of ball bearings with identical outer dimensions.

2.5 Electrical configuration of wind turbine system for bearing current study

Building upon the discussions in section 2.2 and 2.3, which addressed wind turbine drivetrain classification and main shaft suspension systems, this section delves into the primary focus of this work: the analysis of electrical current flow through the main shaft

bearing. Given this research scope, it becomes crucial to study the electrical pathways within the mechanical transmission components of the wind turbine. Consequently, we need to simplify the wind turbine system to facilitate the analysis of the electrical path.

As illustrated in Figure 2.2, wind turbine transmission structures fall into two primary categories: geared turbines and gearless turbines. Building on the introduction of suspension systems for geared and gearless wind turbines in section 2.3, the way of the main bearing is installed varies significantly between these two categories. In geared wind turbines, the main bearing is a separate component mounted on the nacelle frame. Conversely, due to compact structural design considerations, gearless wind turbines normally incorporate the main bearing into the generator. As a result, the analysis of bearing current for geared and gearless wind turbines requires separate discussions.

2.5.1 Geared wind turbine structure

Figure 2.3 illustrates the fundamental structure of geared wind turbines. Within the classification of geared wind turbines, both Fixed-Speed Wind Turbines (FSWTs) and Variable-Speed Wind Turbines (VSWTs) coexist. VSWTs, owing to their enhanced controllability and higher power coefficient, have gained prominence in the wind energy landscape over the past decades, indicating a shift towards their becoming the dominant wind turbine type. However, achieving these benefits requires a more intricate electrical configuration in VSWTs, involving additional electrical subsystems and components, which may influence main shaft bearing currents.

Given the complexity of wind turbine systems, the configuration presented in Figure 2.2, for studying main bearing current in geared wind turbines, is overly simplistic for our purposes. However, as not all subsystems are relevant to the study of main shaft bearing current. Thus, we require a simplified configuration suitable for this specific investigation.

To comprehensively analyze the bearing current in the geared wind turbine, we must consider all subsystems capable of contributing to or transmitting current to the main shaft bearing. Auxiliary subsystems such as the lubrication system and lighting systems can be omitted in this study. Furthermore, the configuration should be adaptable for both FSWTs and VSWTs.

The configuration includes subsystems such as converters and slip rings that do not exist in FSWTs. Therefore, when focusing on FSWTs, their contribution to main bearing current should be disregarded. Common subsystems such as the power generation system, suspension system, and lightning protection system, available in both FSWTs and VSWTs, are situated in the nacelle and basement, respectively. The pitch system, responsible for

controlling blade angles, is positioned inside the hub. The electrical configuration for bearing current study in geared wind turbines is depicted in Figure 2.8, and the relevant subsystems within this configuration will be introduced in the following sections.

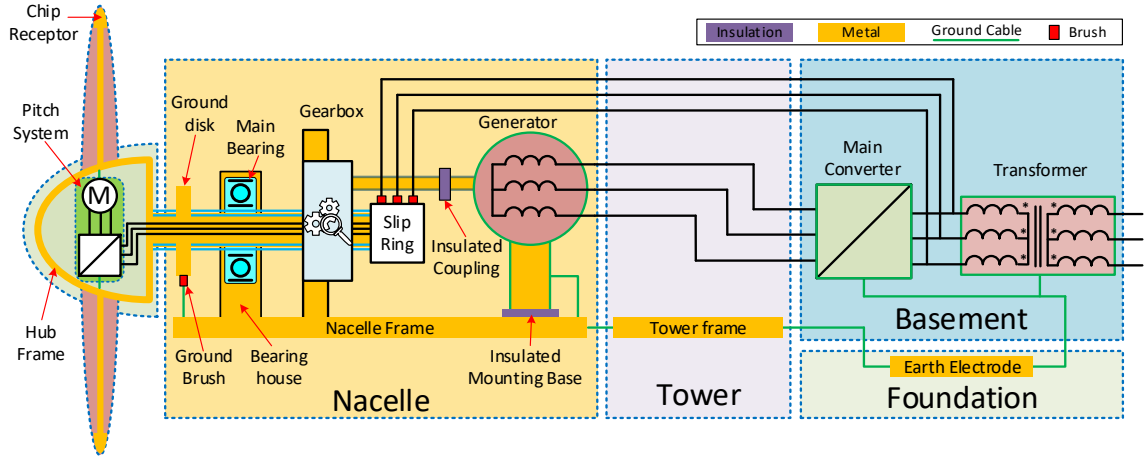

Figure 2.8: Geared wind turbine electrical configuration for the main bearing current study.

Subsystems in geared wind turbine configuration

Power Generation System: Typically, the power generation system consists of a gearbox, generator, and transformer. In VSWTs, an additional converter is required. Within this system, the gearbox and generator are housed in the nacelle. Wind motion impels the rotor, transmitting torque through the gearbox to the generator. The generator generates negative torque to counterbalance wind-induced torque. Power generated by the generator is conveyed to the grid via the converter and transformer, primarily located in the basement. Connections within the nacelle are predominantly mechanical. To mitigate electrical coupling between the main shaft and gearbox, their connection employs an insulated coupling, as depicted in Figure 2.8 and Figure 2.9. Connection between the nacelle and basement involves a group of flexible cables routed along the tower.

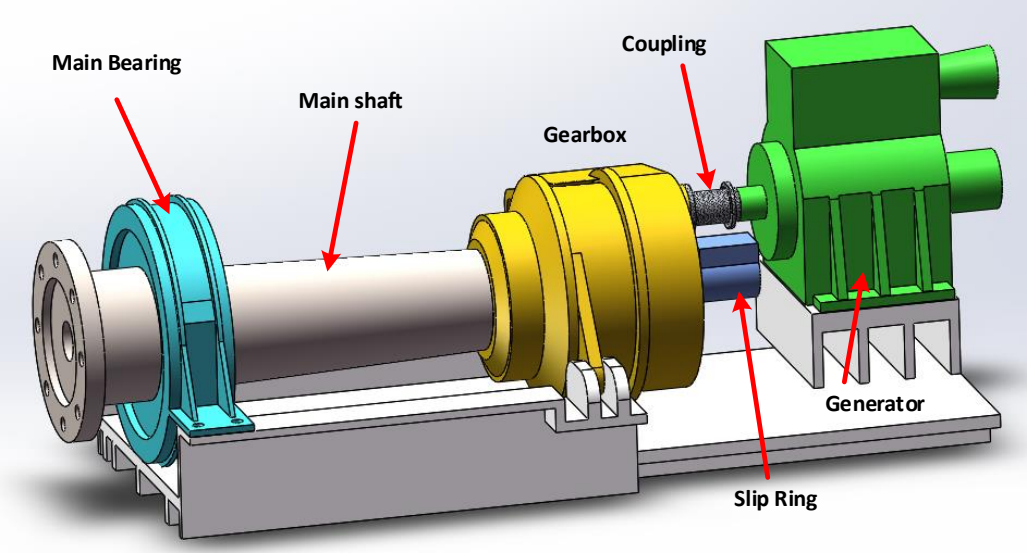

Figure 2.9: Geared wind turbine power generation system.

Suspension System: For electrical modularization purposes, the geared wind turbine suspension system, as introduced in section 2.3, treats double-bearing suspension and single-bearing suspension similarly, with slight variations in bearing capacitance values. To simplify the model, single-bearing suspension is selected as the representative.

Lightning Protection System: The lightning protection system aims to shield the wind turbine from damage caused by lightning strikes. This system channels lightning from the atmosphere to the earth beneath the basement. Key components include the blade's chip receptor, the hub's conductive frame, the main shaft's metal brush, the nacelle frame, the tower frame, and the earth electrode in the foundation [18-23].

Pitch System: In VSWTs, the pitch system assumes a critical role. This system regulates turbine blade angles to optimize operation at varying wind speeds. Increasing wind speed elevates the pitch angle, affecting rotor blade lift forces to keep the wind turbine operating within its rated power range. The pitch system consists of a pitch drive (actuator), a pitch controller, and transmission gear. Options for the pitch drive component include electrical or hydraulic mechanisms. Due to its flexibility, the electrical pitch system represents the future trend. The pitch system is installed within the hub, near the blade's root. The pitch drive component imparts motion to a stationary gear mounted on the drive component. This stationary gear transmits the driving force to a secondary gear mounted on the blade root. Pitch action and a typical 3-blade electrical pitch system are illustrated in Figure 2.10.

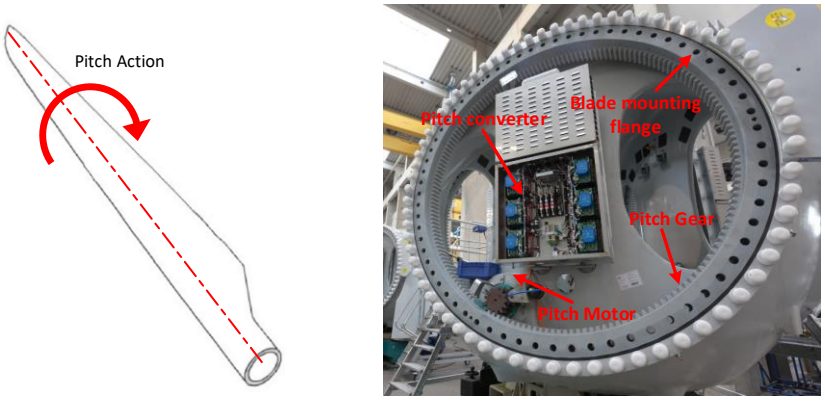

Figure 2.10 Pitch system inside the hub.

As shown in Figure 2.8, in the electrical pitch system, pitch action is driven by a motor controlled by a 3-phase converter. This converter is powered by a bundle of power cables passing through the hollow main shaft. The power cable is connected to the grid via the slip ring mounted on the main shaft.

Grounding System: While not a distinct subsystem within the wind turbine, the way of various components connect to the ground significantly influences main shaft bearing current. Therefore, in this study, we treat ground connections as a subsystem of the wind turbine. In principle, all electrical component frames should be adequately grounded.

- **Lightning Protection System Ground:** As previously discussed, the lightning protection system channels lightning from the clouds through the blade's chip receptor, the hub frame, the main shaft, the ground brush on the main shaft, the conductive cable connecting the brush to the nacelle metallic frame, and finally to the tower metallic frame, which further conducts the electrical charge to the earth electrode in the foundation seen in Figure 2.11.

Blade chip receptor → Hub frame → Main shaft → Ground brush → Brush cable → Nacelle frame → Tower frame → Earth electrode.

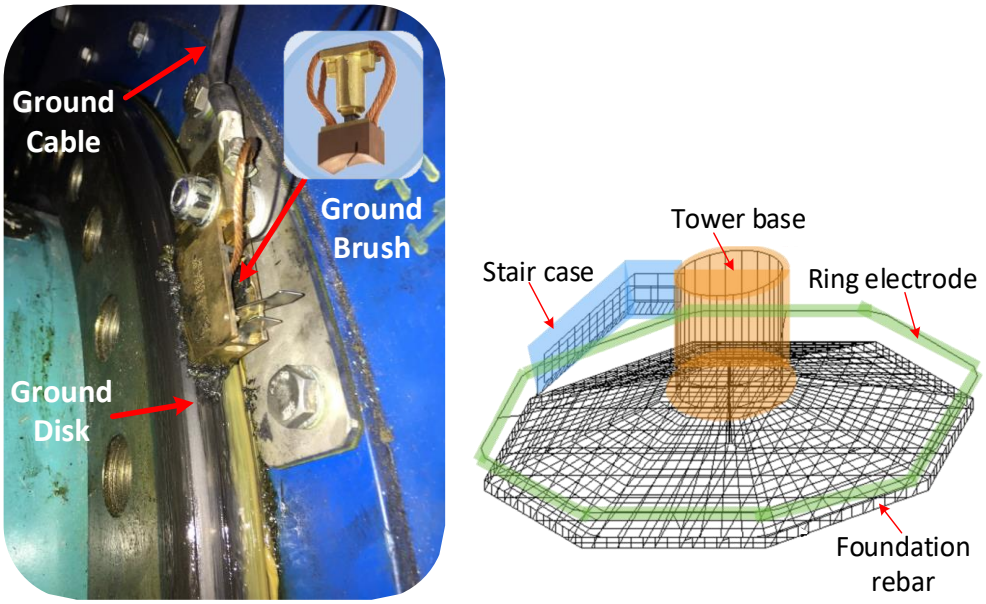

Figure 2.11 Typical wind turbine lightning protection components.

- **Pitch System Ground:** In the pitch system, both the pitch motor and its converter are electrical components. They are mechanically mounted on the hub frame, and their frames are electrically connected to the ground via the hub frame.
- **Main Bearing and Gearbox Ground:** The main bearing is installed within the bearing house, with its outer race electrically connected to the bearing house through its mechanical connection. The bearing house is mounted on the hub frame, which is grounded within the lightning protection system. The inner race of the main bearing is assembled together with the main shaft and grounded via the lightning ground brush.
- **Generator Ground:** While the gearbox and generator are mounted on the nacelle frame, an insulated mounting base separates their frames from the nacelle frame. Consequently, the electrical connection is severed by the insulated mounting base. On the transmission side, insulated couplings are installed between the gearbox, and the generator, shown in Figure 2.13. The gearbox and generator frames are grounded separately via a dedicated ground cable originating in the basement, as illustrated in Figure 2.8, denoted by purple insulation and green ground cable details.

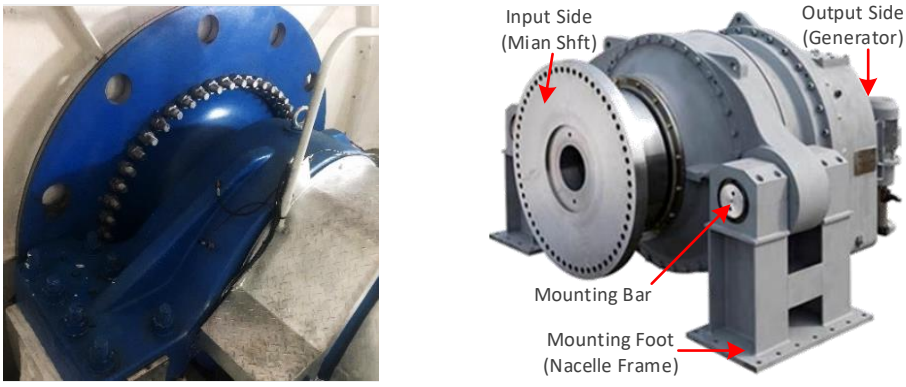

Figure 2.12 Typical wind turbine main bearing house and gearbox.

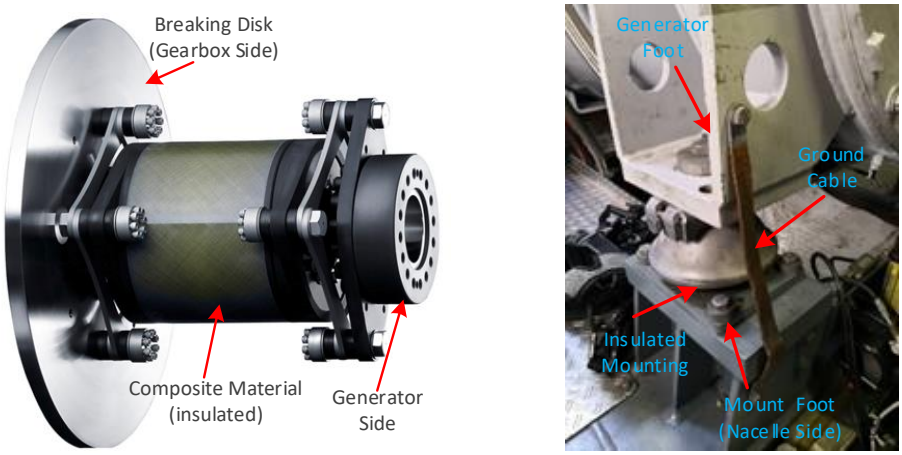

Figure 2.13 Typical wind turbine generator coupling and ground connection.

- **Main converter and transformer ground:** The main converter and transformer are normally situated in the basement, are grounded via the ground cables.

2.5.2 Gearless wind turbine configuration

The development of gearless wind turbines, predominantly used in Variable-Speed Wind Turbines (VSWT), has emerged over the past few decades. The core structure of geared wind turbines is illustrated in Figure 2.5 and Figure 2.6. Their streamlined design integrates the generator's rotor with the wind turbine's rotor, coupling the generator's bearing current path.

As outlined in section2.3, gearless wind turbines are categorized into separate bearing, integrated inner rotor, and integrated outer rotor configurations. While most subsystems remain consistent across different types of gearless wind turbines, there are variances within the generator part.

In the separate bearing gearless configuration, the arrangement differs substantially from the integrated design, yet it bears some resemblance to geared wind turbines. Figure 2.14 illustrates the configuration of a separate bearing gearless wind turbine. The primary distinction lies in the absence of a gearbox, with the main shaft directly connected to the generator shaft, establishing a direct electrical path between the generator and the main bearing.

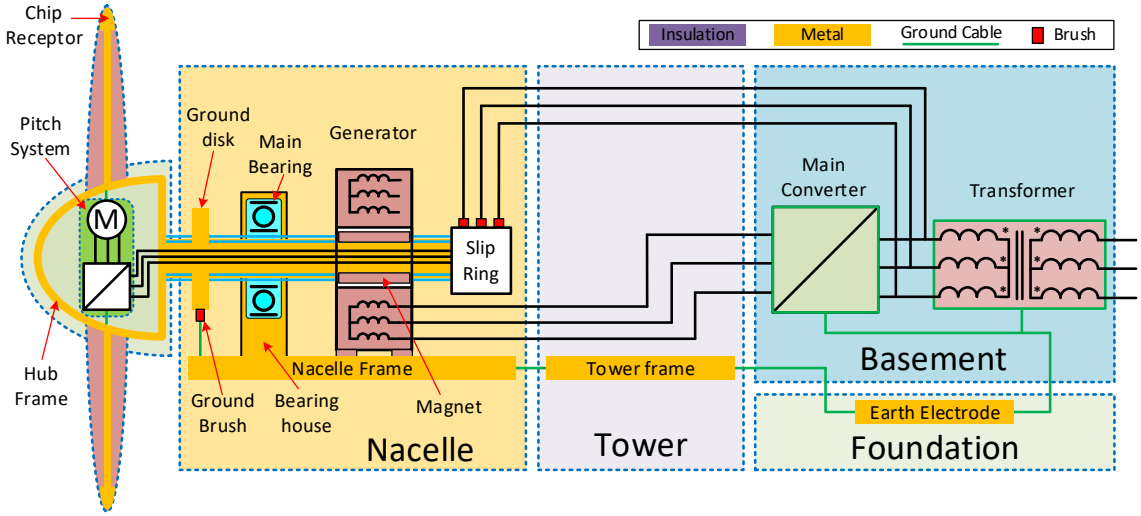

Figure 2.14: Gearless separate bearing wind turbine electrical configuration.

In the integrated gearless wind turbine classification, the main bearings are integrated within the main rotor. Simplified configurations for inner rotor and outer rotor gearless wind turbines are depicted in Figure 2.15 and Figure 2.16, respectively.

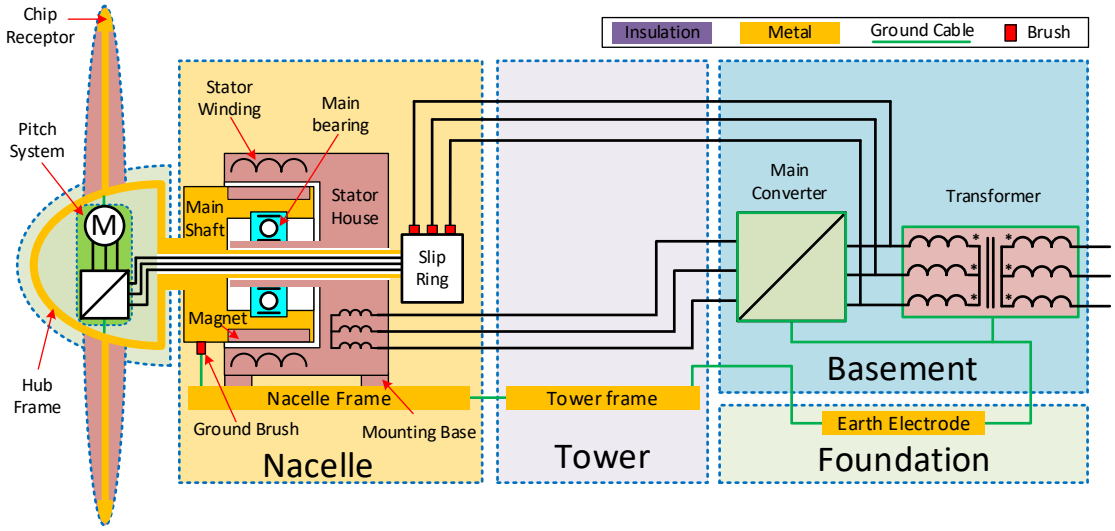

Figure 2.15: Gearless rotor wind turbine electrical configuration.

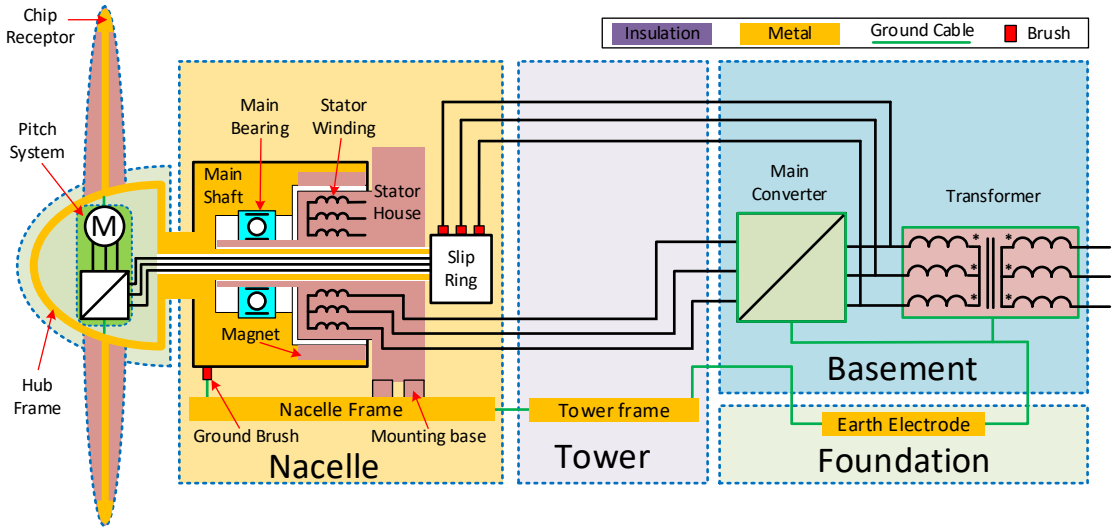

Figure 2.16: Gearless outer rotor wind turbine electrical configuration.

Subsystems in gearless wind turbine configuration

Most subsystems in gearless wind turbines align with their counterparts in geared wind turbines, as introduced in session 2.5.1. Due to the direct drive configuration, there are slight variations in interface and connections.

Power Generation System: In gearless wind turbines, the gearbox is omitted, and the generator connects mechanically to the hub. Consequently, the generator's size surpasses that of geared wind turbines. Electrical power generated by the generator is transmitted to the basement through a cable bundle with length of 50-150 meters running along the tower.

Suspension System: The suspension system may feature either a single main bearing or double bearings, contingent upon wind turbine size. The inner race of the bearing is supported by a hollow shaft, with its outer race rotating concurrently with the main shaft.

Lightning Protection System: The lightning protection system in gearless wind turbines mirrors that in geared wind turbines. The blades and hub channel lightning to the ground via the main shaft and ground brush, connected to the hub frame by a cable.

Pitch System: The pitch system within the hub remains similar to geared wind turbines. However, the power cable traverses the main shaft in gearless wind turbines, while in gearless wind turbines, a cable bundle passes through the entire generator via a hollow shaft. A slip ring on the rear of the generator feeds power to this cable bundle.

Grounding System: Grounding components follow a comparable approach to geared wind turbines, as discussed in session 2.5.1. The primary difference pertains to generator grounding. Due to its larger size, gearless generators often weigh several dozen tons. To ensure stability, generators are typically directly connected to the nacelle frame, creating an electrical pathway for grounding. Refer to Figure 2.14, Figure 2.15, and Figure 2.16 for further details.

2.6 Comparison between different configurations

All configurations of various wind turbine types were introduced in session 2.5. Irrespective of wind turbine type, main bearings are consistently located in the nacelle and connected to the hub and blades via the main shaft. Consequently, the hub, basement, and tower arrangements remain consistent across all configurations, with primary variations residing in the nacelle.

In both geared wind turbines and separate bearing gearless wind turbines, the configurations exhibit similarities. The key distinctions primarily involve the gearbox, main shaft connection, and the generator.

In integrated gearless wind turbines, the main bearing is integrated within the generator. Excluding the hub-side connection, the nacelle contains only a generator, and the main shaft bearing also functions as the generator bearing. Consequently, studying bearing current in integrated gearless wind turbines mirrors the study of bearing current in electrical machines. Bearing current in electrical machines has been extensively investigated, with most mechanisms well-understood. This aspect of the study is introduced in section 1.3.

The study of integrated gearless wind turbine main bearing current extends to its impact on the hub-side connection and, subsequently, on main shaft bearing current. Hub-side connections for different wind turbine types are uniform, allowing this portion of the study to be incorporated into the broader examination of gearless wind turbine main bearing current.

2.7 Summary

In summary, this classification categorizes different wind turbines into two main types: geared and gearless. Geared wind turbines normally feature a separate gearbox and main shaft bearing, while gearless wind turbines integrate the generator with the main bearing. Despite these differences, all configurations share common subsystems such as power generation, suspension, lightning protection, pitch control, and grounding. This classification helps streamline the study of bearing currents in wind turbines, allowing for

more focused research into their electrical systems and current paths, as can be seen in the following chapters.

Chapter 3. Sources and transmission paths of main shaft bearing currents.

3.1 Wind turbine main shaft bearing current paths.

Bearing currents in electrical machines have been extensively studied over the years, with well-defined patterns, mechanisms, and transmission paths. However, the emergence of bearing currents in wind turbine main shafts presents a novel challenge. Limited research has been conducted in this domain, necessitating further exploration into the origins, mechanisms, and transmission paths specific to wind turbine main shaft bearing currents.

The complexity of wind turbine system configurations, involving numerous subsystems and components, distinguishes main shaft bearing currents in wind turbines from those in traditional electrical machines. Consequently, main shaft bearing patterns and mechanisms deviate significantly from their electrical machine counterparts, giving rise to new patterns of bearing currents. In this section, an analytical discussion and simulation are employed to investigate potential sources of main shaft bearing currents based on the configuration outlined in Section 2.1.

3.1.1 Main shaft bearing current paths.

Bearing current, characterized by a flow through the bearing, is driven by a voltage potential between the inner and outer races. In wind turbines, the main shaft's inner race connects to the main shaft, while the outer race links to the bearing house mounted on the nacelle frame. Consequently, a voltage potential exists between the main shaft and the nacelle frame upon bearing current occurrence. The nacelle frame is grounded through the tower frame and a separate ground cable connected to the earth electrode in the ground.

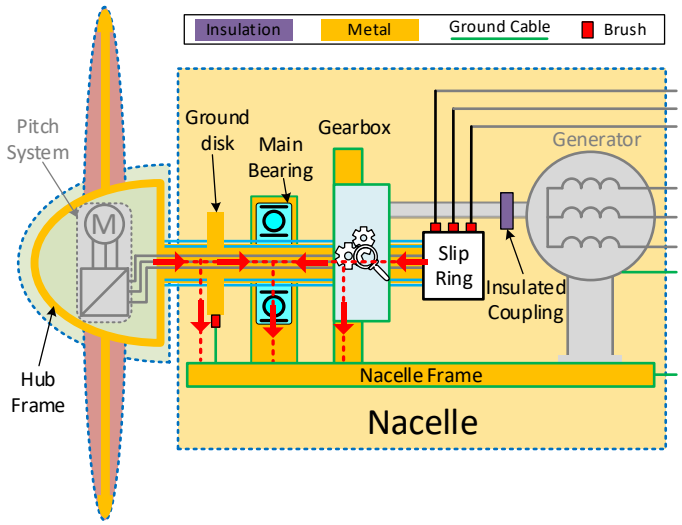

Figure 3.1: Geared wind turbine main shaft bearing current circulation path indication.

The geared wind turbine configuration, shown in Figure 3.1, highlights the main shaft's mechanical and electrical connections to various components such as the hub frame, ground disk, main bearing, gearbox, and slip ring. Voltage potential on the main shaft originates and dissipates through its electrical connections.

The gearbox, a critical component, are illustrated in Figure 3.2 for two typical gearboxes that commonly employed in the wind turbines, I e. parallel shaft and planetary gearboxes. It can be simplistically viewed as a shaft and bearing in series connected to the nacelle frame. Moreover, the slip ring, mounted on the main shaft, facilitates power transfer to rotating subsystems in the hub, constituting an electrical link. Figure 3.3 illustrates a typical slip ring used in wind turbines, featuring metal brushes, conductive channels, and support frames.

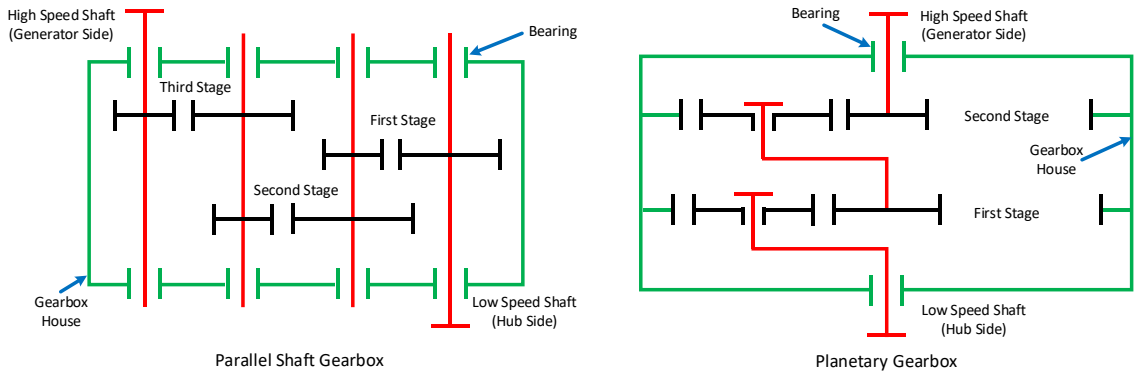

Figure 3.2: Typical wind turbine gearbox structure

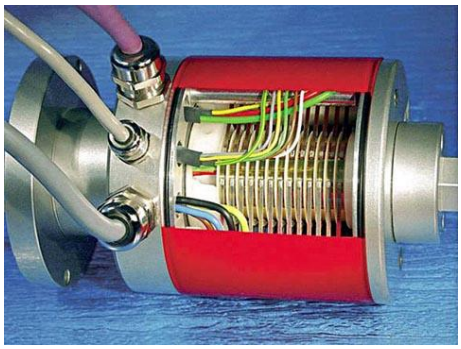

Figure 3.3: Typical slip ring applied in wind turbine.

Within the hub, electrical power from the slip ring, grounded via the main shaft, necessitates a study of the main shaft voltage potential sources. Components such as the main bearing, ground disk, and gearbox contribute to parallel grounding paths for the main shaft voltage potential.

Figure 3.4: Typical ground brush and wind turbine main bearing.

Among these paths, the route crossing the main bearing becomes a critical factor triggering bearing current issues. Significantly, the main bearing's larger size, when compared to the ground brush and ground disk, reduces its impedance, and increases effective interface contact area. Both are shown in Figure 3.4. This size discrepancy significantly influences bearing current patterns. The ground brush, typically made of carbon or alloy, has dimensions of approximately 3cm×5cm, enforced to adhere to the ground disk by a spring. In contrast, the ground disk, affixed to the main shaft, is a steel disk with a width of 3-5cm and a diameter ranging from 1-1.5m. Comparatively, main bearings, elaborated in session 2.4, typically exhibit dimensions around a diameter of 1 meter and a width of 20cm. The main bearing's effective interface contact area is at least ten times larger than that between the ground brush and the ground disk. Furthermore, the impedance ratio across these components ranges more than tenfold, highlighting the need for empirical test data to substantiate these assertions.

The pathway through the main bearing emerges as a focal point for bearing current issues. The pronounced size of the main bearing, in relation to the ground brush and ground disk, accentuates its impedance and effective interface contact area, exerting a substantial influence on bearing current patterns.

3.1.2 Cable Crosstalk in wind turbine and its impact

Crosstalk among adjacent cables plays a significant role in current transmission in wind turbines, presenting a notable coupling path. It is distinguished into conducted mode, inductive mode and radiated mode. Unlike radiated mode, which results from induction without physical contact between conductors, conducted mode arises from the direct physical contact of the conductors.

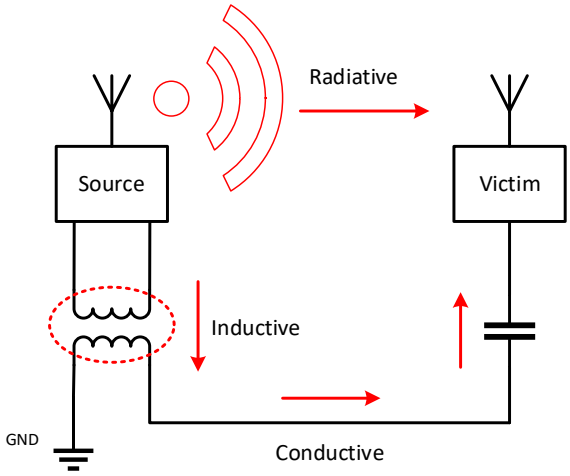

Figure 3.5: Different coupling modes in cabling system.

Figure 3.5 provides a general schematic illustrating various coupling modes, depicting the relationship between noise sources, coupling paths, and victims or receptors. In wind turbines, the cables themselves serve as both sources and victims, acting as perfect antennas capable of sending and receiving signals. The strength of the coupling factor is directly related to cable length and adjacent distances, with longer and closer cables exhibiting stronger coupling effects.

As shown in Figure 3.6, cable bundles responsible for supplying power to different subsystems are situated within the tower. Cables connecting the basement to the tower are as tall as the tower itself. With typical wind turbines rated at 2MW reaching heights of about 80m, and newer 5MW turbines towering at 140m, the length of these cables presents opportunities for both radiative and inductive coupling. And if there is damage on the cables, the conductive mode coupling dominate the transmission.

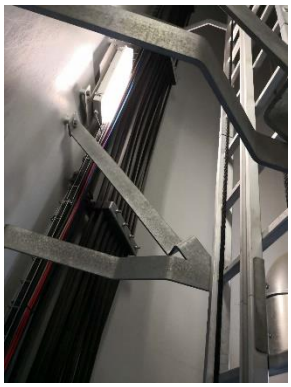

Figure 3.6: Cable bundle inside wind tower.

3.1.3 Shaft magnetization

In this section, we introduced a set of power cables passing through the hollow shaft in wind turbines. These cables facilitate the transmission of both differential mode and common mode currents. While the differential mode voltage forms a closed loop within the cables, the common mode voltage induces an offset voltage and causing current flow along the cables.

As per Maxwell's law, this offset current generates a magnetic field surrounding the cable. As depicted in Figure 3.7, due to practical installation constraints, the cable cannot be perfectly centered in the hollow shaft. Consequently, the offset common mode current carries the potential to magnetize the steel shaft. The rotation of the rotor, in turn, generates a floating voltage potential on the magnetized shaft.

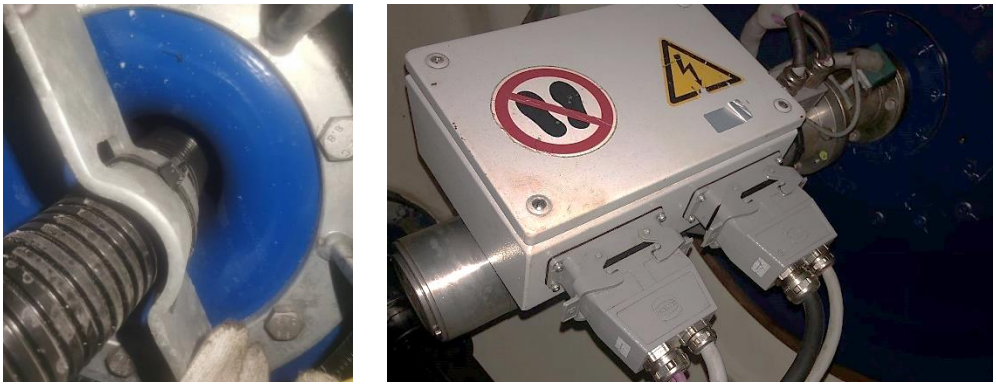

Figure 3.7: Hub power cable through hollow shaft hub side view and nacelle side view with the slipring connection box.

The floating potential on the main shaft attempts to find its path to the ground. As discussed in Section 3.1.1, the ground brush, main bearing, and gearbox serve as primary pathways for the shaft's potential. The intricate details of shaft magnetization and its conductive paths

are shown in Figure 3.8. The magnetization-built shaft voltage is conducted to the ground via the main bearing, the gearbox bearing and the shaft brush.

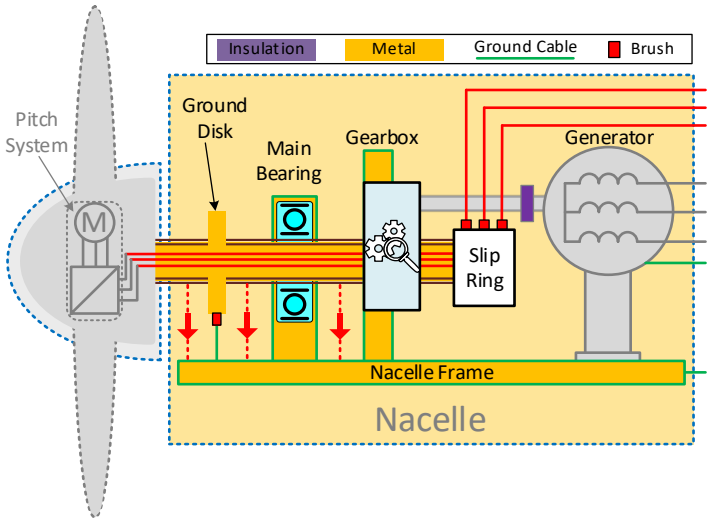

Figure 3.8: Shaft magnetization impact on main shaft bearing current indication.

3.1.3.1 Finite Element Method (FEM) simulation model

Given that the rotor's rotational speed typically ranges from 10 to 30 revolutions per minute (rpm) in a wind turbine, the amplitude of voltage potential induced by shaft magnetization is relatively low. Due to the presence of electromagnetic noise within the wind turbine, detecting the shaft magnetization phenomenon poses challenges. To delve into the effect of shaft magnetization on the main shaft, the Finite Element Method (FEM) is employed for simulation.

An FEM model is constructed, incorporating a group of cables carrying both Differential Mode Voltage (DMV) and Common Mode Voltage (CMV) within a rotating steel hollow shaft. The shaft and the cables are set to rotate at 30 rpm, representing the typical operating speed of a 1MW wind turbine rotor. Key parameters for the simulation are outlined in Table 3.1.

Table 3.1 shaft magnetization simulation parameters.

Shaft length	2 m	Cable diameter	30mm
Shaft out diameter	50 cm	Cable length	2m
Shaft thickness	10 cm	Common mode current	15 A 2.5k Hz
Rotation speed	30 rpm	Differential mode current	50 A 50 Hz

At the excitation side, the cables are fed with a 50A differential mode current (typical 50Hz grid current) and a 15A common mode current (typical switching frequency of the converter at 2.5 kHz). For clarity in results, the amplitude of the common mode current is intentionally set higher than that in a real wind turbine system.

To measure the voltage on the shaft, a 0.1mm diameter bare copper wire cable is placed adjacent to the shaft as a sensor. The sensor cable, situated as close as 0.1mm to the shaft, is stationary in the simulation model, as illustrated in Figure 3.9.

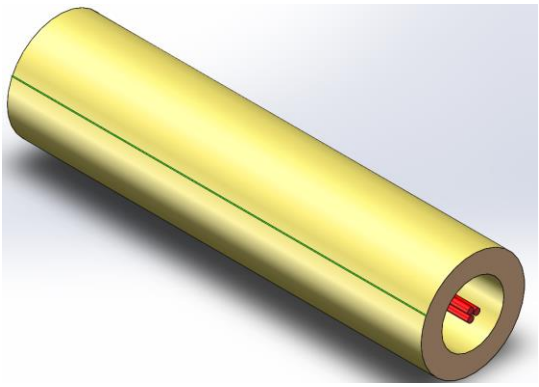

Figure 3.9: Simulation model indication.

3.1.3.2 FEM simulation result

The simulation explores various cable positions, with the concentric and most eccentric cases proving to be the most impactful. The corresponding results are depicted in Figure 3.10 (a) and (b).

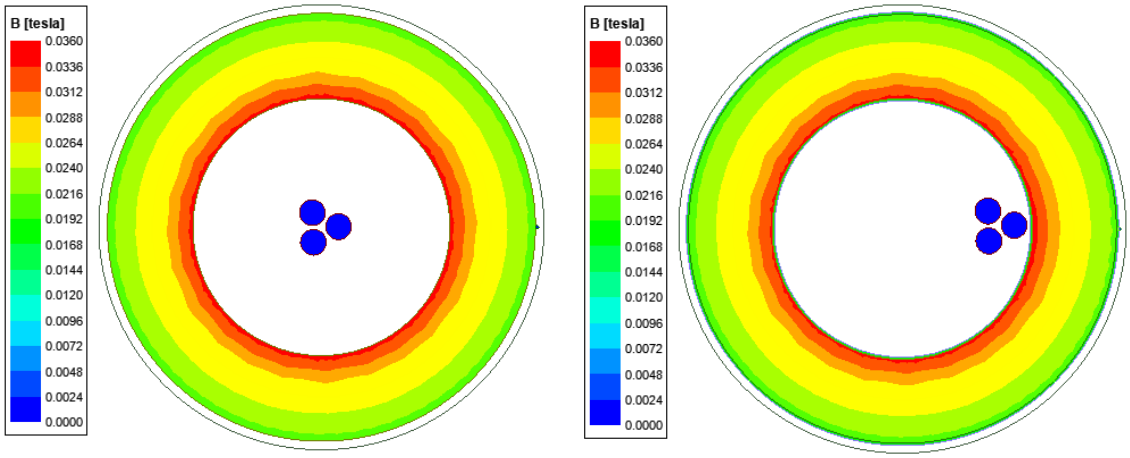

a) Cable in the shaft central b) Cable in the shaft side

Figure 3.10: Shaft magnetization color map at different cable position.

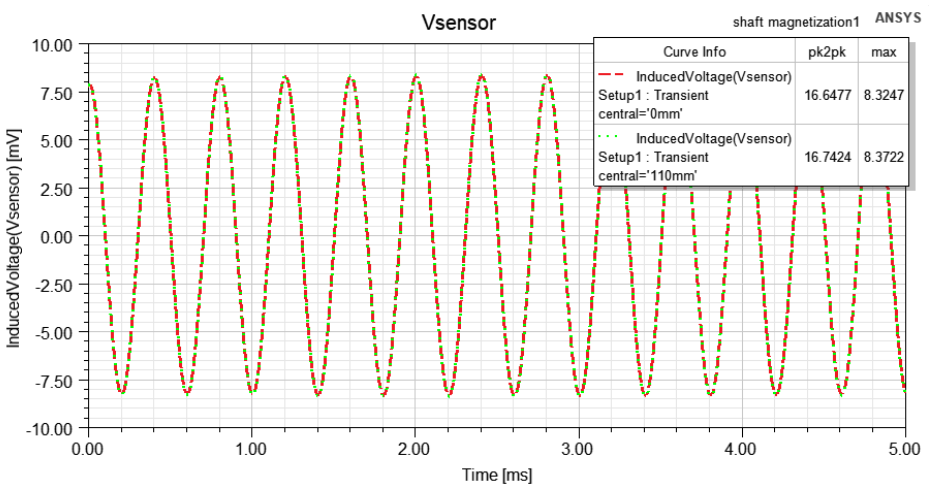

Figure 3.11: Shaft magnetization impatient on main bearing current indication.

From the simulation result in Figure 3.10, the magnetic field cloud maps under different positions of the cable bundle are similar. From the numerical result of the sensor cable in Figure 3.11, the induced voltage under the decentered cable position (green dash curve) is slightly higher than the case of centralized cable position (red dash curve). However, their absolute value is almost the same and the peak value is neglectable. From the simulation results, it can be concluded that the current in cable bundles has no significant impact on shaft magnetization.

3.2 Geared wind turbine main shaft current sources

As outlined in Section 3.1.1, the primary sources of voltage potential on the main shaft in geared wind turbines emanate from the hub side and the slip ring side. On each side, various subsystems contribute to the generation of this potential. Notably, the blades and pitch system on the hub side, along with the power cable passing through the hollow shaft on the slip ring side, are the principal contributors.

Different mechanisms drive voltage potential generation in these subsystems, occurring through various coupling paths. This section explores distinct mechanisms and their associated coupling paths in these subsystems.

3.2.1 Electrostatic discharge (ESD)

Wind, a product of air movement due to temperature variations, carries particles like dust and water droplets. As wind particles collide, microscopic exchanges of electrons occur, generating free charges that accumulate in the atmosphere. This phenomenon contributes to atmospheric events such as thunderstorms and lightning.

In wind turbines, blades can become electrically charged through triboelectric charging when wind interacts with them. Different materials exhibit varying electron affinities, with air likely to release electrons and polymers, such as epoxy and PTFE, having the ability to attract electrons and become negatively charged.

Figure 3.12 shows materials of different electron affinity.

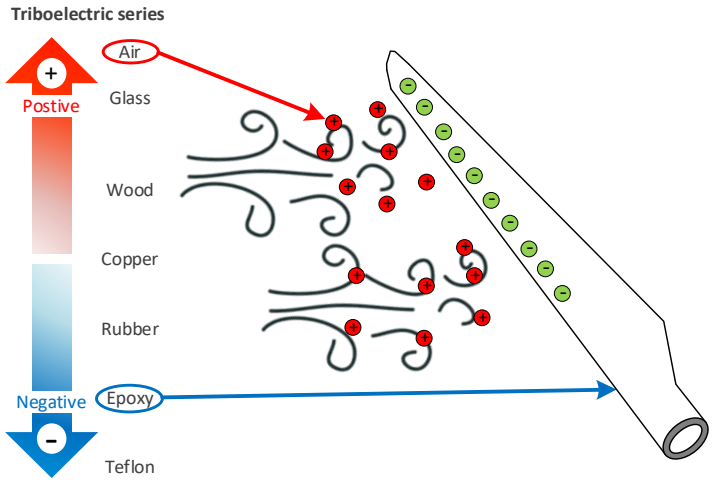

Figure 3.12: Wind blowing over a wind turbine blade.

To mitigate triboelectric effects in engineering applications, static dischargers are employed. In aircraft, for instance, needle-shaped dischargers on wings provide discharge points to dissipate accumulated charges through corona discharges, as depicted in Figure 3.13. Whereas the accumulated charge on wind turbine blades' polymeric dielectric surfaces creates an electric potential that seeks a path to the ground for charge dissipation.

Figure 3.13: Dischargers installed on airplane wings.

3.2.2 Cloud induced current flow.

Clouds in the atmosphere carry charges, and the accumulated charges create an electric field around the cloud. While this field may not be strong enough to induce lightning, it can cause charge imbalances in objects close to the cloud. As illustrated in Figure 3.14, the electric field around the lower cloud repels electrons on wind turbine blades, leading to charge imbalances and the creation of a charge movement, a current, inside the wind turbine.

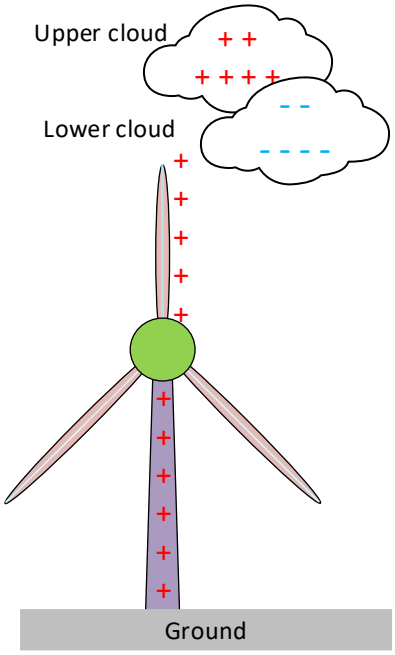

Figure 3.14: Cloud induced charges current path in wind turbine.

3.2.3 Common mode voltage (CMV)

Common mode voltage is active in both input terminals of an electrical system. Unlike differential mode voltage, where current flows forward and back without grounding, common mode voltage seeks paths to the system ground as shown in Figure 3.15 a. In wind turbine drive systems, the generation mechanism and pattern of common mode voltage are explored.

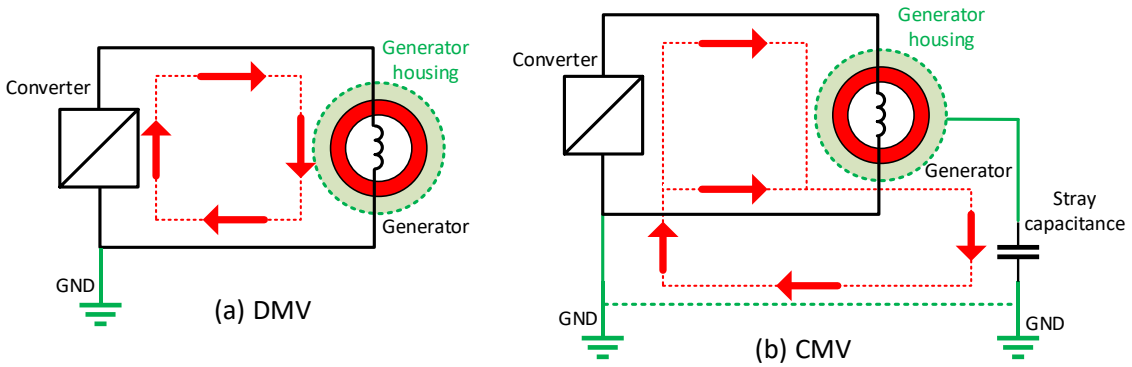

Figure 3.15: Circulation pattern of DMV and CMV.

Different from the differential mode circuit loop, the common mode circuit has a flowing direction in both converter transmission terminal lines, closing the loop via the ground. The common mode voltage pattern involves the converter-originated CMV conducted to the neutral point of motor windings. The windings' neutral point, usually floating to the ground, contains a high-frequency AC voltage, coupling to the ground via the insulation layer's capacitor. This creates a loop to the ground, as shown in Figure 3.15 b.

In wind turbines, various drive systems in different subsystems have the potential to produce CMV. The converters of electrical machines, particularly PWM-driven converters, contribute significantly. Figure 3.16 illustrates the configuration of a typical converter-driven electrical machine via a cable bundle.

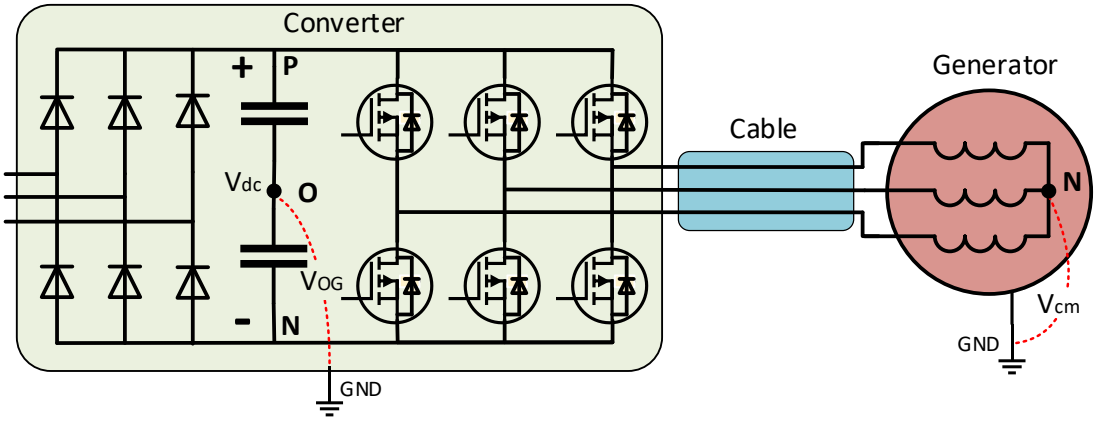

Figure 3.16: Converter-driven electrical machine configuration.

In the configuration, the power electronic side consists of a rectifying circuit and an inverting circuit. In between them is the DC bus which is a capacitor or a group of capacitors. On the inverting circuit side, the middle point of the capacitor (point O) is usually taken as the reference zero for the output phase voltage. The neural voltage of the

winding V_{NO} can be calculated by Equation 3-1. Where U_{AO}, U_{BO}, *and* U_{CO} are the output phase voltages of the inverter circuit.

$$V_{NO} = \frac{U_{AO}+U_{BO}+U_{CO}}{3} \tag{3-1}$$

The common mode voltage of the electrical machine is the voltage potential of the winding neural to the ground. It is the sum of each phase's phase-to-ground voltage potential. Further derivation is shown in Equation 3-2.

$$\begin{aligned} V_{cm} &= \frac{U_{AG}+U_{BG}+U_{CG}}{3} \\ &= \frac{(U_{AO}+V_{OG})+(U_{BO}+V_{OG})+(U_{CO}+V_{OG})}{3} \\ &= \frac{U_{AO}+U_{BO}+U_{CO}}{3}+V_{OG} \end{aligned} \tag{3-2}$$

V_{OG} is the voltage between the inverter reference zero and ground. From the derivation in Equation 3-2 and 3-3, the CMV can be separated into two parts, the inverter side voltage phase to neural voltage V_{NO} and the rectifier side zero to ground voltage V_{OG}.

$$V_{cm} = V_{NO} + V_{OG} \tag{3-3}$$

On the inverter side, the output of phase voltage is achieved by switching each arm alternately. Here, in each arm we mark the upper switch open as "1" and the lower switch close as "0". Thus, there are 2^3 combinations of the switch state in total. These states can be coded under binary (000) to (111), marked as S_0 to S_7. Among them, S_0 and S_7 are not effective output states. In these states, all the DC link voltage V_{dc} is applied to the winding neutral. In the other state, the voltage is fed to the winding via one phase and returns via the other two phases in parallel. The winding neutral to zero voltage V_{NO} can be concluded in Equation 3-4.

$$V_{NO} = \frac{U_{AO}+U_{BO}+U_{CO}}{3} = \begin{cases} \pm\frac{V_{dc}}{2},\ S_0\ \&\ S_7 \\ \pm\frac{V_{dc}}{6},\ S_1 \sim S_6 \end{cases} \tag{3-4}$$

From the equation, it is obvious that the winding to zero voltage is a step waveform instead of a smooth curve. The typical waveform of the three-phase neutral to zero voltage is shown in Figure 3.17.

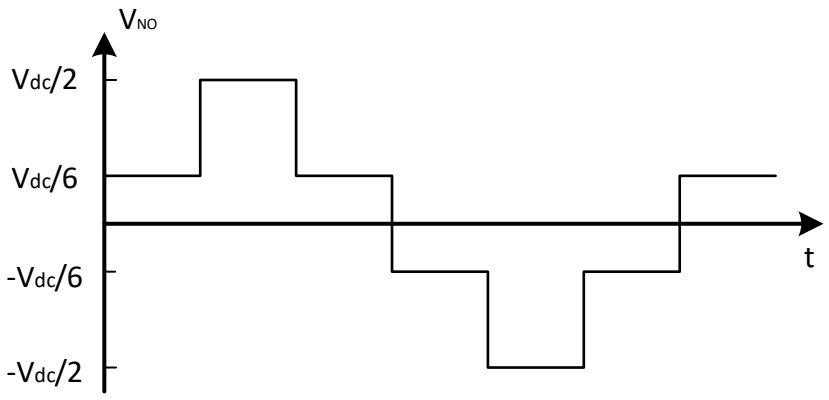

Figure 3.17: Typical PWM-driven inverter output neural to zero-point voltage.

In typical three phase 2 level inverter, SPWM modulation is the wildly used. According to reference[24-26], the phase output voltage can be expanded by Fourier series. Thus, the winding neutral to zero voltage V_{NO} can be derivatized in Equation 3-5.

$$V_{NO} = \frac{U_{AO}+U_{BO}+U_{CO}}{3} \tag{3-5}$$

$$= \frac{V_{dc}}{2} + \frac{2V_{dc}}{\pi} \sum_{m=2k-1}^{\infty} (-1)^{\frac{m-1}{2}} \cdot \frac{1}{m} \cdot J_0\left(m\frac{\pi}{2}M\right) \cos(n\omega_c t)$$

$$+ \frac{2V_{dc}}{\pi} \sum_{m=2k-1}^{\infty} \sum_{n=6l}^{\infty} \cdot \frac{1}{m} \cdot J_n\left(m\frac{\pi}{2}M\right) \sin\left[(m+n)\frac{\pi}{2}\right] \cos[(m\omega_c \pm n\omega_r)t]$$

$$+ \frac{2V_{dc}}{\pi} \sum_{m=2k}^{\infty} \sum_{n=6l-3}^{\infty} \cdot \frac{1}{m} \cdot J_n\left(m\frac{\pi}{2}M\right) \sin\left[(m+n)\frac{\pi}{2}\right] \cos[(m\omega_c \pm n\omega_r)t]$$

Where *k* and *l* are integer numbers, *M* is the modulation index, w_c is the carrier frequency (switching frequency), w_r is the modulating single frequency (usually 50Hz in grid inverters). From the equation, the inverter side common mode voltage V_{NO} shows several characteristics:

a) There is no fundamental frequency component.

b) The carrier frequency harmonics only exist at the odd order of the carrier w_c, with symmetrically attenuated sideband harmonic clusters on both sides. Around the

even carrier harmonic frequency, there is no carrier harmonic but there are also symmetrically attenuated sideband harmonic clusters on both sides.

On the rectifier side, the DC link voltage is the output of the rectifier. The zero-point O is the middle point of the DC link output between point P and point N. The second part of the common mode voltage V_{OG} is the zero point to the ground of the rectifier (the same ground as the converter). The rectifier side common mode voltage can be calculated via Equation 3-6, where U_{PG} *and* U_{NG} are the positive and negative terminals of the DC link.

$$V_{OG} = \frac{U_{PG}+U_{NG}}{2} \tag{3-6}$$

U_{PG} *and* U_{NG} contain the DC component $+V_{dc}/2$ and $-V_{dc}/2$ respectively, and the high-frequency ripple is superimposed on the DC component. This ripple shows a fundamental frequency of 150Hz and its odd-order harmonics.

Traditional electrical machine-driven loads, powered by balanced 3-phase sinusoidal voltage, have no CMV. However, with the advent of power electronics and PWM technology, which enables speed adjustment, the CMV of the converter output voltage is no longer zero due to the presence of switches, as demonstrated in Figure 3.17[27].

In wind turbine subsystems, pitch converters and main converters, both PWM-driven, generate CMV on pitch motors and main generators. This CMV is conducted to the ground via the main shaft and main bearing. Moreover, transmission cables connecting converters and electrical machines carry CMV, potentially coupling to the ground via bearings and other signal cables.

In some wind turbine systems, a CMV filter is adopted at the output side of the converter. And also in some converters, some control strategy that can eliminate the convert output CMV are applied to reduce the CMV in the system. Wind turbine main shaft bearing current transmission paths

In the previous section 3.2, we discussed the existing patterns of voltage potentials. However, the transmission or coupling path of these potentials to the main shaft remained unclear. This section aims to address the transmission paths of these potentials to the main shaft.

3.2.4 Electrostatic discharge (ESD) and lightning transmission path

The accumulated charge on the wind turbine blades' polymeric dielectric surfaces creates an electric potential that seeks a path to ground for dissipating the accumulated charge. A typical wind turbine blade structure is illustrated in Figure 3.18, comprising various layers,

including the blade frame, filling material, lightning protection components, and surface coating. The lightning protection system, consisting of receptors and a copper net [28], provides a path to ground and is crucial for discharging accumulated charges.

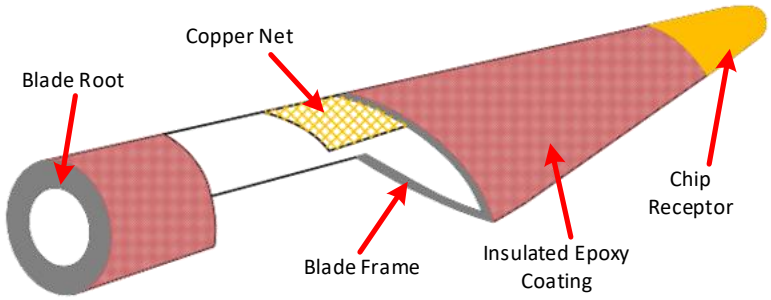

Figure 3.18: Wind turbine blade structure diagram.

At the wind turbine level, accumulated charges on the blades discharge to the lightning protection system, conducting to the ground and resulting in a current flow. In the lightning protection system, the blades are electrically connected to the hub frame and main shaft. The main shaft, fitted with a carbon brush, conducts charges to the nacelle frame and subsequently to the grounding system via the tower frame. However, charges may take different paths from the main shaft to the nacelle frame, including the main bearing and gearbox (geared turbine) or generator (gearless turbine), as indicated by dashed red lines in Figure 3.19. Continuous current flow through the bearing can prematurely age lubrication grease and damage races.

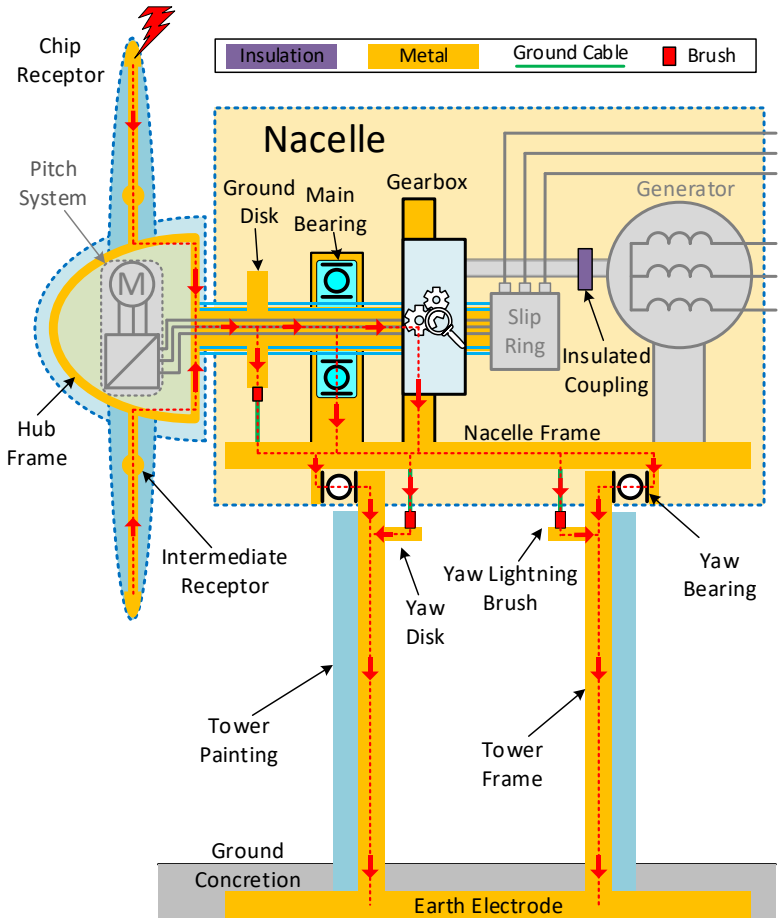

Figure 3.19: A typical wind turbine lightning protection system.

3.2.5 CMV transmission path

In comparison to the ESD effect, CMV is distributed across different subsystems and locations in wind turbines, making their transmission/coupling paths more complex. This section discusses CMV's transmission/coupling paths in different subsystems.

Pitch converter CMV transmission path

The pitch system in a wind turbine, as shown in Figure 2.10 in session 2.5, comprises a pitch converter, pitch motor, and mechanical action devices. Placed in the limited space in the hub, the pitch converter is the CMV source, and the short cable bundle conducts the CMV to the pitch motor winding. The pitch motor then conducts the CMV to the hub frame via the stray capacitance between the motor frame and windings. The hub frame, made of steel and electrically grounded to the main shaft, offers a path for the CMV to the main shaft, as indicated by the red arrow in Figure 3.20.

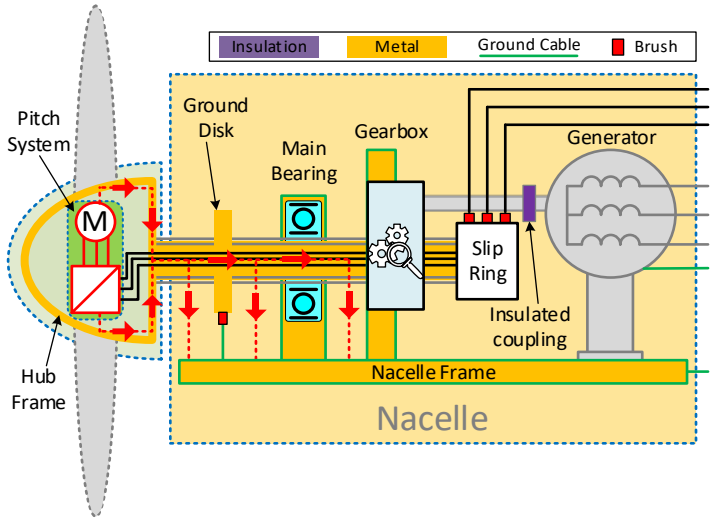

Figure 3.20: Pitch converter CMV main bearing current indication.

Main converter CMV transmission path

Similar to the pitch converter CMV transmission path, CMV originated from the main converter conducts to the generator winding. The generator distributes the CMV through two paths: one to the generator frame and then to the nacelle frame, and the other to the output shaft. The distribution circuit is shown in Figure 3.21. In both loops, the main shaft is not directly involved, indicating that the main CMV has no direct contribution to the shaft voltage potential. The distributed arrangement of the main power generation system, especially in geared wind turbines, introduces complexity in the CMV transmission path. The main converter, located at the basement, connects to the generator in the nacelle via long cables, creating the potential coupled by the inductive path between different group cable bundles.

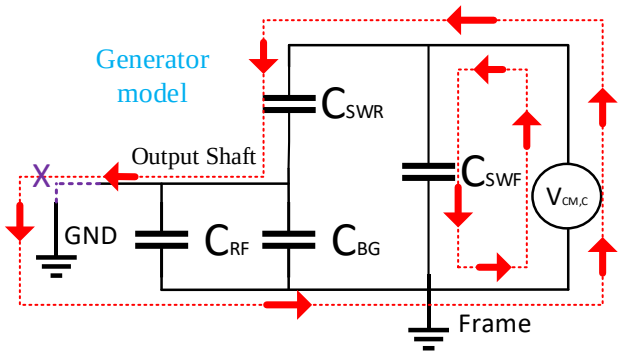

Figure 3.21: CMV distribution inside generator.

$V_{CM,C}$ -- conductive CMV source

C_{SWF} -- the capacitor between stator winding and frame

C_{SWR} -- the capacitor between stator winding and generator rotor

C_{BG} -- the capacitor of generator bearings

C_{RF} -- the capacitor between the generator rotor and frame

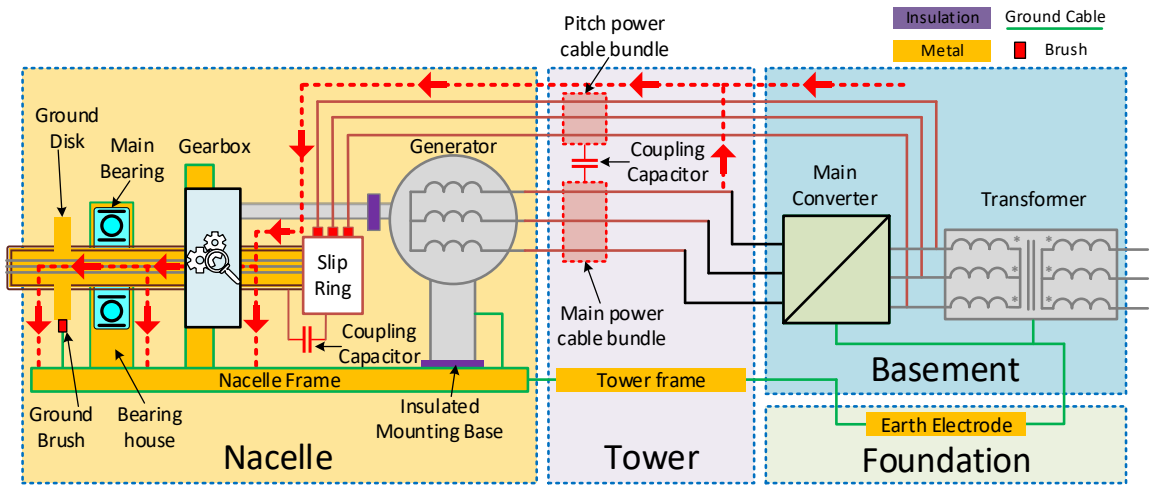

Figure 3.22: Main converter EMI impact on main bearing current indication.

As shown in Figure 3.6, different cable bundles, including main power transmission cables and pitch power feeding cables, are arranged together, leading to crosstalk effects. This crosstalk effect builds a path for CMV transmission from the main power cable bundle and the pitch power cable bundle, as depicted in Figure 3.22.

The pitch power cable bundle feeds power to the pitch system in the hub, conducting power from the stationary part to the rotation part via the slip ring. The slip ring's structure, shown in Figure 3.23, involves components like the stator flange, brush, stator house, rotation part, and bearings. Stray capacitors formed by steel shaft, conduct channels, and insulation materials directly connect channels to the shaft, allowing induced CMV to couple to the main shaft.

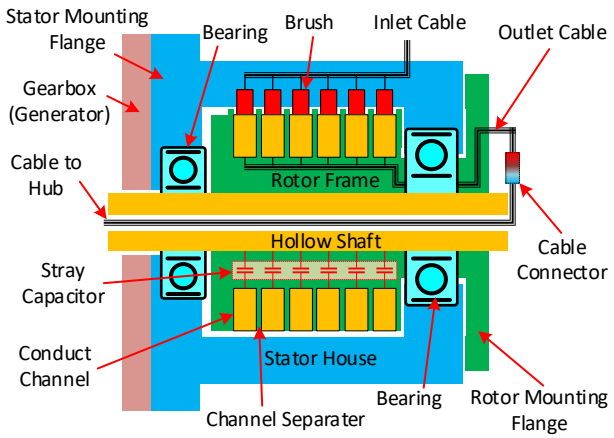

Figure 3.23: Structure of typical slip ring.

As shown in Figure 3.23, the stator house (blue part) and the rotor frame (green part) are made of insulated material to prevent the flashovers. However, the steel shaft, conduct channels and the insulation materials form up a group of stray capacitors. As drawn in Figure 3.23, these stray capacitors directly connect the channels and the shaft together. In this way, the induced CMV can be coupled to the main shaft.

3.3 Summary

This chapter investigates the intricacies of wind turbine main shaft bearing currents, exploring their origins and discharge paths. The unique challenges posed by these currents, distinct from traditional electrical machines, are thoroughly examined. The study highlights the diverse subsystems and components in wind turbines, stressing the importance of specialized research into main shaft bearing currents. Through analytical discussions and simulations, the chapter uncovers potential sources based on wind turbine configurations, revealing a crucial voltage potential between the main shaft and the nacelle frame. Detailed insights into geared wind turbine configurations, components like gearboxes and slip rings, cable crosstalk impact, and shaft magnetization are provided. The investigation extends to common modes like Electrostatic Discharge (ESD) and Common Mode Voltage (CMV), with a focus on transmission paths to the main shaft. The chapter concludes with a comprehensive summary, emphasizing the need for continuous research to enhance understanding and mitigation of wind turbine main shaft bearing currents.

Chapter 4. ESD impact on wind turbine bearing current lab test

4.1 Lab experiment setup

4.1.1 Electrostatic charges vs charge generation sources

Electrical charge flows around in the open air and there are always opportunities for it to attach to wind turbine blades. Due to the large size of wind turbines, the accumulated charge will generate a non-negligible electric potential on the main shaft. This electric potential tries to be neutralized to ground via a path of least resistance.

Above elaborated phenomenon needs to be verified and studied with simplified conductive paths in wind turbine, a downsized lab setup is therefore constructed. Furthermore, due to the turbine's smaller size, the charge accumulated on the lab scale wind turbine blades is not sufficient to generate a sensible current flow and damages to the main bearing. So, an external discharge source is utilized to increase the charge density in the air.

To increase the charge density, a needle panel is used to release charge to the air by means of corona discharges. As shown in Figure 4.1, the needle panel is made of a steel net with number of needles welded onto it and connected to an adjustable negative high-voltage DC source. The panel is mounted in front of an electrical fan which provides a controllable air flow across the needle panel and brings charges into a wind tunnel and increases the charge density inside.

Figure 4.1: Needle panel used to generate charges in air.

4.1.2 Simplified wind turbine configuration

The basic structure of the wind turbine's lightning protection system is introduced in Figure 3.19. In a real wind turbine, different subsystems are mounted inside the nacelle and their layout differs greatly from turbine to turbine. In this study, the main point of interest is the

current in the main shaft bearing. Therefore, in the lab setup, the wind turbine configuration should be simplified to highlight the charge-dissipating path and redundant subsystems are removed.

In a geared wind turbine, the gearbox is mechanically connected to the main shaft and to the generator via an insulated coupling. Thus, the generator has no direct electrical contact to the main shaft. The main shaft voltage is dissipated via the ground brush, main bearing and gearbox bearing.

In a gearless wind turbine, the main bearing is mounted between the main shaft and generator frame. The possible dissipation paths for the main shaft voltage are the ground brush and the main bearing.

In one of the different types of gearless turbines, the main shaft is directly connected to the generator. The configuration is similar to that of the geared wind turbine. The main shaft is grounded via the ground brush, main bearing and generator bearing.

To conclude the different transmission arrangements, the common grounding paths are the ground brush and main bearing. In this study, the main topic of interest is the impact of electrostatic discharge on the main shaft bearing. Thus, the lab setup only considers these two common paths. Figure 4.2 shows the simplified wind turbine configuration. It includes the charge generation subsystem, lightning conducting subsystem, ground brush and main bearing of the turbine suspension system.

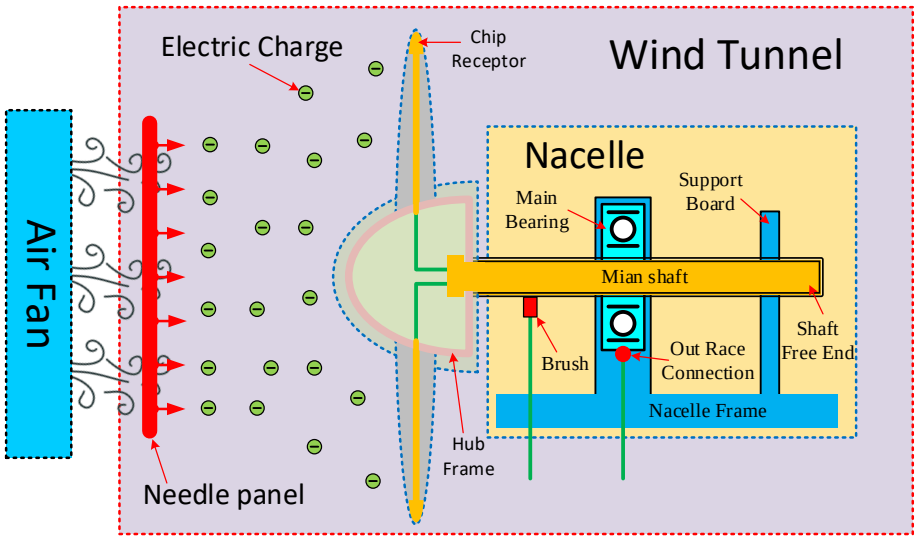

Figure 4.2: Illustration of the simplified wind turbine configuration utilized in lab study.

4.1.3 Simplified wind turbine configuration

The downsized turbine part indicated in Figure 4.2 is located inside the wind tunnel which is made of wood and plastic sheet. Its center height is around 1 m and its diameter about 75 cm. Most components in the downsized turbine are made of non-conductive plastic. This includes the rotor hub and blades, rotor suspension subsystem, lightning protection subsystem and turbine frame.

The suspension subsystem supports the turbine rotor and locks the rotor from axial movement. Its principal components are the main bearings, nacelle frame and slip ring. Its configuration is shown in Figure 4.3. The suspension consists of a two-point system whose rotor is suspended by two bearings. The main bearing inside the bearing housing is a typical cylindrical roller bearing (SKF NU204) that can only support a radial load, while the slip ring bearing inside the slip ring is a typical ball bearing that can support both radial and axial loads. The nacelle frame, bearing housing and mounting board are manufactured as a single unit. The slip ring is mounted on the mounting board, thus locking the slip ring in the axial direction. The main shaft goes through the main bearing and slip ring. At the rear end of the slip ring, the main shaft is locked together with the slip ring by screws. Thus, the rotor is locked in the axial direction by the slip ring and mounting board.

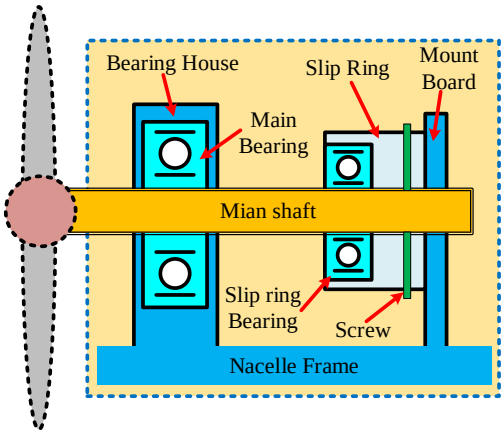

Figure 4.3: Laboratory turbine suspension system.

In the simplified setup, the lightning protection subsystem comprises coated plastic blades, plus the hub connection, main shaft and ground brush.

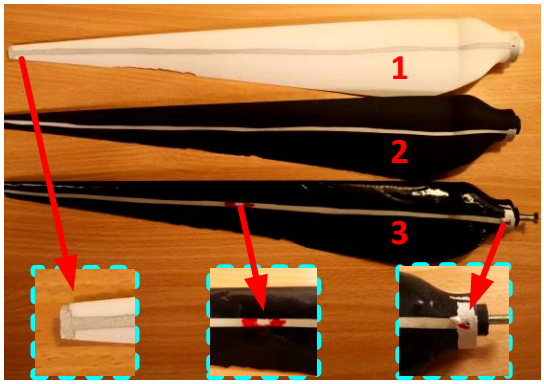

Figure 4.4: Coated wind turbine blades.

Figure 4.4 shows the coated blades. These are 3D printed in different colours of nylon. Electrically conductive silver lines are painted on both sides of the blades to provide the conductive path. Rectangular areas are painted onto the blade tips to simulate the chip receptors. A screw mounted at the root of each blade electrically connects to the silver painted lines via a copper wire. The whole surface of blade 3 in Figure 4.4 has been coated with a layer of epoxy resin, except for the tip and a pit in the middle as lightning receptors.

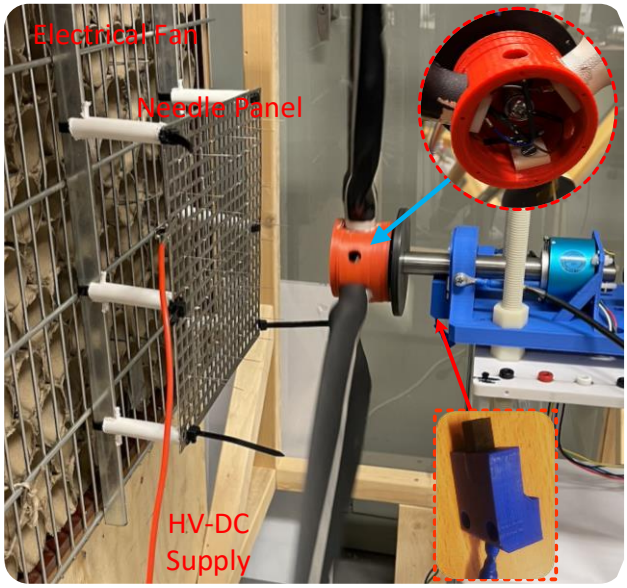

Figure 4.5: ESD impact on the main shaft bearing, test setup.

The main shaft end towards the turbine is front end and the other end is called rear end. The main shaft is a hollow steel, with the hub mounted on the output side by a nut. Inside the hub, the screws into the blade's root are electrically connected to the shaft's front end by three cables. These details also illustrated in the Figure 4.2. On the shaft's drive side (see sub-bottom figure in Figure 4.5), a carbon brush holder is mounted on the nacelle

board and the carbon brush is forced into contact with the surface of the main shaft by a spring. A conductive cable at the end of the brush connects the brush to the system's ground or test equipment.

4.2 Lab test and experiment results

To verify that the electrostatic discharge effect does impact the main shaft bearing, various groups of tests were designed for the downsized wind turbine lab system.

4.2.1 Lab test condition and bearing connection

The bearing operates in the conductive state under low-speed rotation but switches to its insulated state as the speed increases. In a wind turbine, the main bearing normally operates in its insulated state. Under lab conditions, the selected bearing uses an oil based thin lubrication in the cylindrical roller, and thus often operates in its conductive state. To keep the lab turbine main bearing working state similar to the main shaft bearing in wind turbine, grease based thicker lubrication was injected into the space between the rollers and races. The bearing with extra non-conductive grease is shown in Figure 4.6

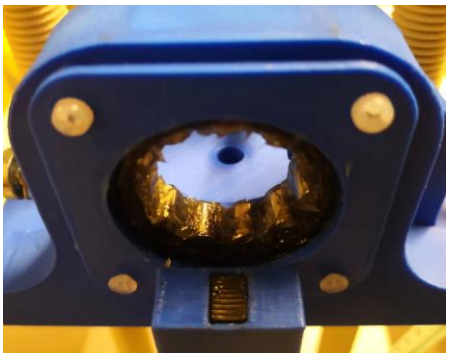

Figure 4.6: Cylindrical roller bearing (in housing) packed with extra lubrication grease.

To keep the test repeatable, a basic test condition was set for all tests in this study. On the charge generation side, the wind speed was kept at a stable value (5-6m/s) and the voltage level was adjusted to achieve different charge densities in the wind tunnel. The turbine was driven by the wind at around 80 rpm and there was no load connected to the main shaft (in other words, the generator was disconnected from the shaft). The distance between the needle panel and turbine hub was fixed at 30 cm to limit the charge travel distance.

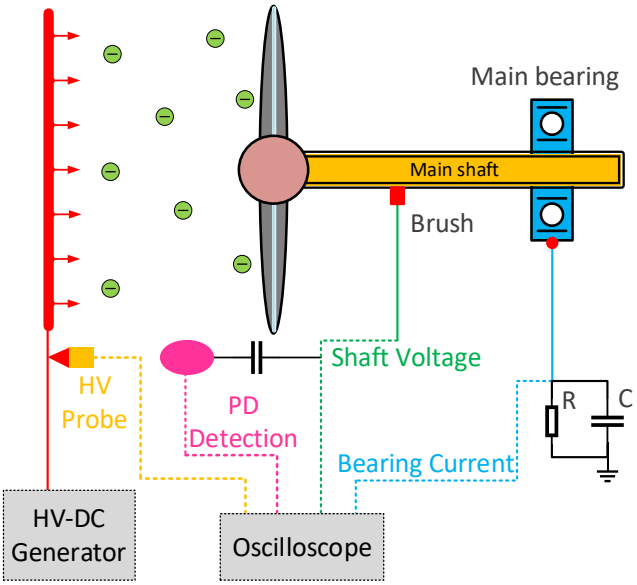

Figure 4.7: Lab test connection.

Focusing on the impact of ESD on the main bearing, the brush serves as a voltage observer (directly connected to the oscilloscope) and the main bearing's outer ring is grounded via a current shunt. Connected in this way all the current will, in principle, pass through the main bearing. Figure 4.7 shows the test connection for the setup.

Inside the bearing, the charge will accumulate at the roller and generate an unevenly distributed electric field within insulated bearing. Once the electric field strength is greater than the withstand strength of the lubrication grease at the bearing, an electric discharge will occur. A strong current will flow through grease and be conducted to ground via the outer ring and ground cable.

The discharge has an extremely high amplitude current flowing for an extremely brief period. This is usually a matter of few nanoseconds with the current amplitude being in the kiloampere range. The amplitude and bandwidth of the discharge current are usually beyond the measurement range of an oscilloscope. To capture the current, the main bearing is grounded via a parallel resistor and capacitor (RC) circuit which measures the bearing discharge current. In this RC circuit, the capacitor slows the current flow, and the shunt resistor converts the current signal into a voltage signal. As shown in Figure 4.8, the RC circuit slows the progress of the discharge current and reduces its amplitude. But the total amount of dissipating charges remains the same.

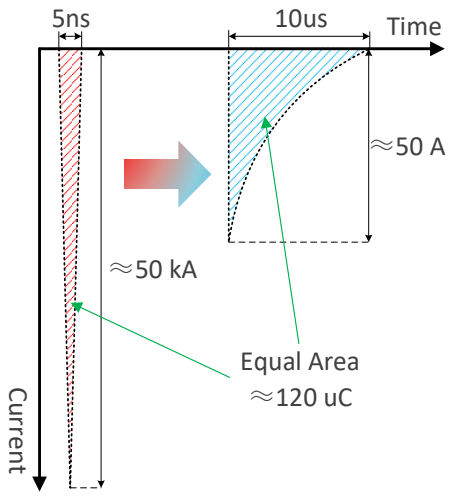

Figure 4.8: Bearing discharge current test method indication.

In the test setup, the used shunt capacitor is 100pF and the shunt resistor is 1kΩ. In the test connection shown in Figure 4.7, one side of the current shunt is connected to ground and the other feeds to the oscilloscope which measures the current passing through the main bearing as a voltage signal.

The input voltage on the needle panel is measured by the oscilloscope via a high-voltage probe. A high-pass filter is connected to the shaft voltage signal and extracts the high-frequency discharge signal from it.

4.2.2 Induced shaft voltage due to charge accumulation

In the setup, different parameters influence the charge density in the wind tunnel. The main purpose of this study is to determine the charge's impact on the main bearing. Thus, the applied voltage to the discharge needles in the test is varied to adjust the charge density generated in the tunnel.

Test A - bearing state measurement:

Due to the extra grease injected into the main bearing, the bearing can operate in its insulated state. The first test verifies the bearing's operating state. Figure 4.9 shows the test connection; a 2.5V square wave voltage signal with frequency of 1k Hz is applied to the shaft via the carbon brush and the main bearing's outrace is connected directly to the oscilloscope to monitoring its voltage.

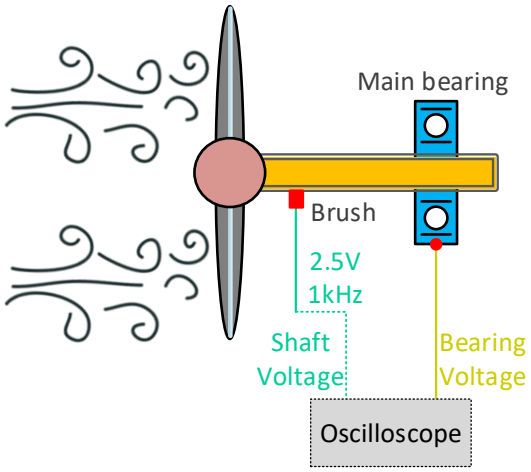

Figure 4.9: Bearing state test connection.

The turbine was rotated by the wind (5-6m/s) at around 80 rpm and no charge generation from the needle panel. The bearing, with and without grease, is shown in Figure 4.10 and Figure 4.11 respectively.

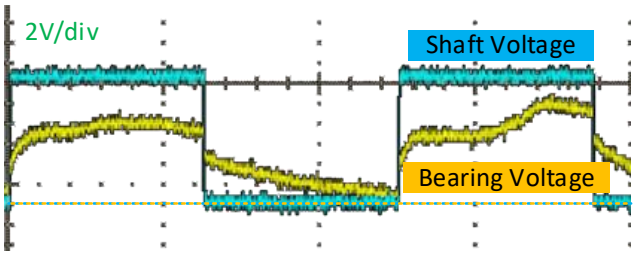

Figure 4.10: Bearing voltage without grease.

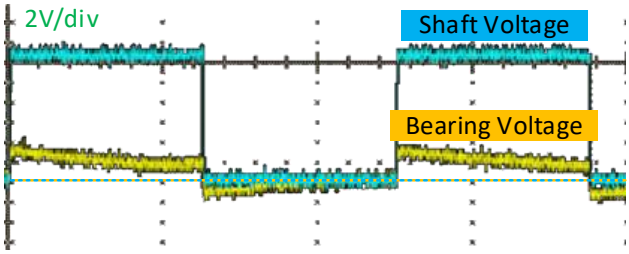

Figure 4.11: Bearing voltage with grease.

In the case of the bearing without grease, the bearing often operates in a conductive state, with the outer race voltage waveform nearly following the input voltage and showing very little voltage drop on the bearing impedance. In the case of the bearing with grease, there was a significant potential difference between the inner and outer races, indicates an insulating state in bearing.

It is clear that injecting grease into the main bearing changes its operating condition from a conductive state to an insulated one. Furthermore, under the insulation state, there was no electrical breakdown in the bearing at 2.5V.

Test B – shaft-induced voltage

Using the test system connection in Figure 4.7, different DC voltage levels were applied to the needle panel. In the test, the charge accumulated / induced on the blade was conducted to the main shaft via the lightning protection system. The charges accumulated on the main shaft are impeded by the grease in the main bearing to the ground. The electrical properties of the main bearing mean that it acts as a dynamic capacitor, blocking DC but conducting AC. The charges from the air are unipolar particles, whose movement generates a negative DC current flow from the blade to the main shaft. These airborne charges are stored on the bearing's inner race and build up a DC electric potential on the main shaft. As shown in Figure 4:12, the needle panel supplied with a voltage of -4kV in channel 1 and in channel 4, a voltage of -10mV is induced on the shaft. Because the airborne charges form negative sources, the voltage on the main shaft is also negative. Based on the bearing's current curve in channel 3, there is no current flowing through the bearing.

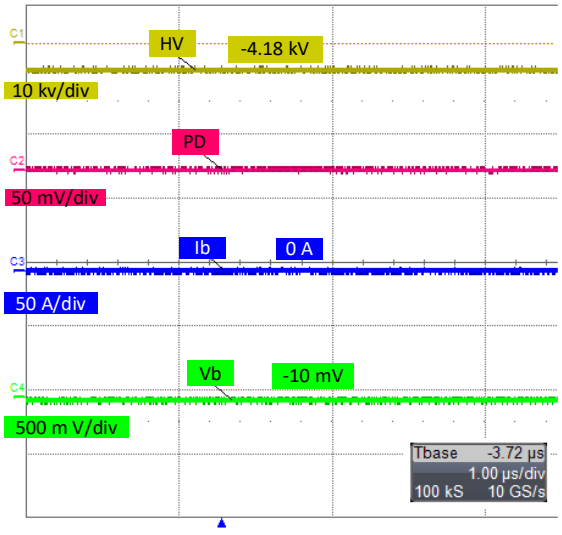

Figure 4.12: Bearing voltage and current at -4.18 kV needle voltage.

Test C – bearing breakdown

In Figure 4.13, with a -6.87kV DC voltage applied to the needle panel, the voltage build-up on the main shaft reached only -93 mV. From the bearing current curve, a breakdown clearly occurred on the bearing and its amplitude reached 62.9 A. During the breakdown process, the induced voltage on the shaft dipped to zero.

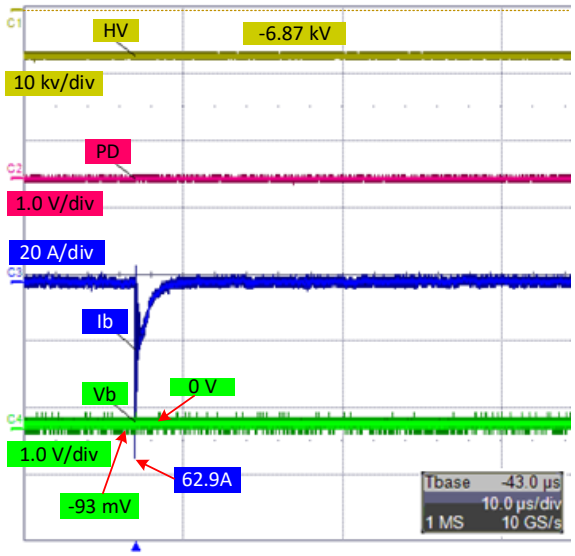

Figure 4.13: Bearing voltage and current at -6.87 kV needle voltage.

With the increasing needle voltage, the charge density in the tunnel further increases. When the needle voltage was increased to -14kV, the bearing broke down more frequently. The test results appear in Figure 4.14, in which the induced voltage reaches -932mV. Within the same timespan as Test B, breakdown occurred three times, with the bearing current amplitude reaching hundreds of amps. During each breakdown, the shaft voltage dipped by several hundred millivolts.

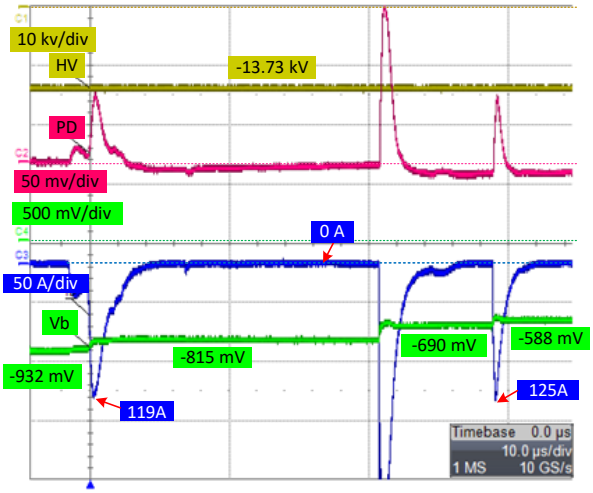

Figure 4.14: Bearing voltage and current at -13.73 kV needle voltage.

Test E – bearing conductive state change

Further increasing the charge density, the applied needle voltage was adjusted to -18.79 kV. As indicated in Figure 4.15, the induced shaft voltage reached -4.83V. The breakdown

occurred in the bearing during rotation, with the current flowing through the bearing peaking at 3.84kA. After the breakdown, the bearing's operating state reverted to a conductive state. There was a continuous current flow through the bearing, even after the voltage had dropped to nearly zero.

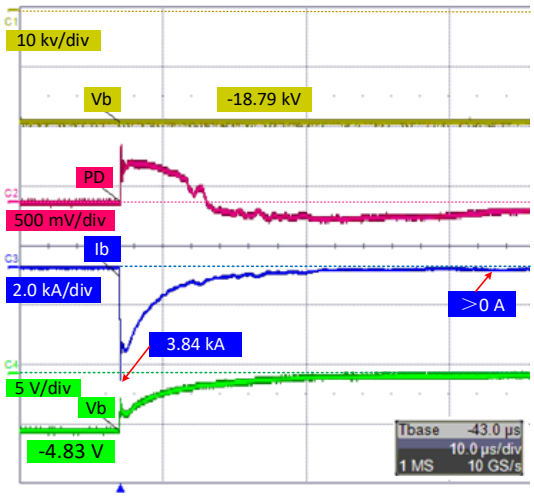

Figure 4.15: Bearing voltage and current at -18.79kV needle voltage.

4.3 Discussion of test results

In Test A, a 2.5V 1kHz AC voltage was applied to the bearing with grease lubrication, no breakdowns / discharges were observed. Comparing to the Tests C and D results, discharges occur more frequently with the shaft voltage was less than 1V, indicating discharges were largely related to charge accumulation at the bearing.

The bearing operated in its insulated state with the wind rotating the lab wind turbine. The grease thickness varies with rotation speed, the rollers' position and the load on the bearing and, from an electrical point of view, the bearing may be modelled as a capacitor. The capacitance varies with the thickness but generally, the capacitance stays within a stable range of dynamic values.

In Test A, a 1kHz AC voltage was applied to the shaft and the charges within the bearing capacitor were periodically polarized and depolarized. During each period, more charges did not have enough time to be accumulated and generated electric field that is strong enough to break down the grease dielectric.

Unlike the test A, the test B, a DC potential was built up at the shaft by means of charges accumulation via the blades. As shown in Figure 4.16 a, the accumulated charges built up a static electric field over the grease. But the amplitude of the electric field on the bearing

grease is not strong enough to break down the bearing. Thus, the potential on the main shaft kept in a stable DC value, as shown in Figure 4.12.

In Test C and Test D, by increasing the voltage level to the needle panel, more charges were generated and travelled to the shaft via blades, and consequently, higher potentials at the shaft. With the rotation of the bearing, the grease thickness changed dynamically, and the electric field strength over the grease was inversely proportional to that thickness. In test C, even though the shaft voltage was only -93mV, the accumulated charges generate a strong enough local electric field to cause breakdowns in bearing when grease dynamically reached to a small enough thickness during rotating.

During the bearing breakdown, the electric arc is generated through the grease and causing a gas channel between roller and outer race. With increasing current flow, A plasma channel can be built (as shown in Figure 4.16 b) and the accumulated charges dissipated to the outrace, which is grounded via the mechanical connection. The shaft voltage dipped to zero and the electric field on the bearing grease was not enough to maintain the plasma channel. Thus, the plasma channel disappeared with the rotation and the breakdown process ended [29].

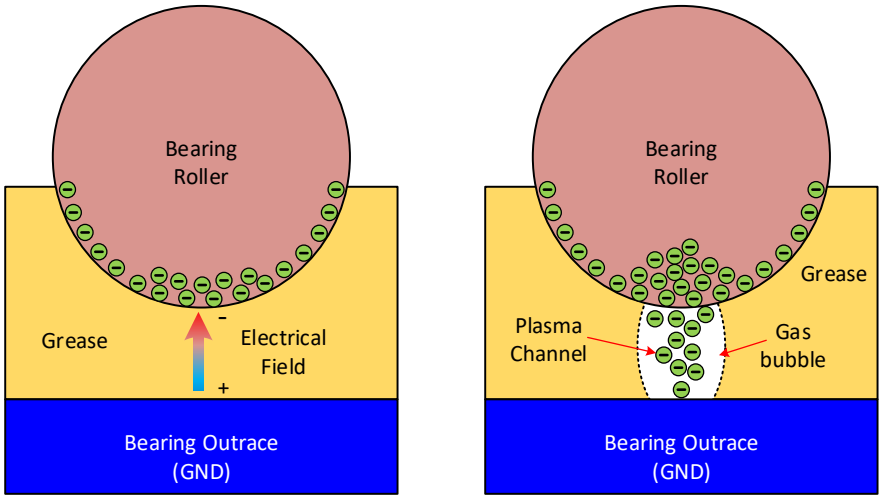

Figure 4.16: Charge movement during breakdown.

In Test E, with increasing charge density in the air, the charges were continuously conducted to the shaft. Once the electric field on the bearing was strong enough, breakdown occurred in the bearing grease. After the breakdown, the charges dissipated to ground via the discharge channel. With subsequent charges from the blades, these charges maintain a continuous flow of current through the discharge channels inside the bearing grease. From the test results shown in Figure 4.15 it is obvious that, after the breakdown, the shaft voltage gradually dropped to nearly zero, but the current maintained to a stable value.

Comparing the test result from Tests C to E, the charge density increased gradually, and the shaft voltage increased from -93mV to -4.8V. It became easier and easier to trigger a breakdown in the bearing. The amplitude of the bearing current began appearing from 63A to 3.8kA. According to Figure 4.8, the current peak was suppressed by the shunt circuit. Assuming a constant discharge duration of 5ns and the amplitude of the currents peak can be calculated as 1.2kA, 60kA, and 210kA in Tests C to E respectively.

4.4 Summary

This chapter has studied and discussed the phenomenon of wind turbine main shaft bearing current. The ESD effect in wind turbines (a new pattern of bearing breakdown) is found in the main shaft bearing. This paper has analyzed its root cause and transmission path. Furthermore, to verify the analysis, a downsized wind turbine was built under lab conditions to simulate a real wind turbine. Several groups of tests were conducted on this lab turbine, with a fatal bearing current amplitude only found at a driven voltage of -93mV. Compared with the AC voltage-driven bearing current, the ESD-driven bearing current appears at a lower trigger voltage and higher current amplitude. Furthermore, based on the charge movement in the test results, the breakdown mechanism of ESD-driven bearing current was studied from a micro-perspective. The analysis and test results prove that the ESD effect in wind turbines is a non-negligible source of main shaft bearing current in wind turbines and that it is much easier to trigger a fatal amplitude current in the main bearing.

Chapter 5. Main shaft bearing current laboratory and field tests

5.1 Common mode voltage transmission path in wind turbine

In this chapter, the focus is on the common mode voltage (CMV) as one of primary sources to main shaft bearing currents in wind turbines, as established in session 3.2.2. Building upon the insights gained from session 3.3.2, which delves into the CMV transmission paths associated with the pitch converter and the main converter, this chapter explores and validates various transmission paths in both laboratory-controlled conditions and real-world field tests.

By bridging theoretical knowledge with experimental evidence, this chapter serves as a crucial link to mitigate and manage main shaft bearing currents in wind turbines. The validation of transmission paths will provide more practical solutions, enabling the industry to enhance the reliability and performance of wind turbine systems.

5.2 Main converter CMV transmission path verification

The common mode voltage (CMV) transmission path originating from the main converter is illustrated in Figure 2.8 the main converter is situated in the turbine's basement, and its associated CMV transmission path in the generator is outlined in Figure 3.21. These paths exhibit intricate interconnections between various subsystems, with diverse mechanisms playing a similar role in transmission. This section investigates these mechanisms through laboratory verification.

5.2.1 Main Converter CMV path lab verification setup

Verification of CMV transmission paths in real wind turbines is challenging due to system complexities and safety regulations. To investigate the different mechanisms within the main converter CMV transmission paths, a scaled-down wind turbine is constructed under controlled laboratory conditions.

The laboratory test wind turbine is based on the K82 model, a commercially available 2 MW geared wind turbine produced by KENERSYS. This model aligns electrically with the configuration showed in Figure 2.8. The lab setup, illustrated in Figure 3.5, includes a

basement, tower, nacelle, and hub, sub-systems such as the transmission system, power generation system, grounding system, and monitor system are integrated.

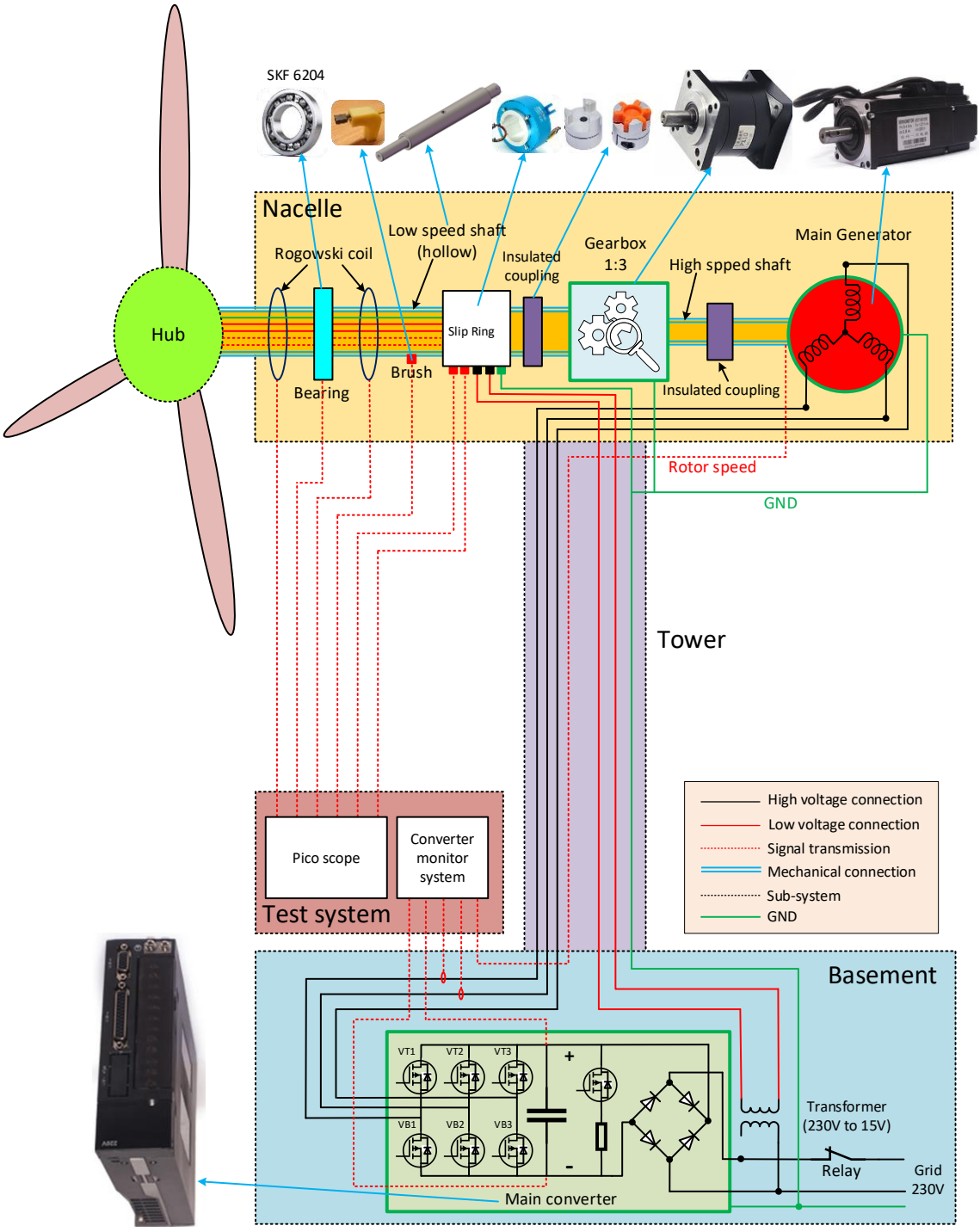

Figure 5.1: Lab wind turbine test setup configuration.

a) Nacelle components

Within the nacelle, a generator, gearbox, and the main bearing are mounted on a nylon board. The gearbox and hub are interconnected by a steel main shaft supported by a SKF ball bearing, detailed in Table 5-1. A carbon brush, housed in plastic, is in contact with the main shaft.

Table 5-1: Main shaft bearing parameters.

Bearing type	Ball-bearing	Inner race diameter (mm)	20
Type number	6204	Width (mm)	14
Brand	SKF	Max speed (rpm)	20000
Outrace diameter (mm)	47	Weight (kg)	0.11

Owing to space constraints, the lab turbine's size and mechanical connections differ from a real turbine. The mechanical connection inside the nacelle is shown in Figure 5.2.

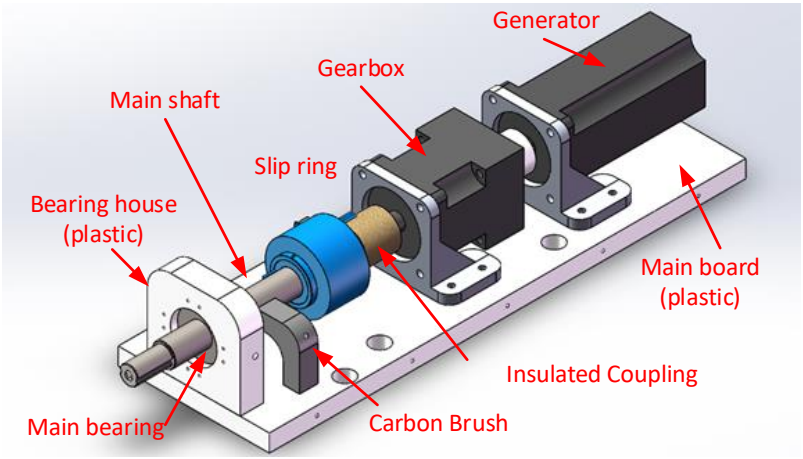

Figure 5.2: Lab wind turbine connection inside the nacelle.

In the planetary gearbox, the input shaft and the output shaft are coaxial, see Figure 3.2 and the output shaft is directly connected to the generator, and the connection is an insulated connection. In order to keep the electrical configuration, the same as the real turbine, the slip ring must be mounted ahead of the generator. However, the connection between the generator and the gearbox takes away the slip ring's installation space. In the lab turbine, the slip ring is mounted ahead of the gearbox, and the hollow main shaft goes through the slip ring.

b) Lab turbine main structure components and ground system

The lab turbine's mainframe, as shown in Figure 5.3, mirrors that discussed in Chapter 4. Notably, the mainframe components are constructed from insulating materials. Ground connections between subsystems are therefore achieved through separate cables, all joining at a common ground bar and thereafter connected to the power grid ground.

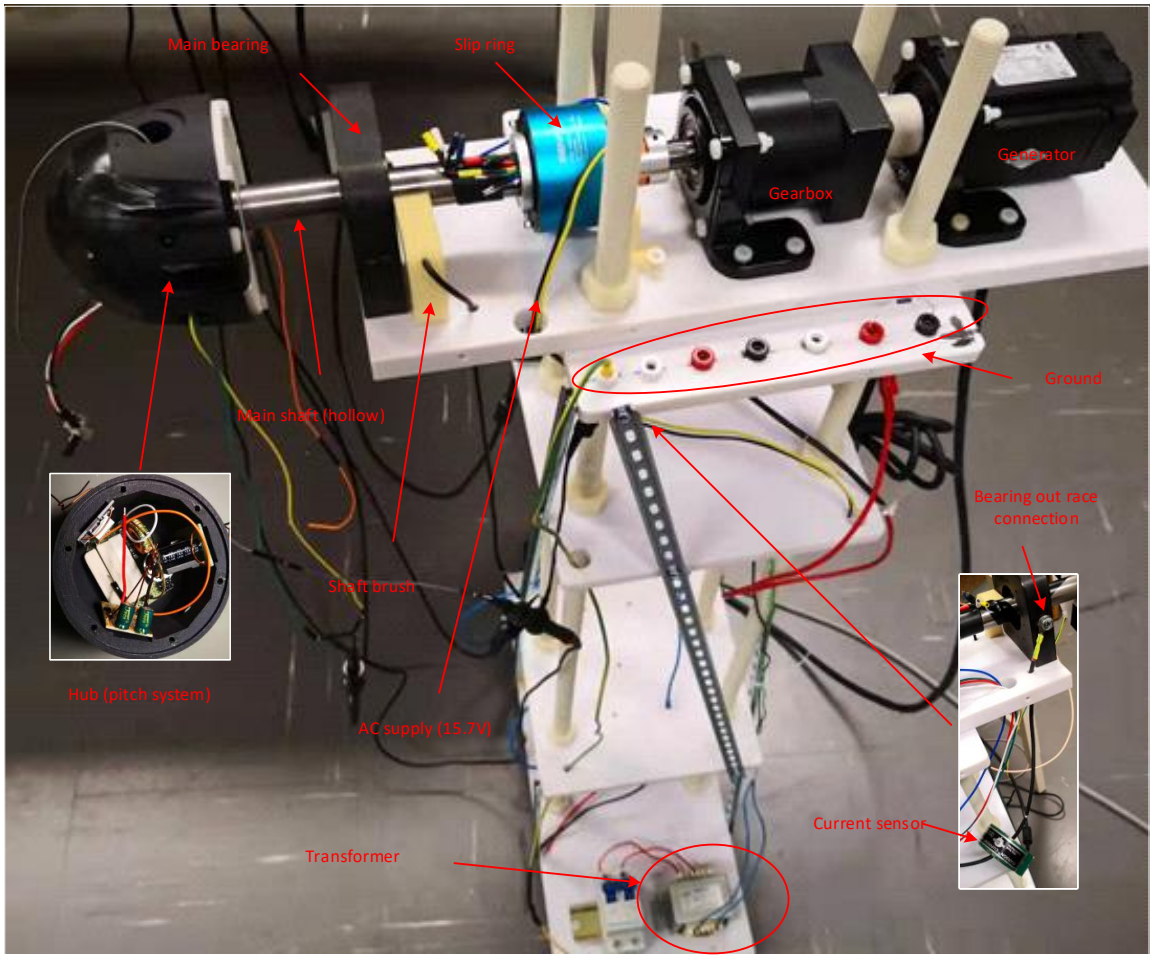

Figure 5.3: Wind turbine lab test setup.

c) Voltage level in the lab turbine system

Voltage level in power generation system: Operated under motor mode, the power generation system's voltage is determined by the converter's driven voltage. In the lab, a single-phase 230V AC voltage source drives the main converter.

Voltage level in the pitch system: Fed by the grid via the slip ring, the pitch system within the hub operates at a lower voltage level than the main power generation system. In the lab, where the main power generation system's voltage is 230V AC, the pitch system's voltage

is set at 15V AC through a transformer connected to the same grid outlet as the main converter.

5.2.2 Study of CMV loop in wind turbine electrical circuit model

The transmission circuit path of common mode voltage to the main shaft bearing is shown in Figure 5.4. One significant source of CMV is the converter located in the basement, which introduces high-frequency components due to fast-switching power electronics. These high-frequency components are transmitted to the generator through phase conductors and crosstalk among bundle cables. The large surface area of the main shaft bearing, its proximity to the generator, and limited space within the nacelle enclosure contribute to the induction of CMVs onto the inner race of the main shaft bearing. As the outer race of the main shaft bearing is grounded, a current flow upon breakdown of the lubrication film between the inner and outer races via a roller, leading to electro-corrosions and bearing damage over time.

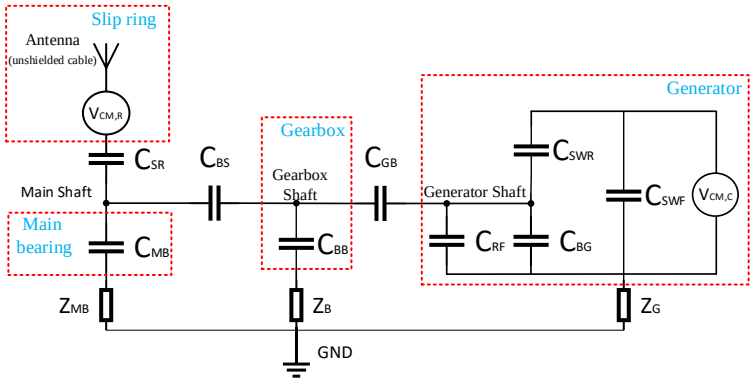

Figure 5.4: CMV transmission path circuit to the main shaft bearing.

Within the nacelle, the CMV source comprises two elements: conductive CMV, which is associated with the physical cable connection, and radiative CMV, transmitted via crosstalk.

$V_{CM,C}$ -- conductive CMV source

$V_{CM,R}$ -- radiative CMV source

C_{SWF} -- the capacitor between stator winding and frame

C_{SWR} -- the capacitor between stator winding and generator rotor

C_{BG} -- the capacitor of generator bearings

C_{RF} -- the capacitor between the generator rotor and frame

C_{GB} -- the capacitor of the coupling between generator and gearbox

C_{BB} -- the capacitor of gearbox bearings

C_{BS} -- the capacitor of the coupling between gearbox and the main shaft

C_{MB} -- the capacitor of the main shaft bearing

C_{SR} -- the capacitor between the slip ring and the main shaft

Z_G -- the grounding impedance of the generator

Z_B -- the grounding impedance of the gearbox

Z_{MB} -- the grounding impedance of the main shaft bearing

In the conductive mode, the modeling of CMV coupling inside the generator is based on a comprehensive study. Here, CMV originates from the generator windings and is subsequently conducted to the generator shaft. The generator shaft connects to the gearbox through a rigid plastic coupling, while the gearbox output shaft is linked via a flexible metal-rubber coupling, as shown in Figure 3.5. The electric couplings among the three distinct shafts are represented as capacitors. Additionally, the grounding cables of the generator, gearbox, and main bearing are modeled as resistors.

In the radiative mode, the electromagnetic field in the nacelle is generated due to the high-frequency content of CMV transmitted along the unshielded phase cable of the generator. In this mode, both the main shaft and its unshielded slip ring cable directly couple to the CMV through crosstalk.

5.2.3 Laboratory setup for lumped circuit model and system simulation

Within the testing environment, the generator and gearbox are considered as voltage dividers responsible for distributing CMV to the transmission shaft in specific ratios. These ratios are determined based on a simplified equivalent circuit model of both the gearbox and generator. In this this study, the primary effort focuses on understanding the transmission dynamics of CMV within the system. Consequently, the circuit model is simplified for clarity and is illustrated in Figure 5.5.

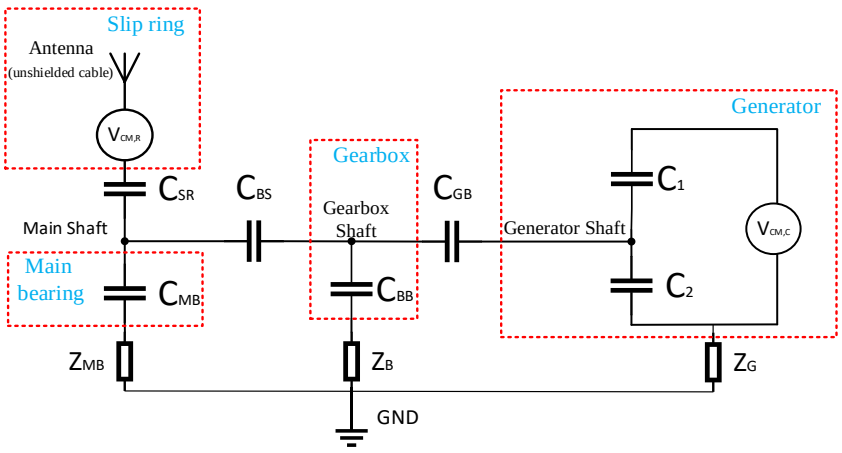

Figure 5.5: Simplified CMV transmission path circuit to the main shaft bearing.

a) Parameter settings

To enhance the precision of the lumped circuit model, various electrical component parameters are determined through a combination of field measurements and laboratory testing. The capacitance values for all capacitors illustrated in Figure 5.5 are obtained from the test bench. To simulate the losses part of these capacitors, a series RC model is employed. These parameters are measured using an LCR meter at frequency of 8 kHz, aligning with the switch frequency of the main converter.

Considering the speed-dependent capacitance of the bearing, the impedance of the generator bearing, gearbox bearing, and main shaft bearing are measured at the turbine system's rated speed. The turbine's rotation speed is set at 1000 rpm, while the generator bearing speed is 3000 rpm. The parameters measured and utilized in the model are detailed in Table 5-2.

Within the generator model, C1 is utilized to denote the insulation between the winding and the stator core, and C2 represents the capacitance of the generator side bearing.

Table 5-2: Impedance of different system components.

C_{MB}	65.4 nF	R_{MB}	153.2 kΩ
C_{SR}	22.93 pF	R_{SR}	45.3 kΩ
C_{BS}	14.3 pF	R_{BS}	18.5 kΩ
C_{BB}	3.6 pF	R_{BB}	41.7 kΩ

C_{GB}	6.95 pF	R_{GB}	38.3 kΩ
C_1	912 pF	R_1	813 Ω
C_2	0.35 uF	R_2	51.3 kΩ

b) System simulation

In accordance with the lumped model illustrated in Figure 5.5 and the parameters obtained from Table 5-2, a simulation model has been developed using ANSYS Simplorer. The simulation includes separate constructions for the conductive mode and radiative mode, as depicted in Figure 5.7 and Figure 5.8, respectively. In the simulation, the common mode voltage (CMV) source is configured as a pure sinusoidal waveform with a frequency of 8kHz, matching the main converter switch frequency. The amplitude of the CMV source is set to 10V, a typical value range for a low-voltage converter.

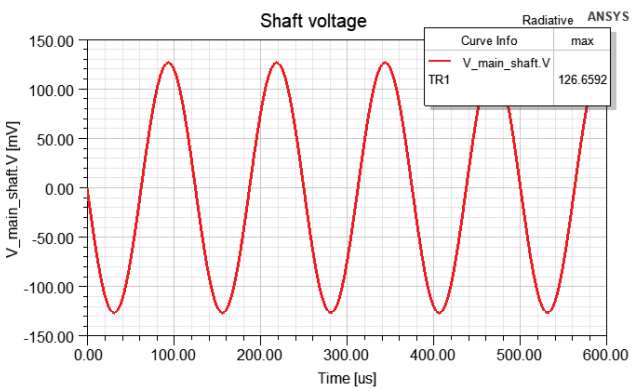

a) Radiative simulation result.

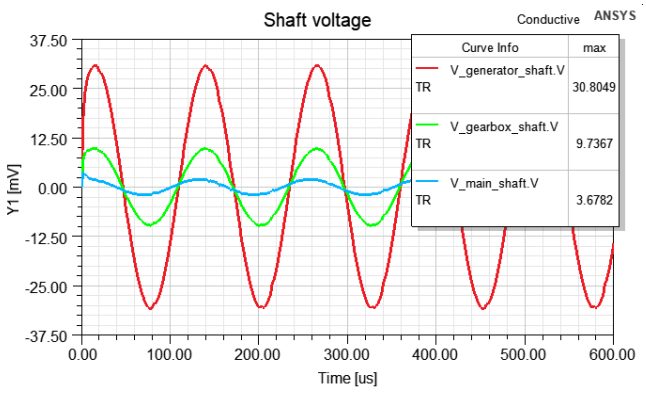

b) Conductive simulation result.

Figure 5.6: The simulated shaft voltages from radiative mode and conductive mode simulations.

The shaft voltages simulated under radiative mode and conductive mode are shown in Figure 5.6 respectively. The highest shaft voltages were found at radiative mode, where it couples about 1.26% of the source voltage. Whereas this voltage is about 40 times lower if it is coupled via the conductive mode.

5.2.4 Laboratory test and verification

To find out different modes of common mode voltage (CMV) coupling capacitances, distinct assessments of conductive and radiative modes were conducted separately on the test bench. For the conductive mode tests, as the slip ring and its cables are predominant sources of radiative CMV, leading to their removal from the test setup. Conversely, in the radiative tests, the conductive sources were isolated, and components separated by the main coupling were disconnected and grounded.

a) Radiative mode CMV circuit test

In the radiative tests, the primary coupling was disconnected, and the gearbox shaft was grounded, with the slip ring fixed onto the main shaft. The voltage on the main shaft was monitored using a directly contacted voltage probe. The schematic representation of the principal test circuits is illustrated in Figure 5.7.

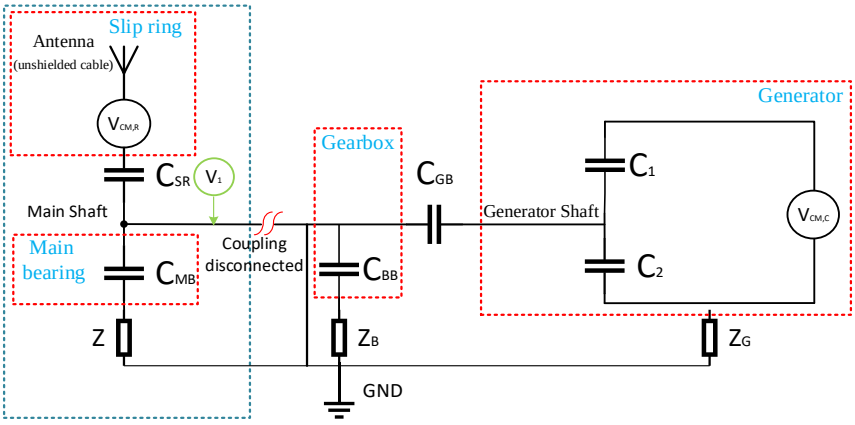

Figure 5.7: Illustration of test circuit used in radiative mode CMV study.

Due to the disconnection of the main coupling, the generator and gearbox sides had no direct electrical connection to the bearing. This allowed for the simplification of the model into a circuit with two series-connected capacitors, as delineated in the blue dashed area in Figure 5.7. In this radiative test mode, C_{SR}, representing the capacitance between the slip ring and the main shaft, emerged as the dominant factor.

b) Conductive mode CMV test circuit

As indicated in Figure 5.8, the radiative source, slip ring, is excluded from the setup, Instead, voltage probes are placed to monitor voltages at various locations along the shaft.

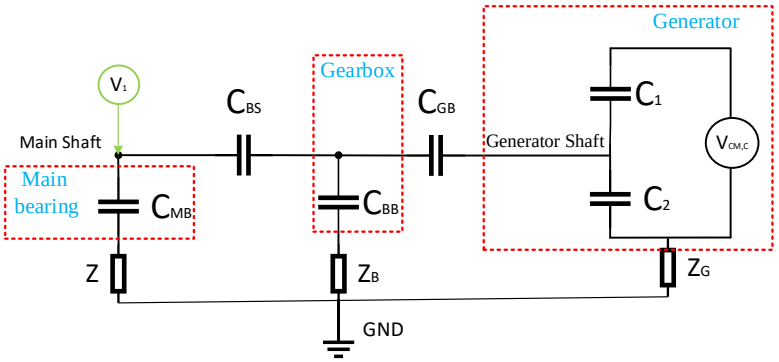

Figure 5.8: Illustration of conductive mode CMV test circuit.

A series of tests were conducted on the laboratory wind turbine, with the generator rotating and operating in motor mode, controlled by the main converter. The test results for both radiative and conductive modes are presented in Figure 5.9. In both waveforms, switching frequency of 8 kHz was identified, revealing high harmonic contribution at the on and off moments of the switches. Comparing these results with the simulated shaft voltages illustrated in Figure 5.6, consistent findings were obtained. This confirms the validation of the proposed circuit models through the laboratory test setup. Furthermore, a small DC offset was observed in the laboratory measurement results, particularly in the conductive mode. This observation suggests potential charge accumulation at the main shaft bearing, indicating a possible source of hazardous inrush current at the main shaft bearing.

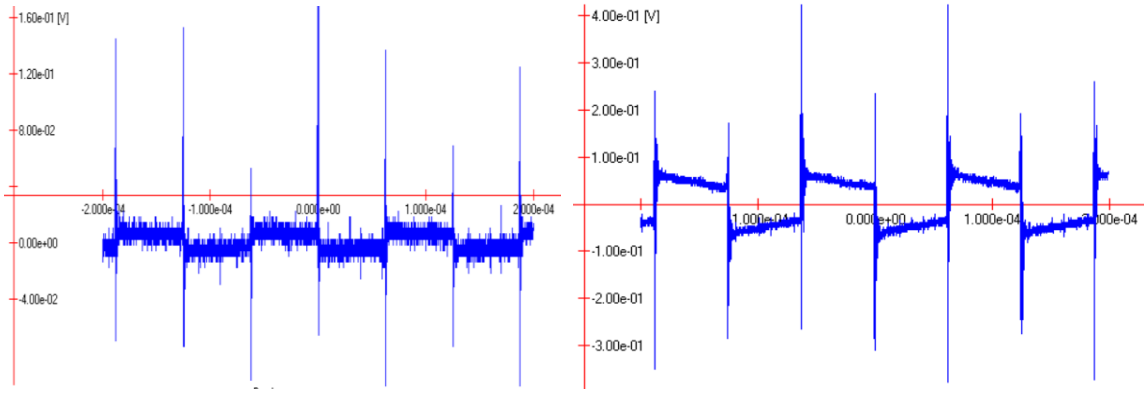

a) Radiative mode. b) Conductive mode.

Figure 5.9: Measured main shaft voltages at radiative and conductive modes.

5.3 Pitch converter CMV transmission path verification

The wind turbine's pitch system emerges as another critical source of Common Mode Voltage (CMV). Typically located inside the hub and rotating with the main shaft, the pitch system includes a pitch converter and a pitch motor for each blade. Both the converter and the motor are directly fastened to the hub frame. The electrically conductive path for the CMV in the pitch system was elucidated in section 3.2.5. To validate this path, a scaled-down pitch system is constructed in the laboratory test bench.

5.3.1 Pitch system CMV path laboratory verification setup

The lab pitch system consists of a transformer, slip ring, rectifier, pitch converter, and pitch motor. The electrical configuration and components of the lab pitch system are shown in Figure 5.10.

a) Lab pitch system

The lab pitch setup shares the same frame as the main converter CMV verification setup shown in Figure 5.3. The hub housing the lab pitch system is attached to the other end of the main shaft. The voltage level for the pitch system is maintained at 15V AC. This is achieved via a transformer where its primary side is connected to the power supply for the main converter.

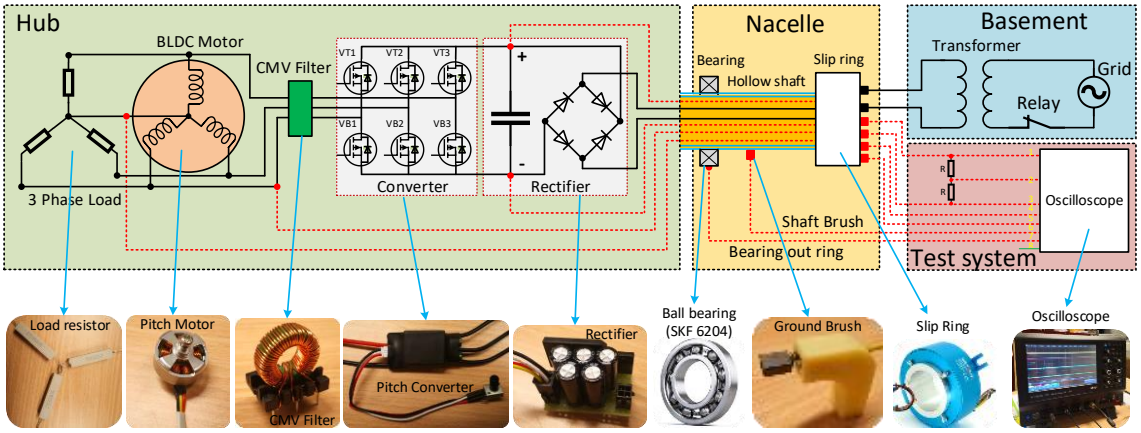

Figure 5.10: Electrical configuration of lab pitch system.

As depicted in Figure 5.11, within the hub, the rectifier, pitch converter, and pitch motor are mounted on the hub frame. Unlike a real wind turbine, the lab setup does not replicate mechanical part of the pitch system. From an electrical perspective, the variation in mechanical connection does not impact the electrical configuration in the pitch system. For this study, with a primary focus on the CMV's transmission path in wind turbines, the electrical connection remains the central point of interest.

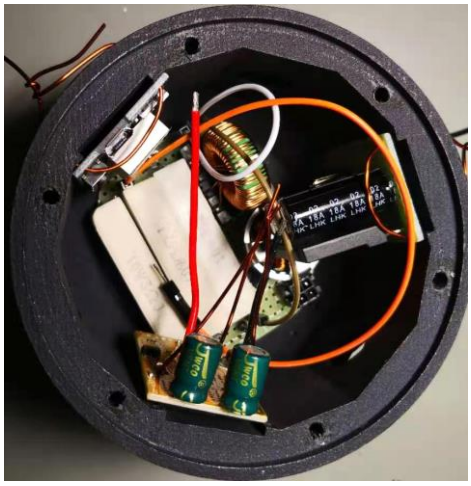

Figure 5.11: Lab turbine pith system in the plastic hub.

In the lab pitch system, due to space constraints inside the hub, it only comprises a single concentrated pitch converter and a pitch motor. The pitch converter is divided into a rectifier and a DC/AC converter. The pitch motor is a three-phase brushless DC (BLDC) motor. To increase the load current, three resistors in star connection are parallelly connected to the BLDC motor's windings. These components are individually shown in Figure 5.10.

b) Monitoring system used in laboratory pitch system setup.

During the development of the laboratory pitch system, careful consideration was given to various signals relevant to the pitch system's common mode voltage throughout the design phase. The red block in Figure 5.10 highlights the collection of different signals in the measurement system.

The winding neutral of the motor, which is the sum of the phase voltages, is regarded as the CMV of the motor. Typically embedded within the winding, in the setup, the motor winding was modified to allow the winding neutral to be extracted as a separate monitor signal.

The DC link voltage of the rectifier is also connected as a monitor signal. Additionally, another signal representing the neutral of the DC link is obtained through the midpoint of two shunt resistors.

To regulate the operational electrical state of the system, the signals from the main shaft brush and the outer ring of the bearing are also extracted. It's important to note that in some instances during testing, the main shaft brush and the bearing outer ring are utilized as ground connections rather than test points.

The specific signals monitored by various oscilloscope channels are outlined in Table 5-3.

Table 5-3: Test channel signal definition.

Name	Signal
Channel 1	Motor neutral voltage (CMV)
Channel 2	DC-link neutral voltage
Channel 3	Shaft brush voltage
Channel 4	Bearing current

5.3.2 Laboratory Testing of Pitch Converter CMV Path

This section focuses on the examination of the pitch system's CMV transmission path. The laboratory setup emulates a downsized pitch system, providing a controlled environment for studying the intricacies of the pitch system's CMV transmission.

Throughout all tests, a consistent load rate is maintained for the pitch converter, operating at the voltage of 15V and a switching frequency of 16kHz. The main shaft and hub are intentionally locked in a random position, and the power supply of the main converter remains in the turned-off state during testing.

A noteworthy aspect of the lab setup is the deliberate use of non-conductive plastic for all structural components. This design choice facilitates a systematic verification of individual paths. Within the defined scope of this study, various test groups are planned and executed on the laboratory turbine, ensuring a thorough exploration of the pitch system's CMV transmission path.

a) Test group A

In test group A, the winding neutral is configured as a floating state, and the access point for the winding neutral serves as a signal collection point only. The states of the main shaft brush and the outer ring connection are altered according to Table 5-4.

Table 5-4: Connection state in test group A.

Case	Bearing out ring	Shaft brush
A1	Ground	Ground

A2	Ground	Float
A3	Float	Ground
A4	Float	Float

The corresponding test configurations are illustrated in Figure 5.12 and Figure 5.14. Case A1, where both the brush and bearing are grounded, represents the typical operational condition in wind turbines.

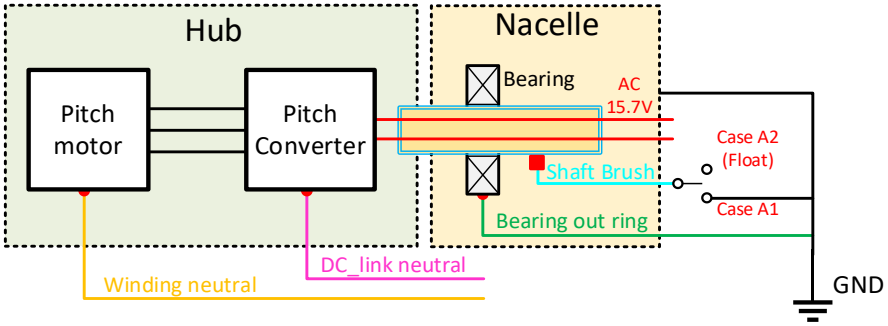

Figure 5.12: Lab pitch test group A (Case A1&A2).

The test results for case A1 are shown in Figure 5.13 (a) and (b). The colors of various signals in the test results align with the corresponding connection sketches. Both the winding neutral and the DC link neutral exhibit mixed frequencies signals. The high-frequency component corresponds to the 16 kHz switching frequency of the pitch converter, clearly visible in the shaft voltage and bearing current as shown in the zoomed-in test result in Figure 5.13 (b). The low-frequency component, at 50Hz, corresponds to the grid frequency, evident in the envelope curve of the neutral voltage switching frequency.

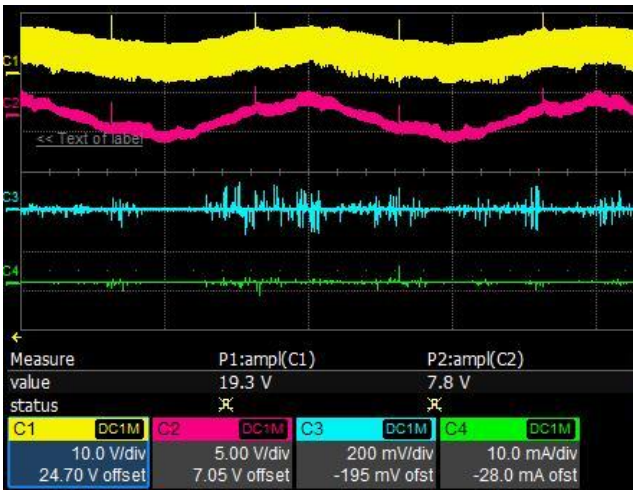

a) Test result of case A1 (both bearing and shaft ground).

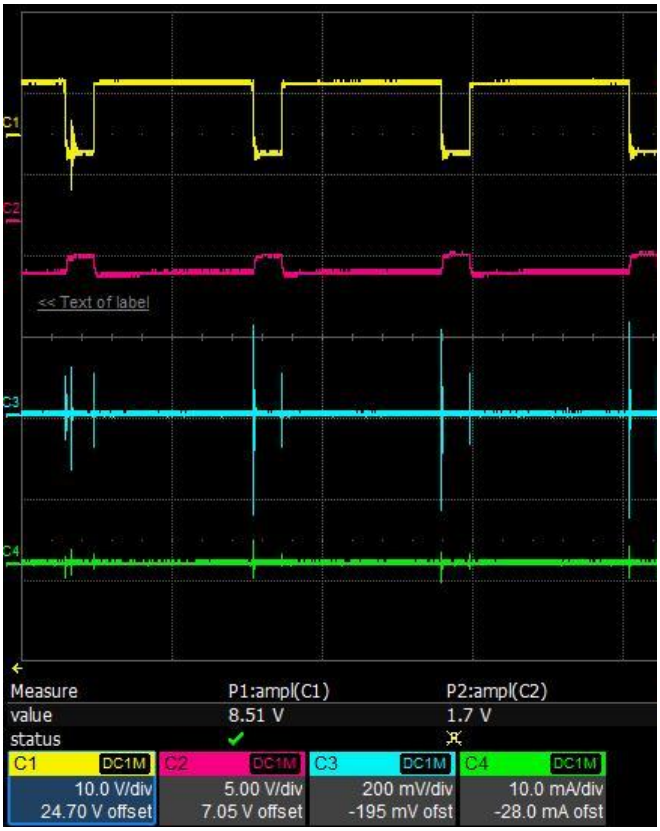

b) Zoom in view of case A1 test result (both bearing and main shaft ground).

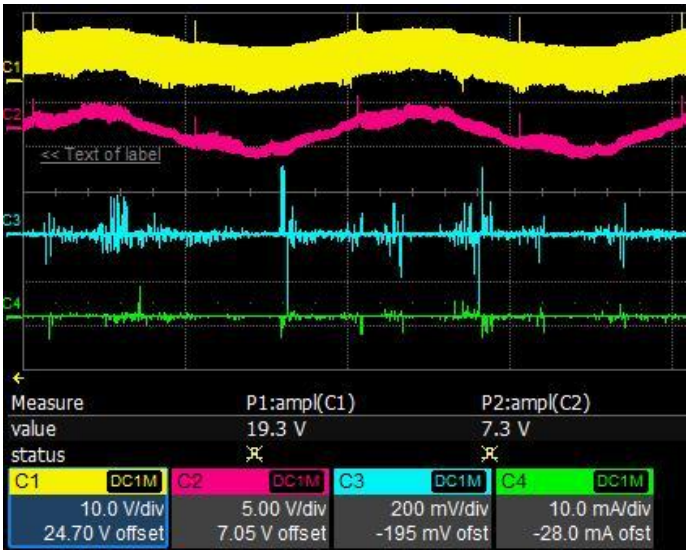

c) Test result of case A2 (bearing ground and main shaft floating).

Figure 5.13: Lab pitch test result of group A (Case A1&A2).

In the A2 test case, the shaft brush is floating. The outcomes are similar to those observed in case A1, albeit with significantly higher amplitudes for both the shaft voltage and bearing current.

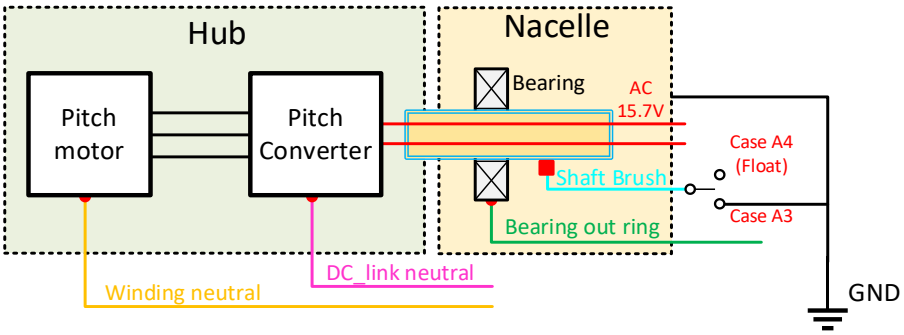

Figure 5.14: Lab pitch test group A (Case A3&A4).

For tests A3 and A4, the bearing outer ring is set as floating. Due to the locked position of the bearing, it operates in a conductive state, causing the bearing outer ring to exhibit shaft voltage. However, this voltage's amplitude is attenuated by the contact resistance of the bearing. The test results for cases A3 and A4 are illustrated in Figure 5.15, with the components of the neutral signals mirroring those observed in case A1.

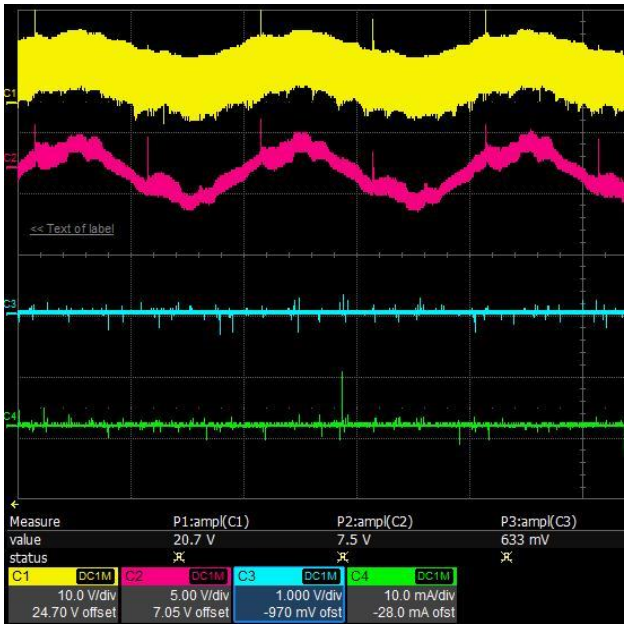

a) Test result of case A3 (bearing floating and main shaft ground).

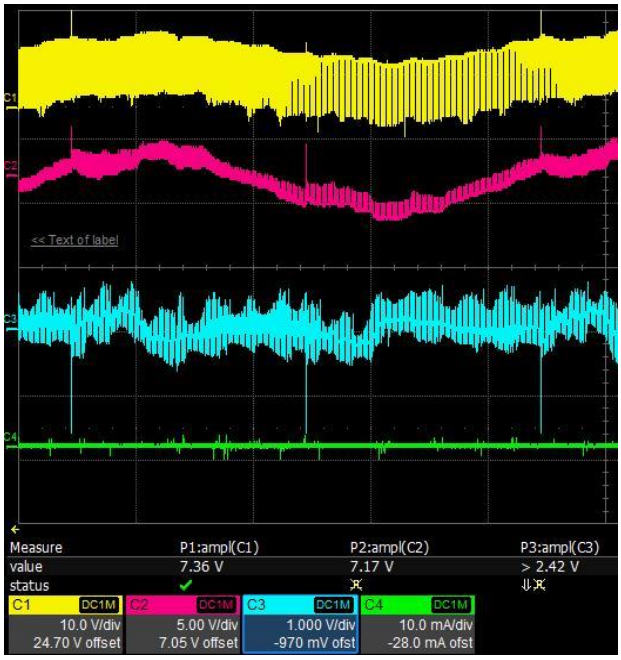

b) Test result of case A4 (both bearing and main shaft floating).

Figure 5.15: Lab pitch test result of group A (Case A3&A4).

In conclusion, the investigation of Test Group A with the winding neutral floating, the deliberate variations in the connection states of the bearing out ring and shaft brush allowed for exploring of different operational scenarios. Notably, Case A1, representing the typical wind turbine operational condition with both the brush and bearing grounded, exhibited mixed-frequency signals, with distinct components corresponding to the pitch converter's switching frequency and the grid frequency. Case A2, with a floating shaft, showed similar outcomes to A1 but with notably higher amplitudes. Tests A3 and A4, where the bearing outer ring was set as floating, demonstrated the impact of the bearing's conductive state on the exhibited shaft voltage.

b) Test group B

In Test Group B, the winding neutral is directly connected to the main shaft, as depicted in Figure 5.16. Similar to Test Group A, other connection state changes remain consistent, and the test connections align with those in Test Group A, as illustrated in Figure 5.17 and Figure 5.18.

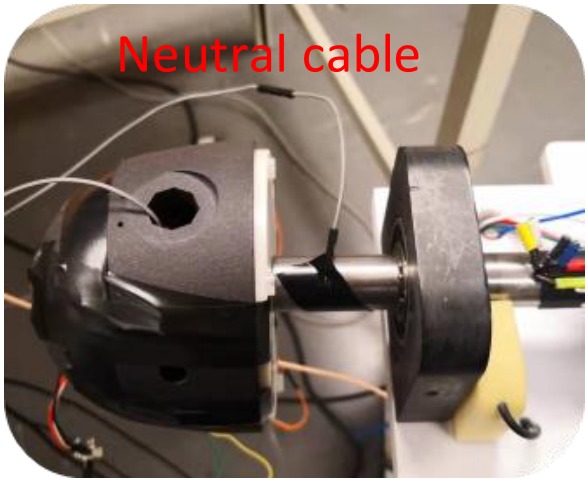

Figure 5.16: Winding neutral connected to the main shaft.

In real-world scenarios, the common mode voltage (CMV) generated by the pitch motor is transmitted to the main shaft via the stray capacitance between the winding and the motor frame. This configuration results in a reduction in the pitch motor CMV level at the main shaft. However, in the laboratory setup, where the hub frame is made of plastic, simplifying CMV coupling to the main shaft, the winding neutral of the pitch motor is directly linked to the main shaft in this test group.

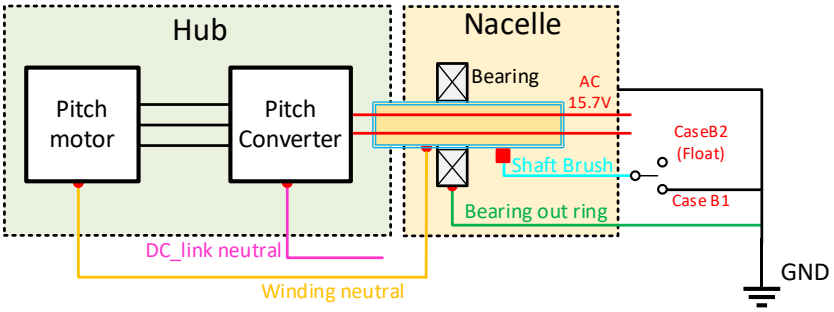

Figure 5.17: Lab pitch test group B (Case B1&B2).

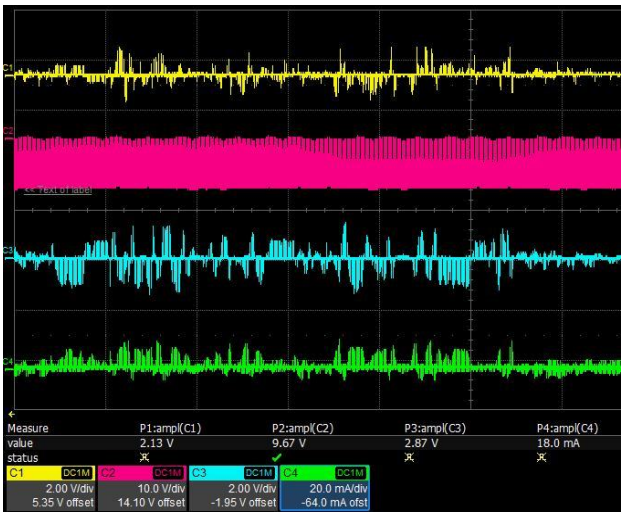

a) Test result of case B1 (both bearing and main shaft ground).

b) Test result of case B2 (bearing ground and main shaft floating).

Figure 5.18: Lab pith test result of group B (Case B1&B2).

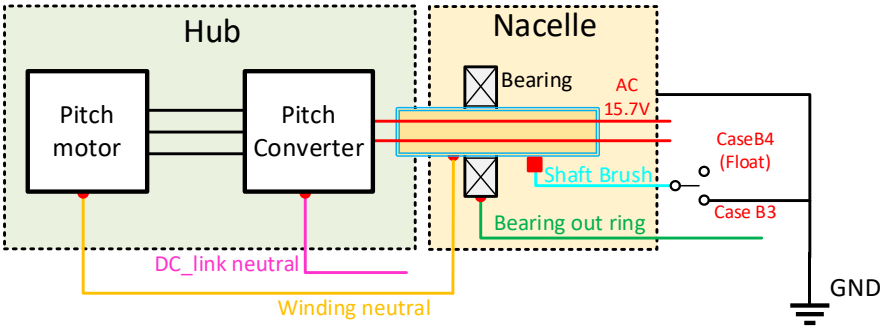

Figure 5.19: Lab pitch test group B (Case B3&B4).

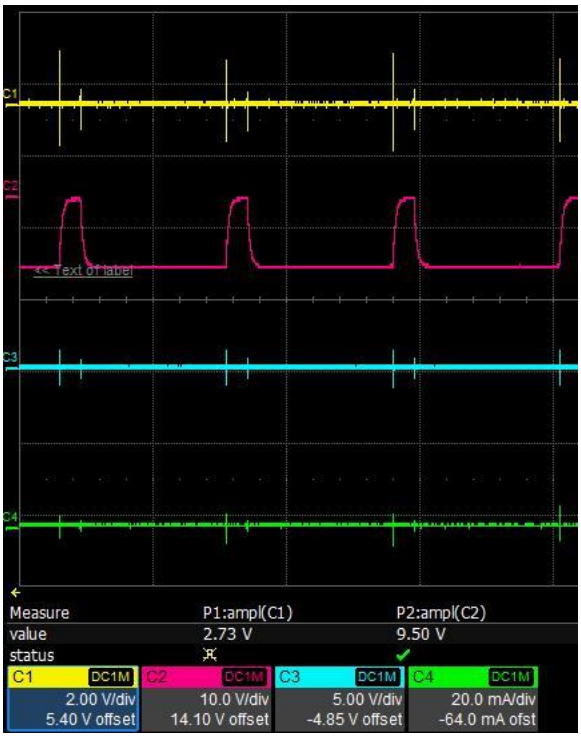

a) Test result of case B3 (bearing floating and main shaft ground).

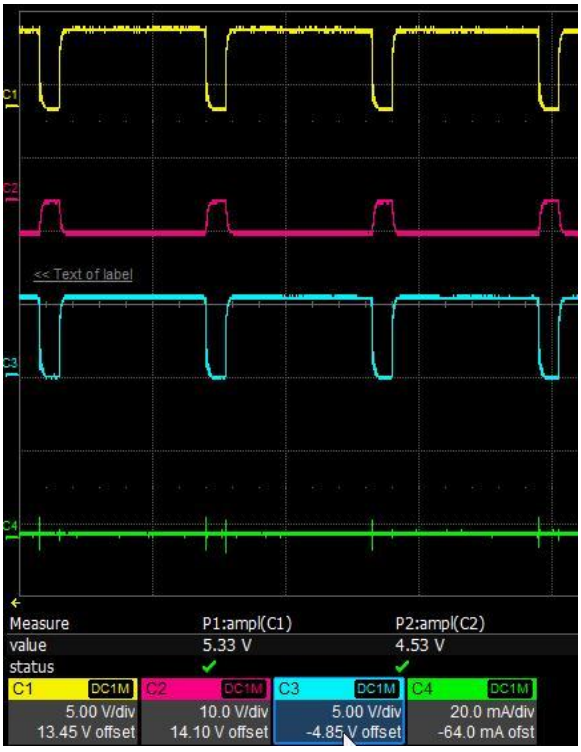

b) Test result of case B4 (both bearing and main shaft floating).

Figure 5.20: Lab pith test result of group B (Case B3&B4).

Results of test group B are shown in Figure 5.18 and Figure 5.20. In contrast to test group A, test group B shows cleaner voltage waveforms for both the neutral winding and the DC link. The low-frequency component is less pronounced, while the high-frequency component remains at the 16 kHz switching frequency of the pitch converter. The direct linking of the winding neutral to the main shaft in test group B results in a notable reduction in the amplitude of the measured neutral voltage. Additionally, this connection significantly mitigates the 50Hz component in the neutral voltage.

5.3.3 Pitch converter CMV contribution discussion

The test results of the CMV from pitch converter in different connections are summarized in Table 5-5.

Table 5-5: Summary of pitch system test results.

Case	Winding neutral	Bearing out ring	Shaft brush	Neutral (CMV)	Brush voltage	Bearing current	Remarks
A1	Float	Ground	Ground	19.3 V	507 mV	7.0 mA	Lowest
A2		Ground	Float	19.3 V	653 mV	17.3 mA	
A3		Float	Ground	20.7 V	633 mV	13.7 mA	
A4		Float	Float	7.36 V	2.42 V	4.7 mA	Radiation dominate
B1	Connect to main shaft	Ground	Ground	2.13 V	2.87 V	18 mA	
B2		Ground	Float	3.6 V	4.07 V	40 mA	Highest
B3		Float	Ground	2.73 V	3.0 V	15.3 mA	
B4		Float	Float	5.85 V	5.99 V	12.7 mA	

From the table, the bearing currents in cases A4 and B4 are the smallest within their respective groups. In these instances, where the brush and bearing are both floating, no current is expected in the test results. However, radiation phenomena dominate the results, and certain signal levels are observed by the oscilloscope. Notably, case A1 stands out as the best scenario, displaying the lowest brush voltage and bearing current. This suggests that the brush plays a critical role in mitigating common mode voltage (CMV) on the main shaft.

Case B2, which conducts all the main shaft CMV to ground via the main bearing, emerges as the worst case across all tests. While such a scenario is likely to appear in practices, where brush traces and heads are often contaminated by non-conductive lubricants, causing a high ohmic resistance (tens of kilohms [30]) in the brushes and consequently leading to a significant increase in bearing current.

5.4 Common mode voltage path verification in wind turbine field test

Building upon the theoretical analysis presented in Chapter 3, a series of field tests have been conducted on an operational wind turbine. The turbine selected for testing is a standard model manufactured by KENERSYS, specifically the K82, which also serves as the basis for the laboratory turbine constructed in this study.

The K82 wind turbine features an electrically excited synchronous generator paired with an IGBT main converter. Positioned at the tower bottom, the main converter system operates at a switching frequency of 2.5 kHz. The pitch system, situated inside the hub, is comprised of a converter and a motor for each blade, with the pitch converter operating at a switching frequency of 4 kHz.

To comprehensively investigate the influence of Common Mode Voltage (CMV) from both the main converter and the pitch converter, two typical operating states have been tested on the wind turbine during the field tests. This empirical approach aims to validate the theoretical insights gained from the earlier analytical study in Chapter 3.

5.4.1 Wind turbine test sensor arrangement

In the field tests, an oscilloscope, along with two Rogowski coils, is employed to monitor current flow at various locations along the main shaft. The positions of these coils are shown in the turbine's electrical connection sketch, as illustrated in Figure 5.21. In this figure, sensor A captures the current from the turbine side, while sensor B captures the current from the generator side. The specific details of the sensors utilized can be found in Table 5-6.

Table 5-6: Field test Rogowski coil information.

No.	Type	Sensitivity	Length	Position (Figure 5.21)
A	Rogowski	50 mV/A	6 m	Turbine side sensor
B	Rogowski	100 mV/A	6 m	Generator side sensor

The calculation of the current passing through the bearing is simply determined as:

$$i_{Bearing} = i_B - i_A \tag{5-1}$$

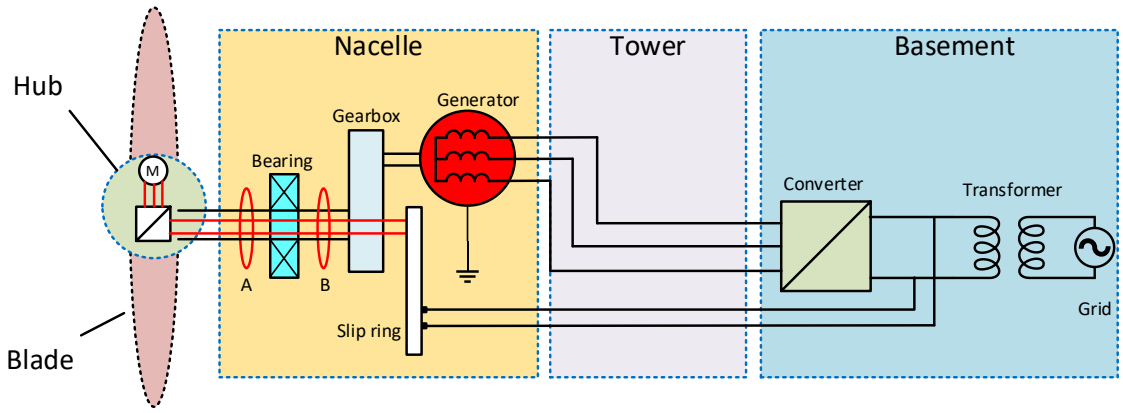

Figure 5.21: Field turbine test sensor arrangement.

5.4.2 Idling operation test

The first operating state under test is the Idling, characterized by the rotor being turned by the wind but without any power generation from the generator nor converter. The pitch system is linked to the power source but does not engage in any pitching action. In this operation, Despite the absence of power output from the main converter, it stays operational in a switching state.

Figure 5.22 illustrates the test results obtained through Rogowski coils and analyses. Plots (a) and (b) present the direct measured data from the oscilloscope, while plot (c) represents the difference between (a) and (b). Plot (d) shows the FFT analysis result derived from the data in plot (c).

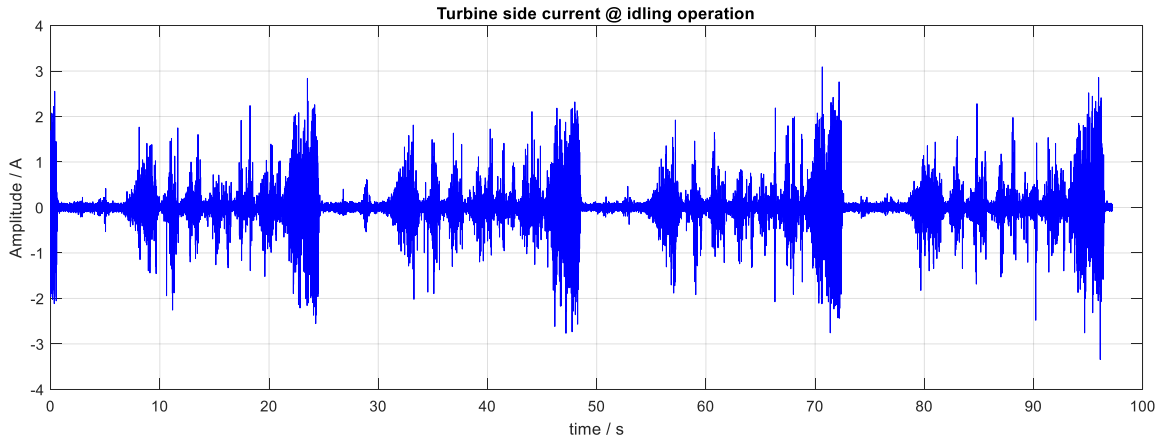

a) Shaft current from sensor A.

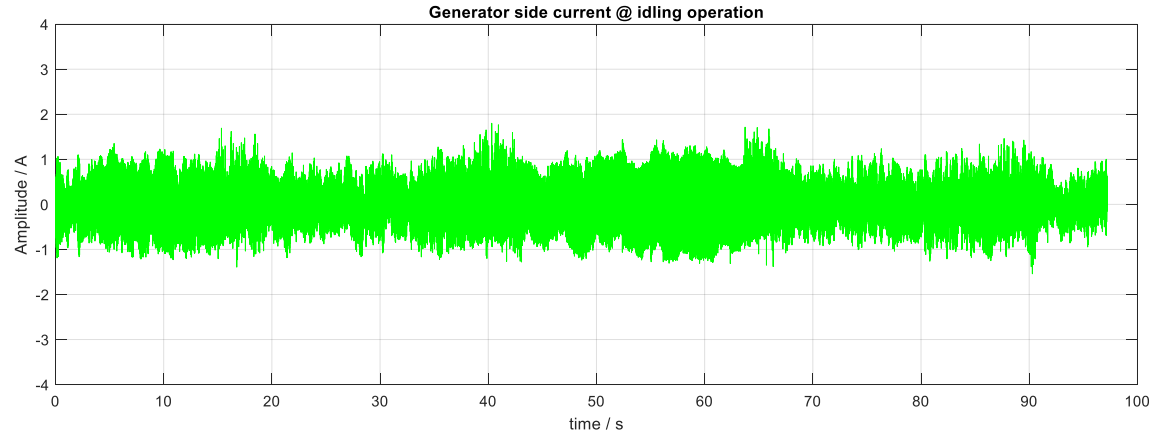

b) Shaft current from sensor B.

c) Bearing current from sensor B-A.

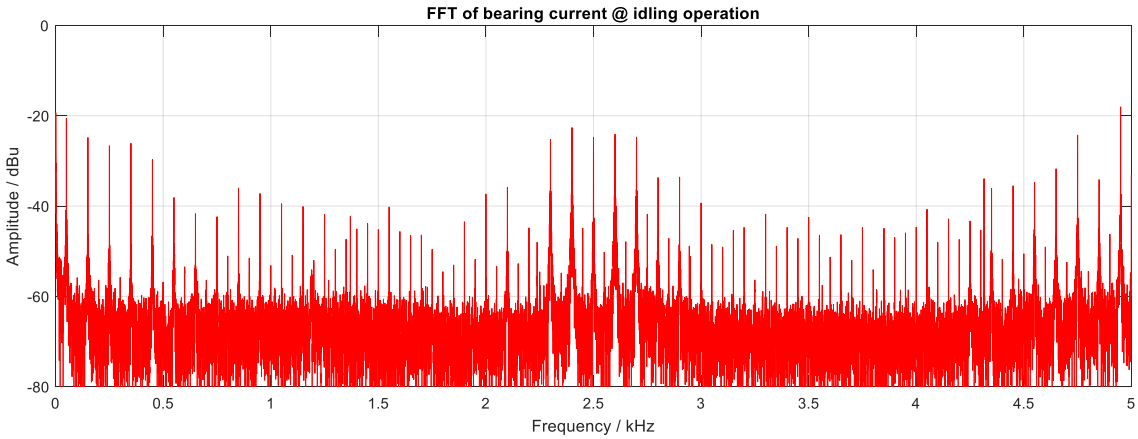

d) FFT result of bearing current.

Figure 5.22: Wind turbine filed test under idling operation (rotor being turned by the wind without power generation nor pitching action).

In the idling operation, the current measured from the turbine side surpasses that on the generator side, indicating a current flow from the turbine to the generator. Although the peak value of the bearing current reaches 2A, its mean value remains relatively small. The primary frequency peaks observed in the bearing current are 50Hz, 2.5kHz, and 5kHz ranges.

5.4.3 Pitching operation test

The pitching operation state is another studied operating condition. Typically, the pitch system is automatically adjusted based on wind; however, for this test, manual control of the pitch system was employed. Throughout the test, the rotor is locked, and the individual blades are collectively pitching.

Figure 5.23 illustrates the test results from Rogowski coils and analyses. Notably, the current on the turbine side, as captured by sensor A, approaches zero. Conversely, the current on the generator side, observed by sensor B, predominates in the bearing current. This indicates a flow of current from the generator side through the main shaft and via bearing to the ground. The peak bearing current reaches 4A, with dominant frequencies at 50/250Hz, 2.5kHz, and 5kHz, aligning with the grid and main converter frequencies. However, the pitch converter frequency of 4kHz is absent in the spectrum, suggesting observed bearing currents are unrelated to pitch switches.

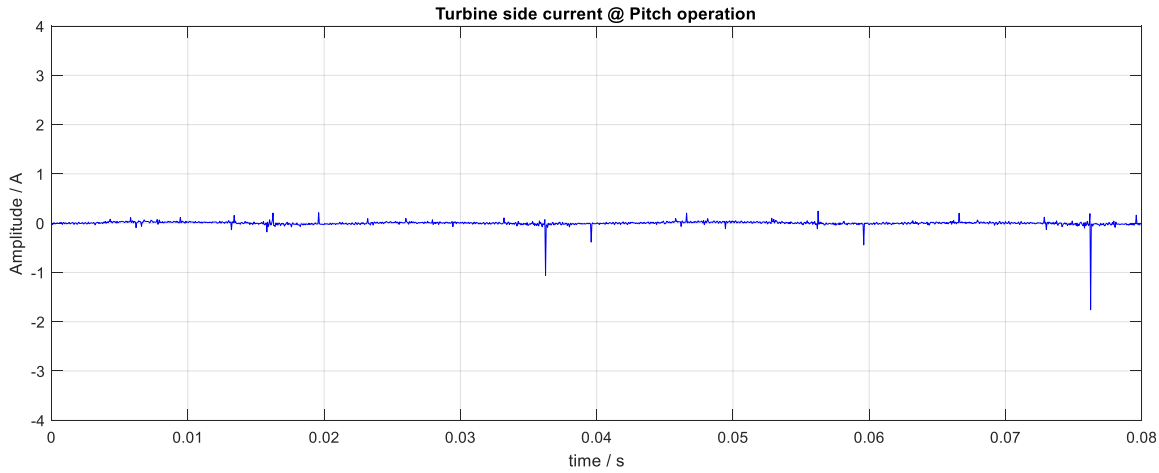

a) Shaft current from sensor A.

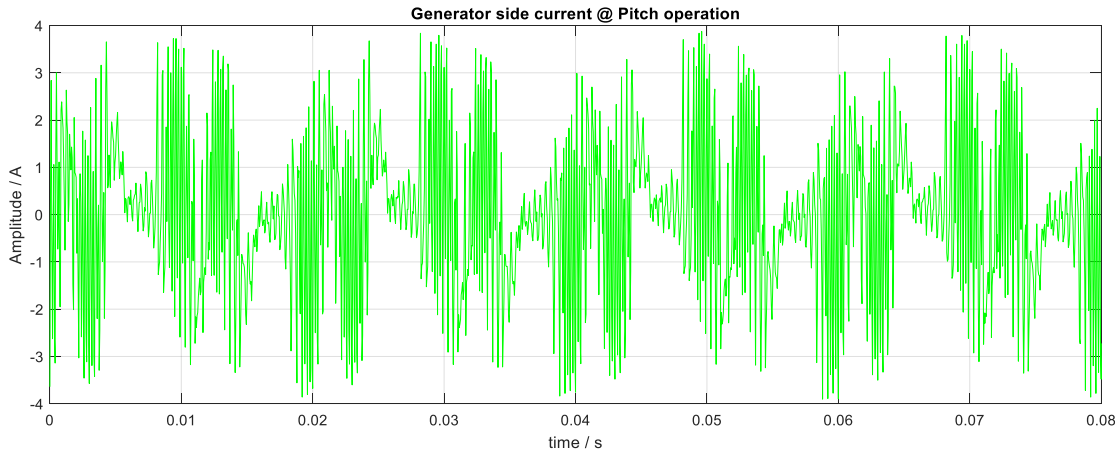

b) Shaft current from sensor B.

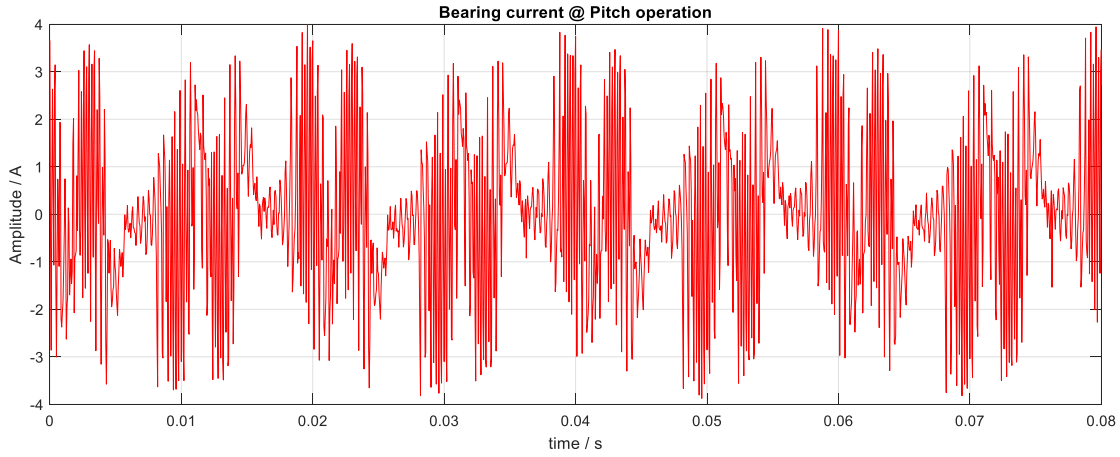

c) Bearing current from sensor B-A.

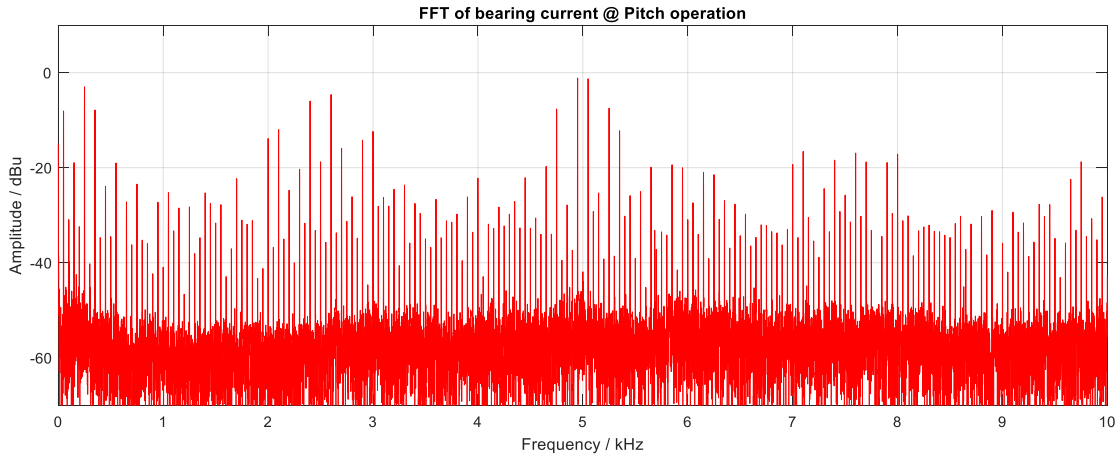

d) FFT result of bearing current.

Figure 5.23: Field turbine test under pitch operation only, with the rotor locked.

5.5 Summary

This chapter discusses the verification of the wind turbine main shaft bearing current path, specifically focusing on the common mode voltage (CMV) transmission paths associated with the main converter and pitch converter. The chapter encompasses laboratory-controlled experiments and field tests to validate theoretical models.

In the main converter CMV transmission path verification, a scaled-down wind turbine is built for laboratory testing, and a circuit model is developed. The model considers conductive and radiative CMV sources, grounding impedances, and capacitors representing various components. The laboratory tests and simulations confirm the circuit model's accuracy, revealing insights into CMV transmission dynamics.

We also explore the pitch converter CMV transmission path through a laboratory setup. Different test groups and configurations are examined to understand the impact of various connections on CMV. Test results highlight the importance of the brush in mitigating CMV on the main shaft and reveal the influence of different connections in the loop.

Additionally, field tests on an operational wind turbine are conducted during idling and pitching operation states. The results indicate a current flow from the turbine to the generator, with the bearing current exhibiting dominant frequencies aligned with grid and main converter frequencies. The absence of the pitch converter frequency in the spectrum suggests detected bearing currents are unrelated to pitch switches in the tested wind turbine.

Chapter 6. Conclusion and discussion

6.1 Main shaft bearing currents

Aiming at studying the wind turbine main shaft bearing current, in this thesis first categorizes different type of wind turbines into geared wind turbine and gearless wind turbine. Despite different type of wind turbines different a lot, all configurations share common main subsystems such as power generation, suspension, lightning protection, pitch control, and grounding. This classification helps streamline the study of bearing currents in wind turbines, allowing for more focused research into their electrical systems and current paths.

Secondly after the classification, through analytical discussions and simulations, based on wind turbine configurations potential sources are discussed. Detailed insights into geared wind turbine configurations, components like gearboxes and slip rings, cable crosstalk impact, and shaft magnetization are provided.

Thirdly, shedding light on their diverse sources, mechanisms, and transmission paths. Through comprehensive wind turbine and lab tests, two primary sources are identified: Common Mode Voltage (CMV) and wind blade Electrostatic Discharge (ESD) effects. Their impact and transmission paths are discussed separately. With an downsize lab turbine, their contribution and pattern are verified respectively.

Finally, it can be concluded that the CMV effect exhibits a periodic current pattern, its frequency determined by converter and grid frequencies. On the other hand, the wind blade ESD effect on bearing identified in this study, characterized as an instantaneous current with high amplitude, causing significant partial discharges in bearing grease and subsequent heat release, thereby reducing bearing lifespan.

6.2 Suggestion for bearing current eliminating

To safeguard the bearing from harmful currents, the primary strategies involve eliminating the current source and altering the current path.

Addressing the source, it is established that Common Mode Voltage (CMV) and the Electrostatic Discharge (ESD) effect are contributors to main shaft-bearing current. CMV originates from the main converter and pitch converter in wind turbines. To mitigate CMV,

the utilization of a CMV filter or select a PWM patten with reduction of harmonics in the voltage is a viable option for reducing CMV originating from the converters.

Regarding the transmission path, the study thoroughly analyzes and validates the paths for CMV and ESD effect. Within these transmission paths, the main shaft ground brush emerges as a crucial component safeguarding the main bearing from bearing current. However, its maintenance in wind turbines is not consistently optimal, potentially leading to an increased current ratio in the main shaft bearing. A more effective approach to maintaining the main shaft ground brush is imperative to minimize the current passing through the bearing.

6.3 Future work

Future research will delve into a more detailed examination of the electrostatic discharge (ESD) effect and the induced current flow by charge clouds. This exploration will assess their contributions to the main shaft bearing current and evaluate their impact on bearing lifetime, in comparison to various common mode voltage (CMV) sources. The study underscores the necessity for both theoretical analysis and practical laboratory tests to comprehensively understand bearing lifetimes under various bearing current sources, including their discharge pathways.

Reference

[1] C. Radu. (March 2020) The Most Common Causes of Bearing Failure and the Importance of Bearing Lubrication. *RKB Technical Review, Switzerland*. Available: https://www.bearing-news.com/the-most-common-causes-of-bearing-failure-and-the-importance-of-bearing-lubrication/

[2] Y. Gemeinder and M. Weicker, "Application Guide Bearing Currents_V2.3," in "Technical report," 2021-09-28. [Online]. Available: https://tuprints.ulb.tu-darmstadt.de/id/eprint/19393

[3] J. Ribrant and L. M. Bertling, "Survey of Failures in Wind Power Systems With Focus on Swedish Wind Power Plants During 1997–2005," *IEEE Transactions on Energy Conversion,* vol. 22, no. 1, pp. 167-173, 2007, doi: 10.1109/TEC.2006.889614.

[4] *ISO 15243 Rolling bearings damage and failures*, 2017.

[5] SKF, "Bearing damage and failure analysis," https://www.skf.com/binaries/pub12/Images/0901d1968064c148-Bearing-failures---14219_2-EN_tcm_12-297619.pdf.

[6] H. Tischmacher, "Bearing Wear Condition Identification on Converter-fed Motors," in *2018 International Symposium on Power Electronics, Electrical Drives, Automation and Motion (SPEEDAM)*, 20-22 June 2018 2018, pp. 19-25, doi: 10.1109/SPEEDAM.2018.8445293.

[7] A. Muetze, "Bearing Currents in Inverter-Fed AC-Motors ", TU Darmstadt, 2004. [Online]. Available: https://api.semanticscholar.org/CorpusID:112828069

[8] A. Muetze and A. Binder, "Don't lose your bearings," *IEEE Industry Applications Magazine,* vol. 12, no. 4, pp. 22-31, 2006, doi: 10.1109/MIA.2006.1678327.

[9] S. Yagi and N. Ninoyu, "Technical Trends in Wind Turbine Bearings," NTN technical review, 2008.

[10] P. Dvorak and J. Gavilanes. "Cable designs to meet wind industry standards." Wind power development. (accessed.

[11] P. Dvorak and J. Smalley. "Turbine components: bearings." Windpower engineering & development. (accessed.

[12] E. Hart *et al.*, "A review of wind turbine main bearings: design, operation, modelling, damage mechanisms and fault detection," *Wind Energ. Sci.,* vol. 5, no. 1, pp. 105-124, 2020, doi: 10.5194/wes-5-105-2020.

[13] J. Carroll, A. McDonald, and D. McMillan, "Failure rate, repair time and unscheduled O&M cost analysis of offshore wind turbines," *Wind Energy,* vol. 19, 08/01 2015, doi: 10.1002/we.1887.

[14] J. Keller, S. Sheng, J. Cotrell, and A. Greco, *Wind Turbine Drivetrain Reliability Collaborative Workshop: A Recap*. 2016.

[15] B. AlikhanzadehAlamdari, G. Tekin, R. G. Sengoga, and W. Yuan, "Causes of currents in the wind turbine bearings," 2023:2, 2017.

[16] *IEC 61400-27-1*, IEC, 2015.
[17] P. Sørensen, B. Andresen, J. Fortmann, and P. Pourbeik, "Modular structure of wind turbine models in IEC 61400-27-1," in *2013 IEEE Power & Energy Society General Meeting*, 21-25 July 2013 2013, pp. 1-5, doi: 10.1109/PESMG.2013.6672279.
[18] R. G. Deshagoni, "Design and Analysis of Earthing System for Wind Turbine Generators from Lightning Discharge Currents," Victoria University of Wellington, 2020.
[19] Y. M. Hernández *et al.*, "An Insight on the IEC 61400-24 Ed2: Lightning Protection of Wind Turbines," in *2019 International Symposium on Lightning Protection (XV SIPDA)*, 30 Sept.-4 Oct. 2019 2019, pp. 1-6, doi: 10.1109/SIPDA47030.2019.8951662.
[20] V. Peesapati and I. Cotton, "Lightning protection of wind turbines — A comparison of lightning data & IEC 61400-24," in *2009 International Conference on Sustainable Power Generation and Supply*, 6-7 April 2009 2009, pp. 1-7, doi: 10.1109/SUPERGEN.2009.5348088.
[21] *The update of IEC 61400-24 lightning protection of wind turbines*, T. Soerensen *et al.*, 2008.
[22] R. Rodrigues, V. M. F. Mendes, and J. Catalão, "Analysis of Transient Phenomena Due to a Direct Lightning Strike on a Wind Energy System," *Energies,* vol. 5, 12/01 2012, doi: 10.3390/en5072545.
[23] *IEC 61400-24*, IEC, 2019.
[24] A. L. Julian, G. Oriti, and T. A. Lipo, "Elimination of common-mode voltage in three-phase sinusoidal power converters," *IEEE Transactions on Power Electronics,* vol. 14, no. 5, pp. 982-989, 1999, doi: 10.1109/63.788504.
[25] P. M. Sunitha, B. Banakara, and S. Reddy, "Modeling, simulation and analysis of common mode voltage, bearing voltage and bearing current in PWM multilevel inverter fed induction motor with long cable," in *2017 2nd IEEE International Conference on Recent Trends in Electronics, Information & Communication Technology (RTEICT)*, 19-20 May 2017 2017, pp. 1161-1167, doi: 10.1109/RTEICT.2017.8256781.
[26] A.-R. Haitham, M. Mariusz, and A.-H. Kamal, "Common‐Mode Voltage and Bearing Currents in PWM Inverters: Causes, Effects and Prevention," in *Power Electronics for Renewable Energy Systems, Transportation and Industrial Applications*: IEEE, 2014, pp. 664-694.
[27] A. Joshi, "Electrical Characterisations of Bearings," Phd thesis, 2019.
[28] Y. Méndez, J. Birkl, S. F. Madsen, T. Sørensen, J. A. Plumer, and J. Montanya, "The 2018 Revision of the Standard IEC 61400-24: Lightning Protection of Wind Turbines," in *2018 34th International Conference on Lightning Protection (ICLP)*, Rezeszow, Poland, 2-7 Sept. 2018 2018, pp. 1-6, doi: 10.1109/ICLP.2018.8503411.
[29] U. Maradia and K. Wegener, "EDM Modelling and Simulation," M. P. Jahan Ed.: Publisher: Nova Science, 2015, pp. 67-121.

[30] J. Zhao, X. Xu, and O. Carlson, "Electrostatic discharge impacts on the main shaft bearings of wind turbines," *Wind Energ. Sci. Discuss.,* vol. 2023, pp. 1-19, 2023, doi: 10.5194/wes-2023-46.

Appendix A Lab turbine key components

No	Name	Description	Picture
1.	Converter	Servo converter 220V Max 5A	
2.	Generator	PMSM servo motor 200W 3000rpm 0.6 Nm With optical encoder	
3.	Gearbox	Gear ratio i=1:3	

4.	Generator & gearbox support	Aluminum	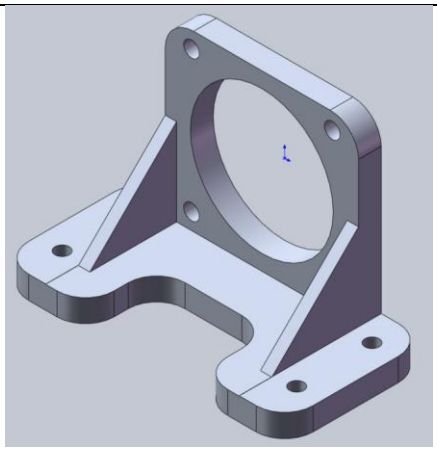
5.	Insulated shaft	Plastic	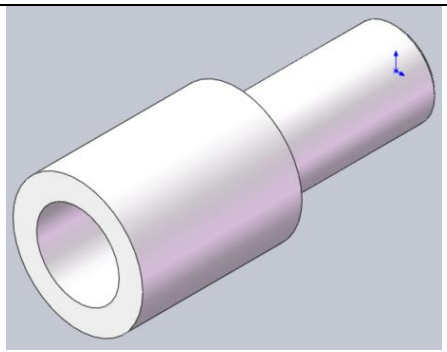
6.	Coupling	Aluminum & rubber ϕ 14mm	
7.	Slip ring	6 channel Max2A 250 rpm	

8.	Main shaft	Steel hollow shaft	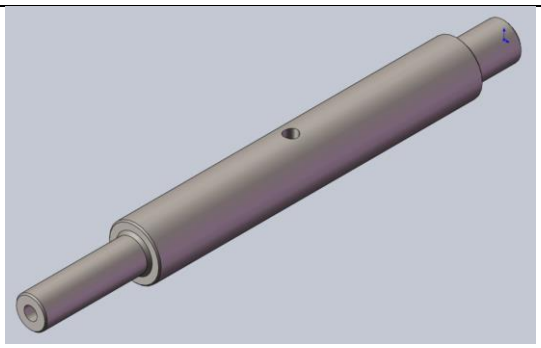
9.	Shaft ground brush	Carbon brush	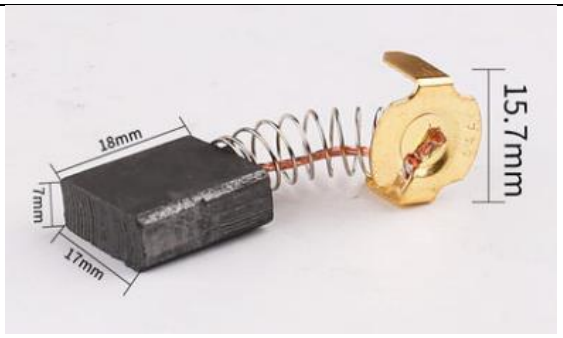
10.	Main bearing	SKF Roller Bearing NU2204E	
11.	Main bearing	SKF Ball Bearing 6204	

12.	Bearing house	Hold the main bearing Plastic (Teflon)	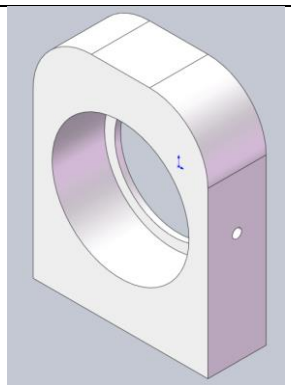
13.	Hub	3D Printing Plastic (Nylon)	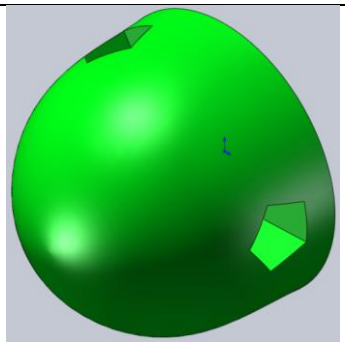
14.	Blade	3D Printing Plastic (Nylon)	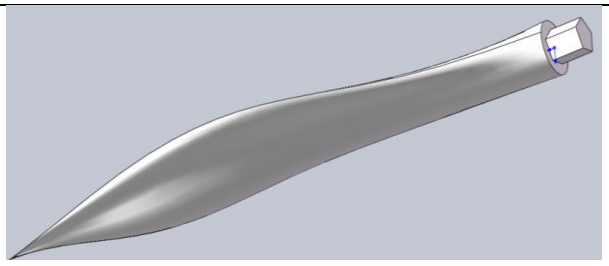
15.	Nacelle bottom board	Support all the component on the nacelle Plastic (Teflon)